

LIBRARY  
OF THE  
UNIVERSITY  
OF ILLINOIS  
620.1123  
I & 59i  
v. 3-5  
cop. 2

~~ENGINEERING~~

The person charging this material is responsible for its return to the library from which it was withdrawn on or before the **Latest Date** stamped below.

**Theft, mutilation, and underlining of books are reasons for disciplinary action and may result in dismissal from the University.**

**To renew call Telephone Center, 333-8400**

**UNIVERSITY OF ILLINOIS LIBRARY AT URBANA-CHAMPAIGN**

SC 02 1981

L161—O-1096



Digitized by the Internet Archive  
in 2011 with funding from  
University of Illinois Urbana-Champaign

<http://www.archive.org/details/inelasticdesigno35univ>



WADD TECHNICAL REPORT 60-580

Part III

INELASTIC DESIGN OF LOAD CARRYING MEMBERS

Part III The Significance of an Inelastic Analysis of  
Eccentrically-Loaded Members

O.M. Sidebottom

Theoretical and Applied Mechanics

University of Illinois

WRIGHT AIR DEVELOPMENT DIVISION



**WADD TECHNICAL REPORT 60-580**  
**Part III**

**INELASTIC DESIGN OF LOAD CARRYING MEMBERS**

**Part III The Significance of an Inelastic Analysis of  
Eccentrically-Loaded Members**

**O.M. Sidebottom**

**Theoretical and Applied Mechanics**

**University of Illinois**

**September 26, 1960**

**Materials Central  
Contract No. AF 33(616)-5658  
Project No. 7351**

**Wright Air Development Division  
Air Research and Development Command  
United States Air Force  
Wright Patterson Air Force Base, Ohio**



620.1123

95-71

1.3-15

1.1

Engin.

ENGINEERING LIBRARY

FOREWORD

7200-3

This report was prepared by the University of Illinois under USAF Contract No. AF 33(616)-5658. This Contract was initiated under Project No. 7351 "Metallic Materials", Task No. 73521, "Behavior of Metals". It was administered under the direction of the Materials Central, Directorate of Advanced Systems Technology, Wright Air Development Division with Mr. R.F. Klinger acting as the Project Engineer.

This report covers work conducted from November 1, 1959 to October 31, 1960.

The work was conducted in the Department of Theoretical and Applied Mechanics in the Engineering Experiment Station, University of Illinois, Urbana, Illinois. Professor O.M. Sidebottom was the Project Supervisor.



## ABSTRACT

The author has worked with others on ten investigations, sponsored by Wright Air Development Division, which have considered the theoretical and experimental inelastic analyses of eccentrically-loaded tension and compression members. In all cases good agreement was found between theory and experiment for numbers tested at room temperature and at elevated temperatures. This investigation was undertaken to consider the significance of an inelastic analysis of eccentrically-loaded members. If the inelastic deformation can be considered time independent, a choice has to be made between an elastic and an inelastic solution. A study was made of the effect of several variables on the ratio of the load necessary to produce a specified inelastic deformation to the maximum elastic load. If the inelastic deformation is time dependent (creep), the only choice is an inelastic solution.

## PUBLICATION REVIEW

This report has been reviewed and is approved.

## FOR THE COMMANDER

W.J. Trapp  
Chief, Strength and Dynamics Branch  
Metals and Ceramics Laboratory  
Materials Central



TABLE OF CONTENTS

	Page No.
I . INTRODUCTION	1
II . THEORETICAL APPROACH	2
III . ELASTIC VERSUS INELASTIC ANALYSES	5



## LIST OF FIGURES

Figure No.		Page No.
1.	Idealized Stress-Strain Diagram for Time Independent Inelastic Deformation	12
2.	Constant Depth of Yielding Interaction Curves for Rectangular Section Member ( $\alpha = 0$ ).	13
3.	Family of Curves for Rectangular-Section Member Giving Relation Between $\Delta$ , q, and K.	14
4.	Family of Curves for Rectangular-Section Member Giving Relation Between P, q, and K.	15
5.	Configurations of Eccentrically-Loaded Tension Members and Columns.	16
6.	Cross-Sections for Eccentrically-Loaded Members.	17
7.	Ratio of Collapse Load to Maximum Elastic Load for Rectangular-Section Eccentrically-Loaded Columns.	18
8.	Ratio of Collapse Load to Maximum Elastic Load for Circular-Section Eccentrically-Loaded Columns.	19
9.	Ratio of Collapse Load to Maximum Elastic Load for Angle-Section Eccentrically-Loaded Columns.	20
10.	Ratio of Collapse Load to Maximum Elastic Load for T-Section Eccentrically-Loaded Columns.	21
11.	Ratio of Collapse Load to Maximum Elastic Load for I-Section Eccentrically-Loaded Columns.	22
12.	Ratio of Collapse Load to Tangent Modulus Load for Eccentrically-Loaded Columns Made of a Material that Creeps.	23



## I. INTRODUCTION

Modern design, particularly in the aircraft and missile fields, requires that load carrying members be used to the limit of their capacity. In many applications the peak loads are applied only a small number of times so that fatigue is not a problem. For the design of these members, the engineer has to choose between an elastic and an inelastic analysis. Because of its ease of application and the confidence which the engineer has in its application, the engineer would prefer to use the elastic solution. However, the elastic solution is too safe in many applications, and the engineer must use an inelastic design to utilize the increase in load carrying capacity which is possible if small, inelastic strains are allowed. The percentage increase in load above the maximum elastic load depends upon such variables as type of member, shape of cross-section, shape of stress-strain diagram of the material, and the amount of inelastic deformation. In the case of design for an elevated temperature of sufficient magnitude to produce creep, an inelastic analysis is always required.

The difficulty of an analysis depends upon the type of relation used to represent the stress-strain diagram for the material. Linear elasticity uses one of the simplest relations, namely, a straight line. If the material has a yield point and the member is designed for strength rather than deformation, a fully plastic analysis may be used; the resulting solution may be easier to apply than an elastic solution.\*A fully plastic analysis cannot be used in a large number of instances if any one of the following conditions are present:

1. The member is made of a material which does not have a yield point.
2. It is necessary to know the load-deformation relation for inelastic conditions.
3. The member may become unstable before reaching the fully plastic condition as is the case of an eccentrically-loaded column.

In most cases, the loads on the members are assumed to maintain their same relative magnitude and to increase in magnitude so that a nonlinear elastic analysis can be used. In deriving the theoretical relations, the stress-strain diagram of the material is represented by one non-linear function or two functions. At room temperature, two functions are usually used to represent the stress-strain diagram for metals, and the resulting solution is called an elastic-plastic solution.

Because of the ever increasing interest in the inelastic analysis of load carrying members, it is necessary that theoretical inelastic analyses be developed for all types of load carrying members. Furthermore, it is necessary that these theories be checked experimentally for the following reasons:

1. Frequently simplifying assumptions are used in order to reduce the complexity of the theory so that the theory can be readily applied by the design engineer. It is necessary to determine the influence of these simplifying assumptions on the agreement between theory and experiment.



2. It is logical that the engineer does not have the same confidence in an inelastic analysis which he has in an elastic analysis. Experimental verification of inelastic theories helps promote confidence in those theories.

Some of the investigations (1 through 10)\* sponsored by the Wright Air Development Division have considered the theoretical and experimental inelastic analyses of eccentrically-loaded tension and compression members. These investigations have considered a large number of variables, namely:

1. Several types of ductile metals such as S.A.E. 4340 steel, 7075-T6 aluminum alloy, type 304 stainless steel, 17-7PH stainless steel, and Ti 155A titanium alloy.
2. Several types of cross-sections such as rectangular, angle, and T-sections.
3. Several end conditions for the columns such as fixed ends and pivot ends with equal and unequal end eccentricities of various magnitudes.
4. Several slenderness ratios for the columns.
5. Both room temperature and elevated temperatures.

In all cases good agreement was found between theory and experiment indicating that the theory was sufficiently exact to be used in the design of eccentrically-loaded members. Since the theory was found to be reliable, was the increase in load carrying capacity of a member (which resulted from the inelastic deformation) of sufficient magnitude to justify the increase in labor necessary to complete an inelastic analysis? Answers to this question vary from yes for some cases to no for other cases. In order to obtain definite answers to the question, the theory will be reviewed so that the effect of various variables on the increase in load carrying capacity of eccentrically-loaded members can be determined.

## II. THEORETICAL APPROACH

In deriving theoretical, load-deflection relations for eccentrically-loaded members, the procedure is to equate the internal load and moment at every section of the member to the applied load and moment. For elastic conditions, Timoshenko (11) has presented closed solutions for rather general loading conditions. Closed solutions have not been found for inelastic conditions. Several analyses requiring a trial and error solution have been presented (2,3,5,6,7,8,9,10,12,13,14). In each case, a family of interaction curves was constructed to give a relation between the internal load, moment, and curvature at any section of the member. A relation between applied load, moment, and curvature was obtained by approximating the configuration of the deformed member.

---

\* Numbers in parenthesis refer to correspondingly numbered entries in the Bibliography.



At least three different types of interaction curves have been used in the analyses of eccentrically-loaded columns in which the inelastic deformation was primarily time independent. Chwalla (13) and Bijlaard (12) used a family of curves giving the relations between the average stresses of originally straight, centrally-loaded columns and the post-buckling deflection. Galambos and Ketter (14) used dimensionless, moment versus curvature curves for specified loads. Sidebottom and Clark (2) approximated the stress-strain diagram of the material by two straight lines (see Fig. 1), and constructed dimensionless, moment versus load curves for constant depths of yielding. These curves are shown in Fig. 2 for rectangular-section members made of a material with  $\alpha' = 0$  (see Fig. 1). In Fig. 2,  $P_e = \sigma_e A$  and  $M_e = \sigma_e I/c$ . It is the author's opinion that constant depth of yielding interaction curves are the easiest to construct and use.

In case the inelastic deformation is time dependent (creep), Sidebottom, Clark, and Dharmarajan (6) approximated the isochronous stress-strain diagram\* of the material by an arc hyperbolic sine curve of the form

$$\sigma = \sigma_0 \operatorname{arc} \sinh \frac{\epsilon}{\epsilon_0} \quad (1)$$

in which  $\sigma_0$  and  $\epsilon_0$  are experimental constants. Since the stress distribution in the eccentrically loaded member changes with time and  $\sigma_0$  and  $\epsilon_0$  were obtained from constant stress creep curves, Eq. 1 does not accurately represent the stress-strain relation in the member at a specified time. Good agreement was found between theory and experiment (9,10) by decreasing  $\sigma_0$  by 10 per cent for eccentrically-loaded tension members and by increasing  $\sigma_0$  by 10 per cent for eccentrically-loaded columns. Based on Eq. 1, two families of interaction curves were constructed as indicated in Figs. 3 and 4 for a rectangular-section member. In these figures  $\Delta$  is the distance from the action line of the load to the centroidal axis of the member at the point of maximum deflection,  $h$  is the depth of the member,  $qh$  is the distance from the most strained fiber to the neutral axis, and  $K$  is the ratio of the maximum strain at a given section to  $\epsilon_0$ .

Using the interaction curves shown in either Fig. 2 or Figs. 3 and 4, the deflection, load, and curvature can be computed for any assumed point on any of the curves. Another relation for the curvature of an eccentrically-loaded member is obtained in terms of the configuration of the member. A trial and error solution is required in order to determine the point on a given interaction curve which will make the two curvatures equal. One point on the theoretical load-deflection curve for the eccentrically-loaded member may be obtained from each interaction curve.

Consider the eccentrically-loaded tension member shown in Fig. 5a. Since the exact configuration of the member was difficult to obtain for inelastic conditions, the axis of the member was assumed (2,5,6,7,8,9) to deform into a

\*Diagram obtained by plotting values of stress and strain obtained at a given time from constant stress creep curves.



segment of a circle. This configuration assumes that every section has the same curvature as that for section C. Since every other section has a curvature greater than that at C, the resulting theoretical deflection will be less than actual, i.e. nonconservative. The error is small if  $\epsilon$  is large compared to  $\delta$ .

In the case of an eccentrically-loaded column (see Fig. 5b), Chwalla (13) and Galambos and Ketter (14) have presented procedures to approximate the configuration of the inelastically deformed column as accurately as desired. These procedures could also be used in the analysis of eccentrically-loaded tension members and columns having end conditions other than that shown in Fig. 5b. However, these exact solutions are extremely time consuming. Since a column having any known end condition deforms into a sine curve elastically, Bijlaard (12) suggested that the inelastic column also be assumed to deform into a sine curve. For the column shown in Fig. 5b, the curve DCF can be represented by the following relation:

$$y = \Delta \sin \frac{\pi x}{L} \quad (2)$$

The curvature of the column at section C can be obtained from Eq. 2 to be equated with the curvature obtained from the assumed point on a given interaction curve. The correct point on the interaction curve will satisfy the condition that  $y = e$  when  $x = u$ . Solutions for general end conditions are presented in references 10 and 12. Theoretical (12) and experimental (10) investigations have shown that relatively small errors are introduced by the assumption that the inelastic column deforms into a sine curve.

In several investigations (3,5,9), the curve ACB was represented both by a segment of a circle and a sine curve of the form

$$y = \delta \sin \frac{\pi x}{\ell} \quad (3)$$

Since neither of these approximations introduced another unknown (such as L when using Eq. 2), they are easier to work with than Eq. 2. For a given load, the segment of a circle approximation gives a deflection greater than actual (conservative), while Eq. 3 gives a deflection less than actual (nonconservative). Good agreement was found (3,5,9) between theoretical collapse loads based on Eq. 3 and the experimental collapse loads. Furthermore, the ratios of collapse loads to maximum elastic loads are nearly identical for theories based on Eq. 2 and Eq. 3. Computations have been made for eccentricities as large as 25 per cent of the column depth.



### III. ELASTIC VERSUS INELASTIC ANALYSES

The discussion which follows will consider the ratio of the load necessary to produce a specified amount of inelastic deformation to the maximum elastic load for eccentrically-loaded members. For a given member this ratio depends upon the amount of inelastic deformation, the shape of cross-section, and the magnitude of  $\alpha$  (see Fig. 1). The ratio is also greatly influenced by the type of loading. In the case of an eccentrically-loaded tension member, the ratio continues to increase with inelastic deformation (limited by the fully plastic condition when  $\alpha = 0$ ). The ratio reaches a maximum at the collapse load in the case of eccentrically-loaded columns. Separate discussions will be presented for each type of member. In each case data will be presented for the five cross-sections shown in Fig. 6. The I-section member is assumed to deform without local buckling.

Eccentrically-Loaded Tension Members. As indicated in Fig. 5a, the section of an eccentrically-loaded tension member having maximum moment is located at either end of the member. Since small deformation theory is used, the moment remains constant and equal to  $P_e$ . If the inelastic deformation is primarily time independent, the stress-strain diagram of the material is approximated by two straight lines as indicated in Fig. 1, and interaction curves similar to those shown in Fig. 2 are used in the inelastic analysis. Since the ratio of moment to load remains constant, the load necessary to produce any depth of yielding in an eccentrically-loaded tension member may be obtained from a radial line drawn from point O in Fig. 2. The slope of line OB in Fig. 2 is equal to the ratio of  $M/M_e$  to  $P/P_e$  and can be shown to be equal to  $ec/r^2$  where  $c$  is the distance from the centroidal axis to the outermost fiber of the member, and  $r$  is the radius of gyration of the cross-section with respect to the same centroidal axis.

The maximum elastic load and the load necessary to produce any depth of yielding are easily obtained from the radial line in Fig. 2. The ratio of the load necessary to produce a specified depth of yielding to the maximum elastic load increases from 1.00 for  $\theta = 0$  (centrally-loaded tension member) to a maximum for a value of  $\theta$  between 0 and  $\pi/2$ . When  $\theta$  is equal to  $\pi/2$ , the member is subjected to pure bending.

The line OB shown in Fig. 2 has a slope of 1.5. The ratio of the load necessary to produce one half depth of yielding to the maximum elastic load was computed for a slope of 1.5 for all of the cross-sections shown in Fig. 6. These data are shown in Table 1 for values of  $\alpha = 0$  and  $\alpha = 0.20$ . It will be noted that an appreciable increase in load carrying capacity resulted from allowing the inelastic deformation. The increase is greatly influenced by the shape of cross-section and by the strain hardening factor,  $\alpha$ . The increase in deflection for this increase in load may be obtained using the theories presented in references 2,5,6,7,8, or 9. The deflection necessary to produce one half depth of yielding at each end of an eccentrically-loaded tension member is in the neighborhood of twice the maximum elastic deflection.



In case the inelastic deformation is time dependent (creep), there is no choice between an elastic and an inelastic design since any design for creep is based on an inelastic analysis. The load necessary to produce a specified strain in the most strained fibers can be obtained using the procedure outlined in references 6, 7, 8, 9, or 10. This procedure uses interaction curves such as those shown in Figs. 3 and 4.

Eccentrically-Loaded Columns. As indicated in Fig. 5b, the maximum moment in the eccentrically-loaded column occurs at the section which has the maximum deflection  $\Delta$ . Thus, an inelastic analysis requires that the load-deflection curve for the column be obtained. If the inelastic deformation is primarily time independent, constant depth of yielding interaction curves similar to those shown in Fig. 2 are used in the inelastic analysis. By the procedure outlined in references 3, 5, 9, or 10, a moment-load curve similar to curve OD in Fig. 2 can be constructed for a given column from which the load-deflection curve is obtained. It will be noted that the load carried by the eccentrically-loaded column does not continue to increase with an increase in depth of yielding but that the load is limited to the collapse load.

The effect of inelastic deformation on the load carrying capacity of eccentrically-loaded columns will be indicated by the ratio of the collapse load to the maximum elastic load. This ratio is influenced by such variables as cross-section, slenderness ratio, yield strain, strain hardening factor  $\alpha$ , and initial eccentricity. The two variables, slenderness ratio and yield strain, can be replaced by one variable  $\epsilon_e(\ell/r)^2$ .

Ratios of the collapse load to the maximum elastic load are shown in Figs. 7 through 11 for the 5 cross-sections shown in Fig. 6. Data is given in each case for two initial eccentricities of 5 and 25 per cent of the column depth and for two strain hardening factors of zero and 0.20. It will be noted that the ratio of the collapse load to maximum elastic load approaches 1.0 for large values of  $\epsilon_e(\ell/r)^2$ ; furthermore, the effect of  $\alpha$  on the ratio is small for large values of  $\epsilon_e(\ell/r)^2$ . The magnitude of  $\epsilon_e(\ell/r)^2$  at which the ratio becomes small depends upon the shape of cross-section and upon the initial eccentricity. The effect of shape of cross-section can be represented, at least partially, by the variable  $ch/r^2$  where  $c$  is the distance from the neutral axis to the outermost fibers of the member. Consider the dimensionless product,

$$S = \frac{ch}{r^2} \frac{1}{(1 - /h)^2 \sqrt{(\ell/r)^2 \epsilon_e}} \quad (3)$$

If  $S$  is less than or equal to 17, the ratio of collapse load to maximum elastic load will be less than 1.05 for all of the variables considered in Figs. 7 through 11. In the case of the T-section member, the ratio will be less than 1.05 for values of  $S$  as large as 28. When these conditions are satisfied, an inelastic analysis is not justified. The minimum slenderness ratio, for several materials and for three eccentricities, necessary to have the ratio less than 1.05 were calculated and are shown in Table 2 for the cross-sections



shown in Fig. 6. As indicated in Table 2, there are many applications for which an inelastic analysis is not justified, particularly for eccentrically-loaded columns made of high strength, low modulus materials for which the initial eccentricity is small. It should be noted that the aforementioned values of S are valid for unequal eccentricities if the larger value of  $e/h$  is substituted in Eq. 3.

If S is greater than 28 for the T-section member and greater than 17 for the other cross sections shown in Fig. 6, an inelastic analysis may result in an appreciable saving in weight and cost. As indicated in Figs. 7 through 11, the ratio of collapse load to maximum elastic load may be as large as 2.00 in some instances. This ratio will be larger for larger initial eccentricities.

In case the inelastic deformation is time dependent (creep), the design of an eccentrically-loaded column must be based on an inelastic analysis. For centrally-loaded columns with pivot ends, the collapse load is the tangent modulus load which is easily computed using Eq. 1. Since Eq. 1 does not accurately represent the stress-strain relation for the material in the column at the specified time (see Section II), the actual collapse load will be greater than the tangent modulus load by 10 per cent. The ratio of the collapse load of an eccentrically-loaded column for a specified time to the tangent modulus load for the same time was computed for the rectangular-section, the T-section, and the I-section and are shown in Fig. 12. For zero initial eccentricity, the column is centrally-loaded and the collapse load is 10 per cent greater than the tangent modulus load as explained in Section II. The experimental data presented in references 9 and 10 indicate that, for a given cross-section and a given initial eccentricity, the ratio of the collapse load to the tangent modulus load is not influenced by either the slenderness ratio or the time to collapse if the tangent modulus load is calculated for the specified time.



## BIBLIOGRAPHY

1. Brush, D.O., Sidebottom, O.M. and Smith, J.O., "Axial Tension and Bending Interaction Curves for Members Loaded Inelastically," WADC Technical Report, February, 1952.
2. Sidebottom, O.M. and Clark, M.E., "The Effects of Inelastic Action of the Resistance to Various Types of Loads of Ductile Members Made from Various Classes of Metals -- Part I Eccentrically-Loaded Tension Members Having Angle-and T-Sections," TAM Report No. 100, March, 1956, WADC Technical Report, April, 1957.
3. Clark, M.E. and Sidebottom, O.M., "The Effects of Inelastic Action on the Resistance to Various Types of Loads of Ductile Members Made from Various Classes of Metals -- Part IV Eccentrically-Loaded Columns Having Angle-and T-Sections," TAM Report No. 112, November, 1956, WADC Technical Report.
4. Maeda, Y., Van Lierde, P., Sidebottom, O.M., and Clark, M.E., "The Effects of Inelastic Action on the Resistance to Various Types of Ductile Members Made from Various Classes of Metals -- Part VI A Digital Computer Analysis of Bending Moment -- Axial Load Interaction Curves," TAM Report No. 115, January, 1957, WADC Technical Report.
5. Sidebottom, O.M. and Clark, M.E., "A Theoretical and Experimental Analysis of Members Loaded Eccentrically and Inelastically," Bulletin Series No. 447, Engineering Experiment Station, University of Illinois, 1958.
6. Sidebottom, O.M., Clark, M.E., and Dharmarajan, S., "The Effects of Inelastic Action on the Resistance to Various Types of Loads of Ductile Members Made from Various Classes of Metals -- Part VIII Eccentrically Loaded Tension Members Made of Two Stainless Steels tested at Elevated Temperatures," TAM Report No. 132, April, 1958, WADC Technical Report, October, 1958.
7. Sidebottom, O.M. and Dharmarajan, S., "The Effects of Inelastic Action on the Resistance to Various Types of Loads of Ductile Members Made from Various Classes of Metals -- Part IX T-Section Eccentrically-Loaded Tension Members Made of Type 304 Stainless Steel and Tested at 1000°F," TAM Report No. 134, May, 1958, WADC Technical Report, October, 1958.
8. Sidebottom, O.M. and Dharmarajan, S., "The Effects of Inelastic Action on the Resistance to Various Types of Loads of Ductile Members Made from Various Classes of Metals -- Part X T-Section Eccentrically-Loaded Tension Members of 17-7 PH Stainless Steel and Tested at 1000°F," TAM Report No. 144, November, 1958, WADC Technical Report, May 1959.



9. Sidebottom, O.M., Dharmarajan, S., Gubser, I.L. and Leasure, J.D., "The Effects of Inelastic Action on the Resistance to Various Types of Ductile Members Made of Various Classes of Metals -- Part XII Eccentrically-Loaded Tension Members and Columns Made of 17-7 PH Stainless Steel and Ti 155A Titanium Alloy and Tested at Various Temperatures," TAM Report No. 154, October, 1959, WADC Technical Report.
10. Costello, G.A., Sidebottom, O.M., and Pocs, E., "Inelastic Design of Load Carrying Members -- Part II The Effects of End Conditions on the Collapse Loads of Columns," TAM Report No. 178, September, 1960, WADD Technical Report.
11. Timoshenko, S., "Theory of Elastic Stability," McGraw-Hill Book Co., Inc., New York, 1936.
12. Bijlaard, P.P., "Buckling of Columns with Equal and Unequal End Eccentricities and Equal and Unequal Rotational Restraints," Proceeding of the Second U.S. National Congress of Applied Mechanics, 1954, pp. 555-562.
13. Chwalla, E., "Aussermittig gedruckte Baustahlstäbe mit elastisch eingespannten Enden und verschieden grossen Augriffshebeln," Der Stahlbau, 1937, Nos. 7-8.
14. Galambos, T.V. and Ketter, R.L., "Columns Under Combined Bending and Thrust," Proceedings ASCE, Vol. 85, No. EM 2, April 1959.



TABLE 1

Ratio of Load Necessary to Produce One Half Depth of Yielding in  
 an Eccentrically-Loaded Tension Member and Maximum  
 Elastic Load

Strain Hardening Factor $\alpha$	Ratio when $\tan \phi = 1.5$				
	Rectangular- Section	Circular- Section	Angle- Section	T-Section	I-Section
0	1.43	1.53	1.51	1.27	1.22
0.2	1.66	1.74	1.78	1.62	1.46



TABLE 2

**Minimum Slenderness Ratios for Eccentrically-Loaded Columns  
for which an Inelastic Analysis is Not Justified**

Material	$\sigma_e$ (psi)	$\epsilon_e$	Slenderness Ratio for				
			Rectangular-Section	Circular-Section	Angle-Section	T-Section	I-Section
$e/h = 0.05$							
Steel	30,000	.0010	124	165	202	98	70
Steel	90,000	.0030	71	95	117	57	40
Steel	180,000	.0060	50	67	82	40	29
17-7PH	183,000	.065	49	65	79	39	28
7075-T6	80,000	.0078	44	59	72	35	25
Ti 155A	164,000	.0092	41	54	67	32	23
$e/h = 0.25$							
Steel	30,000	.0010	198	265	324	157	113
Steel	90,000	.0030	115	153	187	91	65
Steel	180,000	.0060	81	108	132	64	46
17-7PH	183,000	.0065	78	104	127	62	44
7075-T6	80,000	.0078	71	95	116	56	40
Ti 155A	164,000	.0092	65	87	107	52	37
$e/h = 0.50$							
Steel	30,000	.0010	446	595	729	354	253
Steel	90,000	.0010	258	344	421	205	146
Steel	180,000	.0060	182	243	298	145	103
17-7PH	183,000	.0065	175	234	286	139	99
7075-T6	80,000	.0078	160	213	261	127	91
Ti 155A	164,000	.0092	147	196	240	117	83



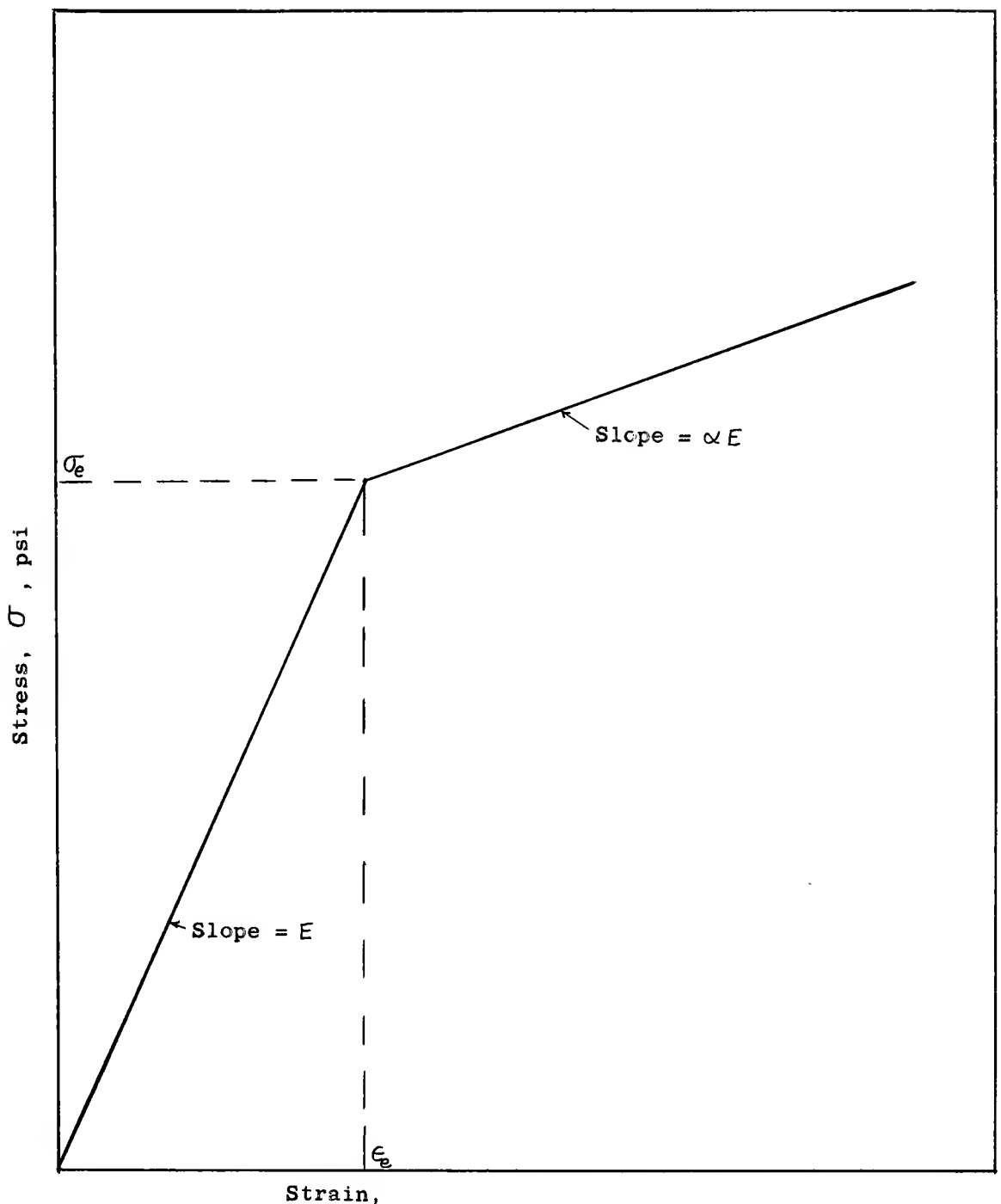


Fig. 1      Idealized Stress-Strain Diagram for Time Independent  
Inelastic Deformation



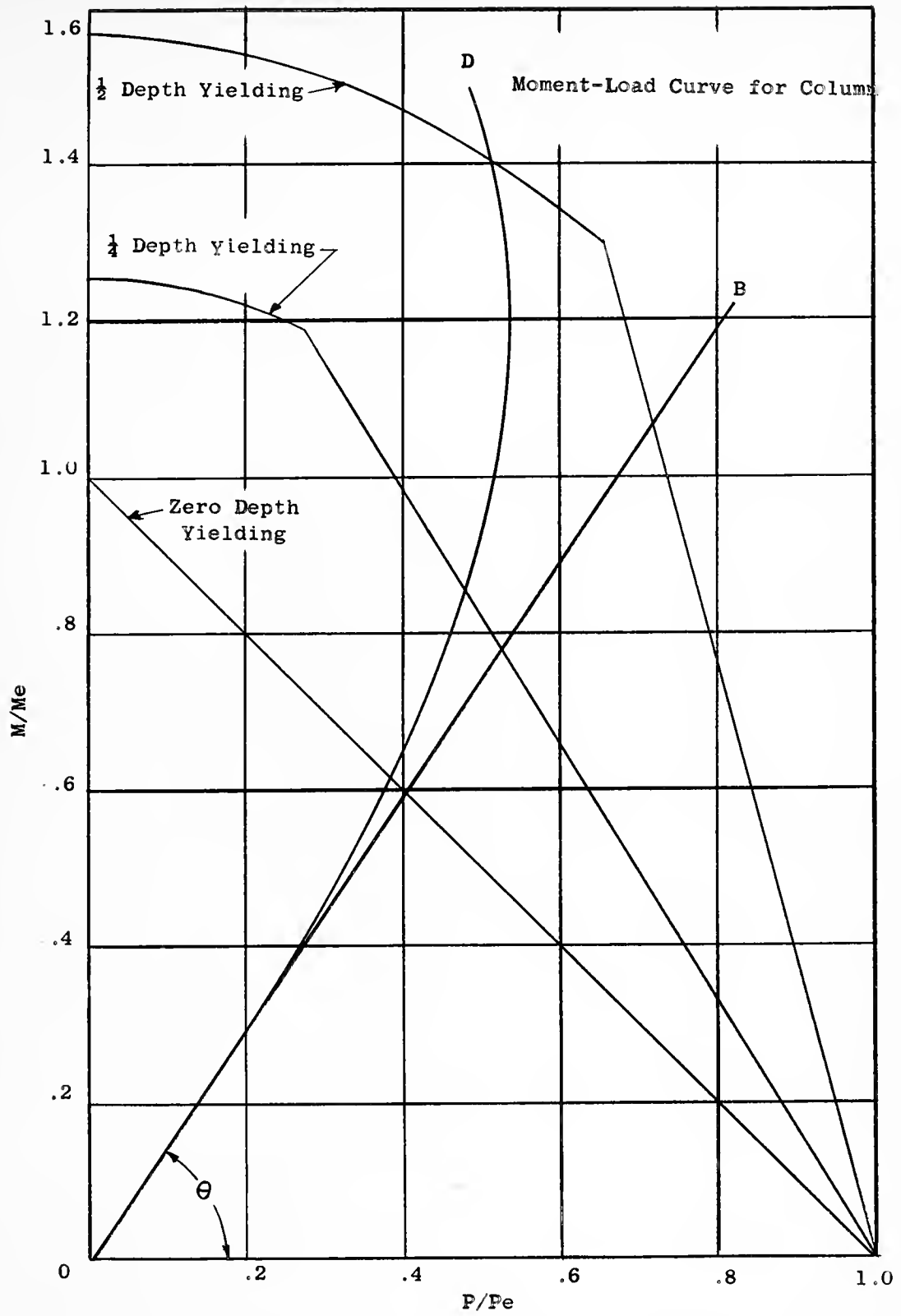


Fig. 2 Constant Depth of Yielding Interaction Curves for Rectangular-Section Member ( $\alpha = 0$ ).



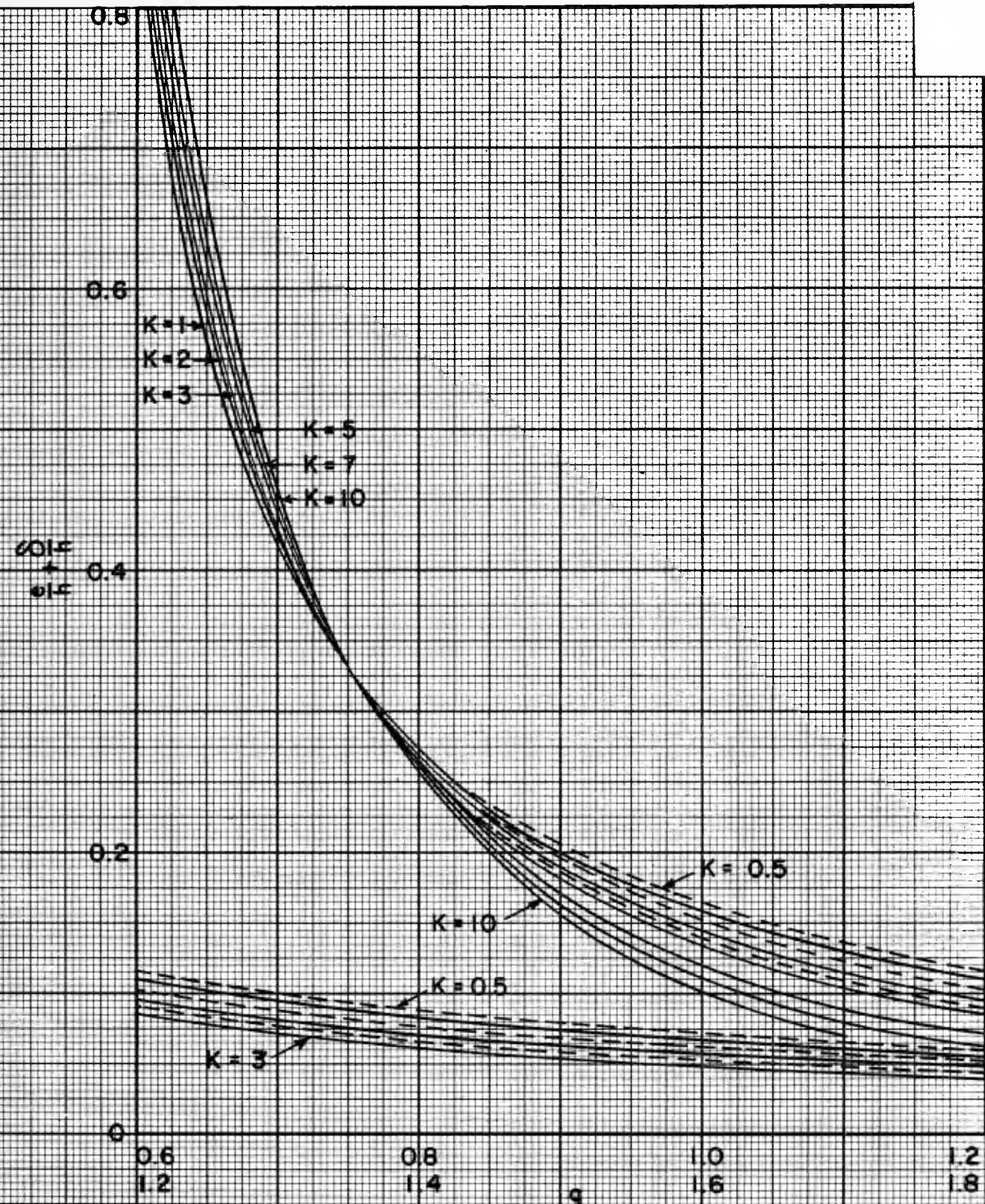
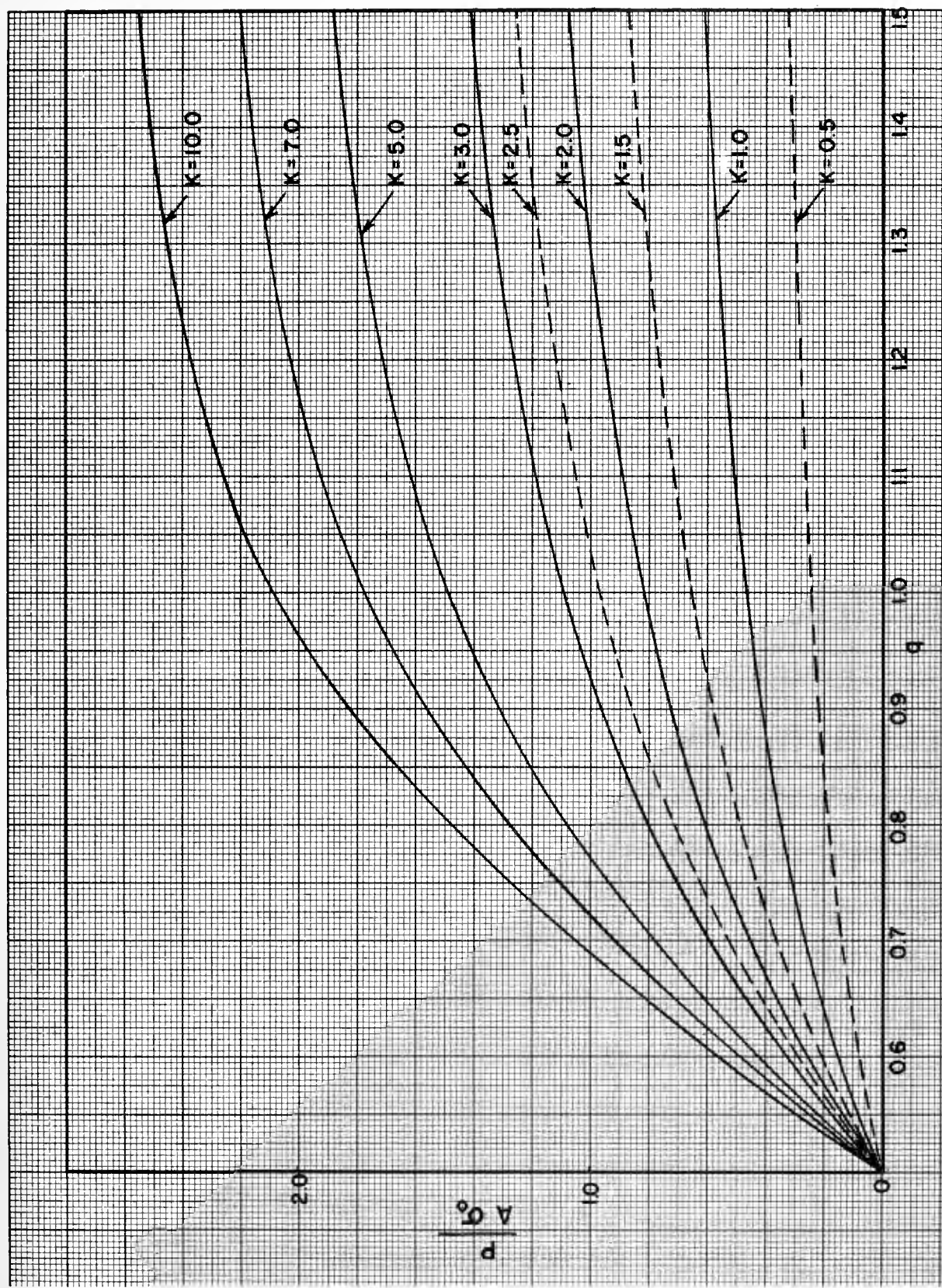


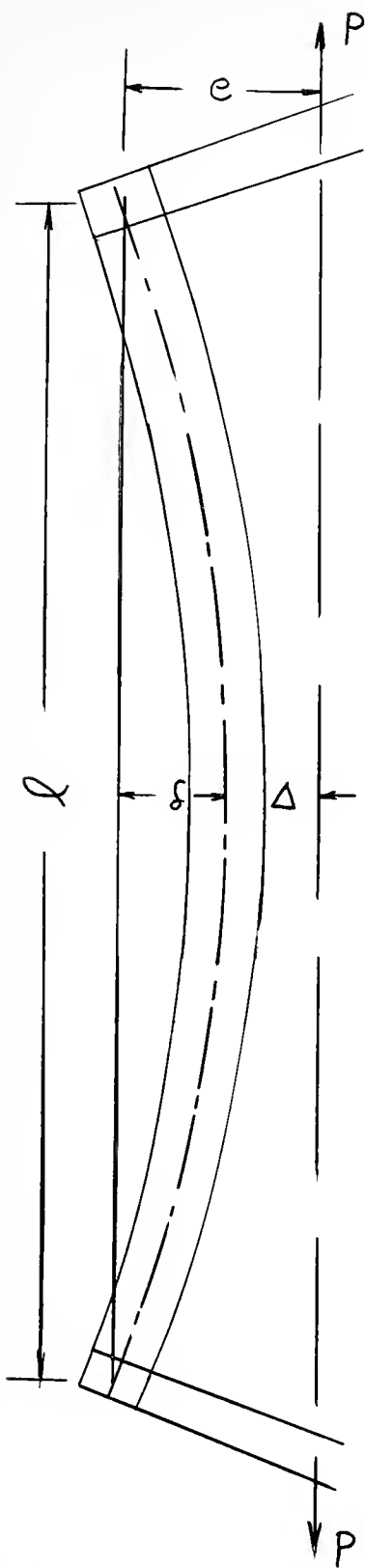
Fig. 3. Family of Curves for Rectangular-Section Member Giving Relation Between  $\Delta$ ,  $q$ , and  $K$



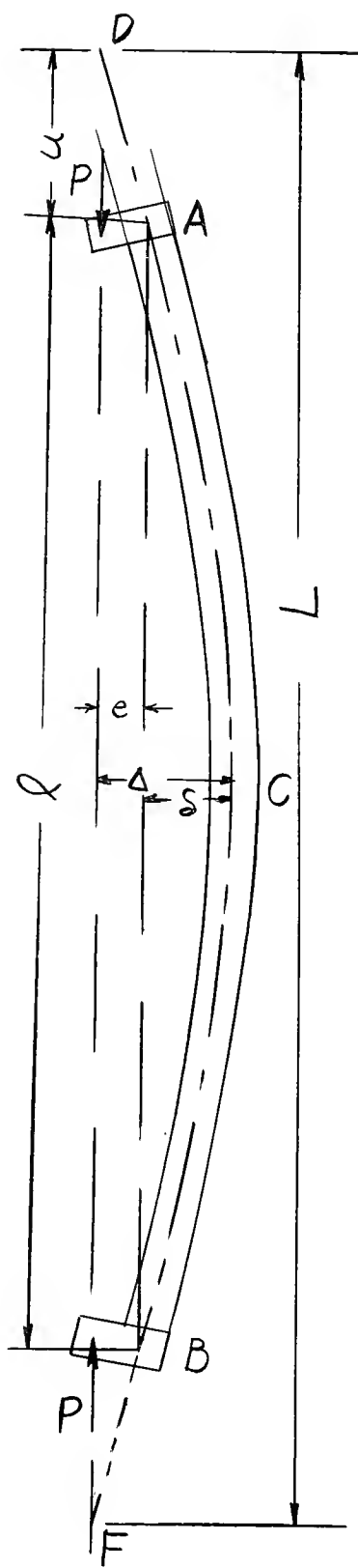
Fig. 4. Family of Curves for Rectangular-Section Member Giving Relation Between  $P$ ,  $q$ , and  $K$ .







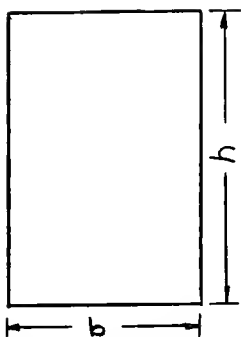
(a) Eccentrically-Loaded Tension Member



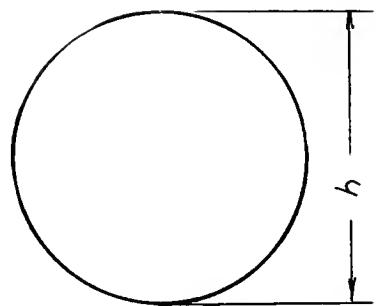
(b) Eccentrically-Loaded Column

Fig. 5 Configurations of Eccentrically-Loaded Tension Members and Columns.

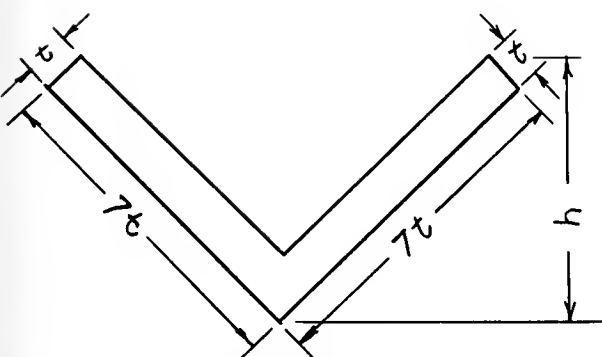




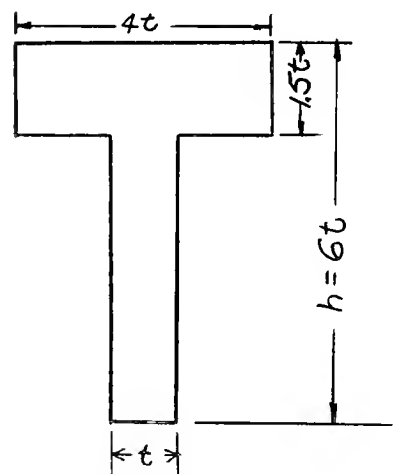
(a) Rectangular-Section



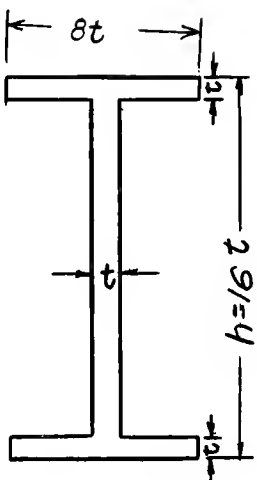
(b) Circular-Section



(c) Angle-Section



(d) T-Section



(e) I-Section

Fig. 6 Cross-Sections for Eccentrically-Loaded Members



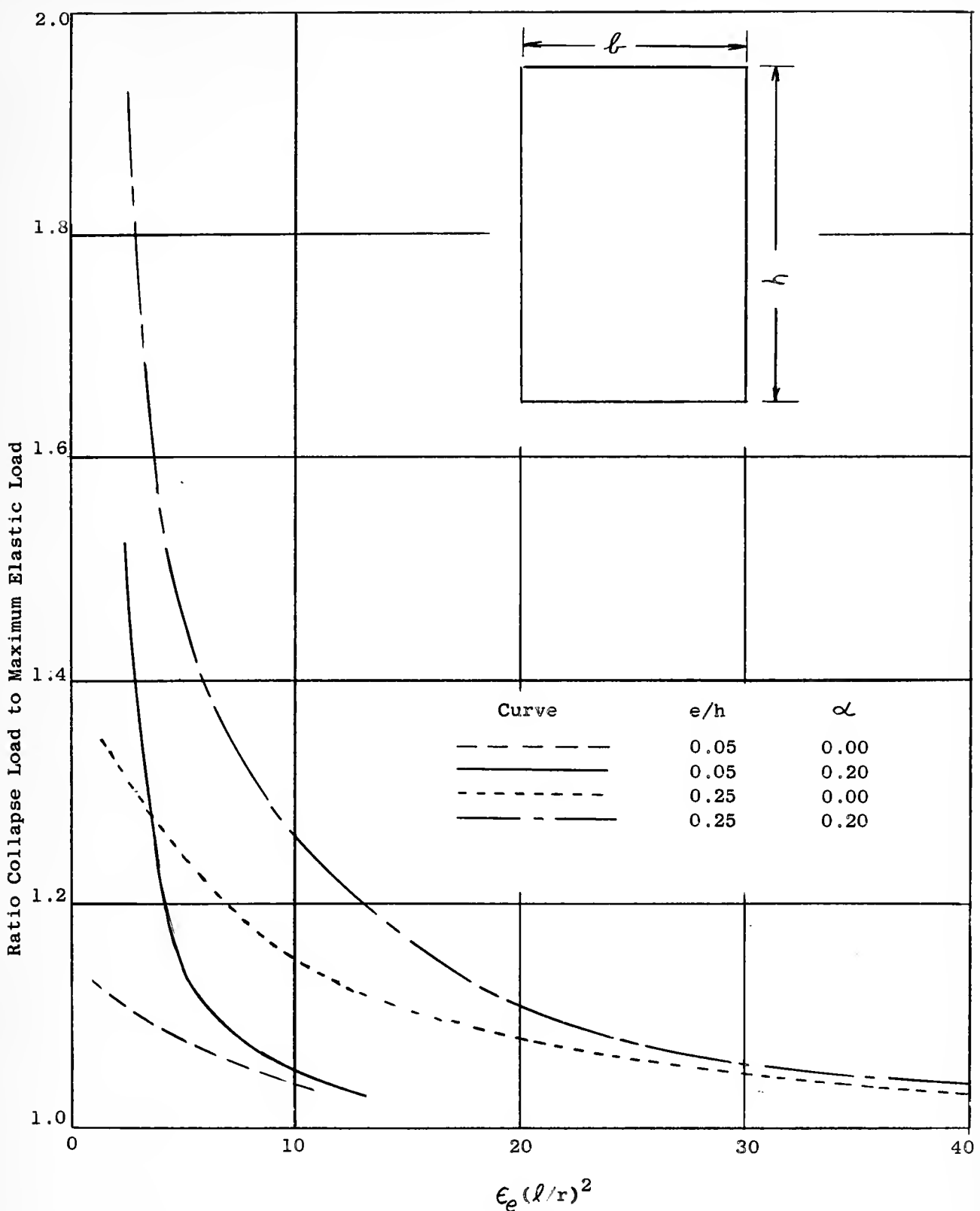


Fig. 7 Ratio of Collapse Load to Maximum Elastic Load for Rectangular-Section Eccentrically-Loaded Columns



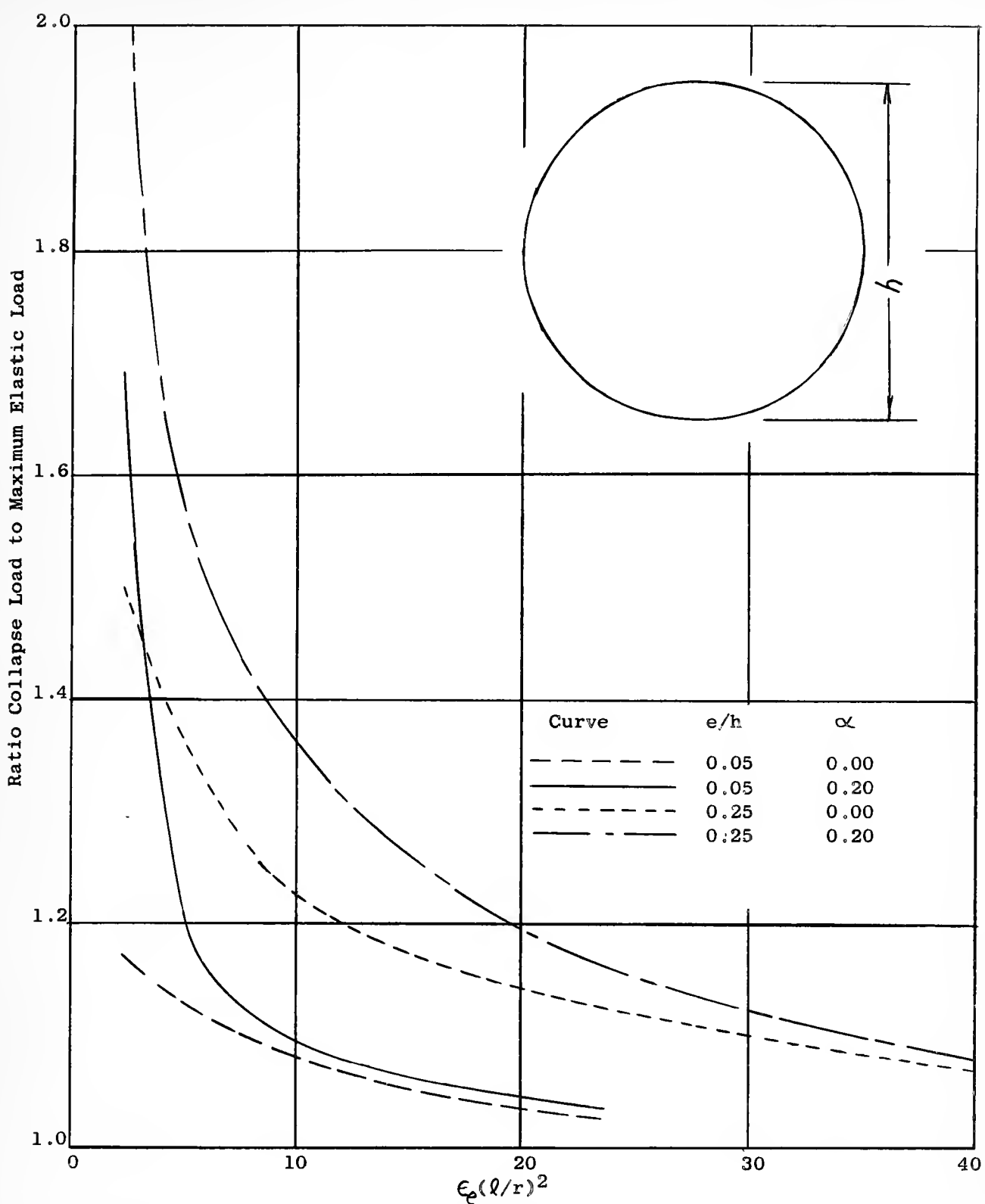


Fig. 8 Ratio of Collapse Load to Maximum Elastic Load for Circular-Section Eccentrically-Loaded Columns



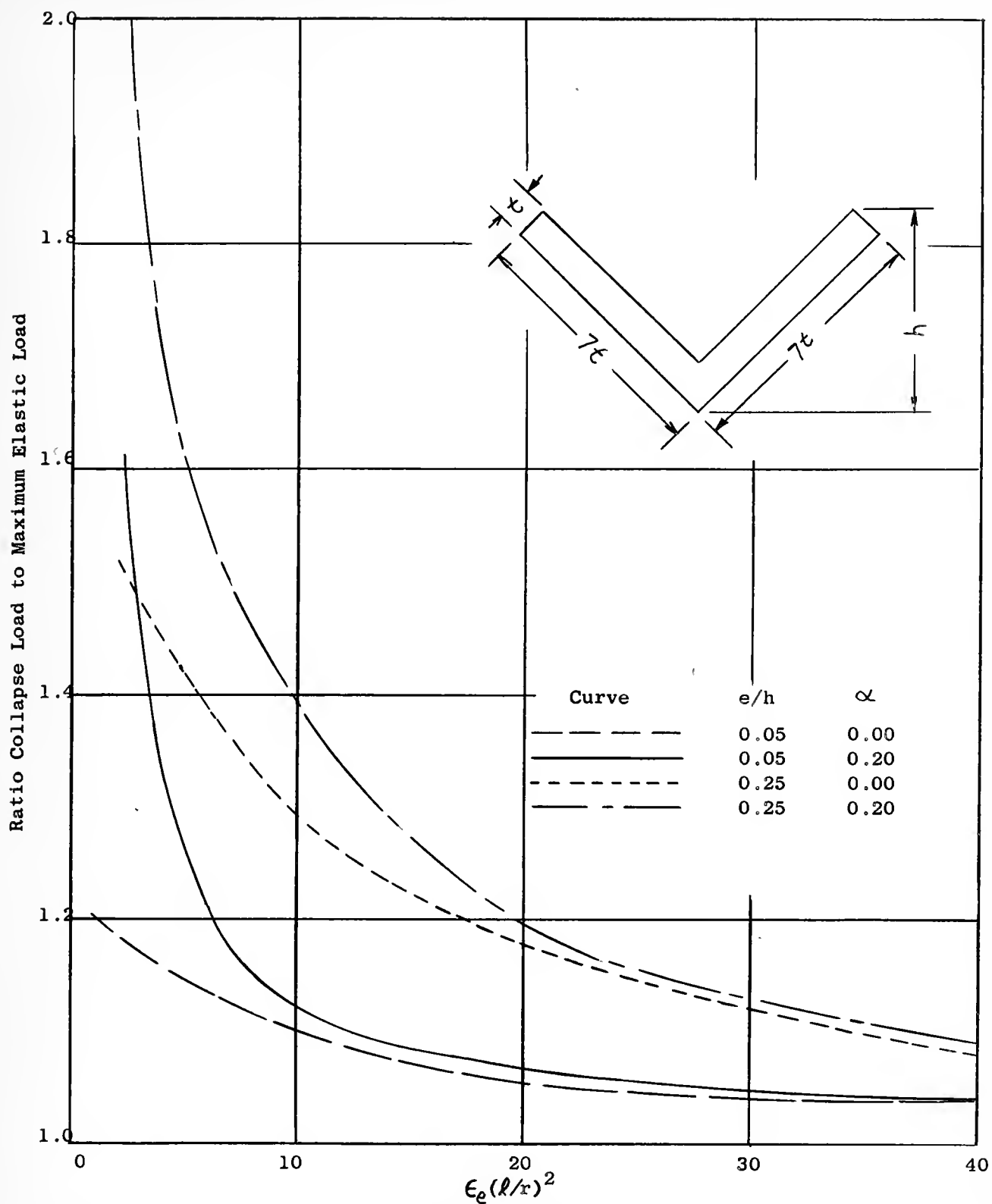


Fig. 9 Ratio of Collapse Load to Maximum Elastic Load for Angle-Section Eccentrically-Loaded Columns



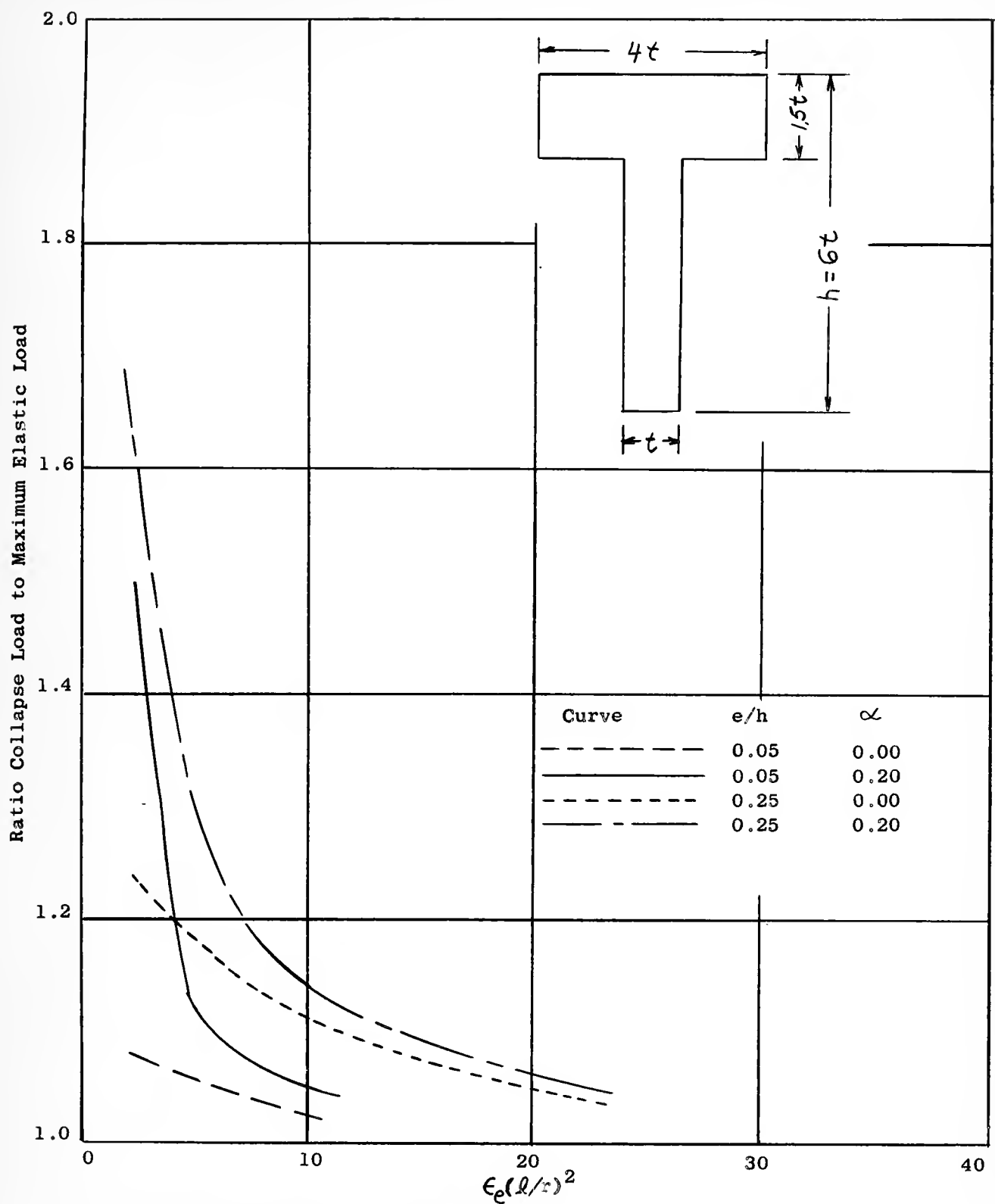


Fig. 10 Ratio of Collapse Load to Maximum Elastic Load for T-Section Eccentrically-Loaded Columns



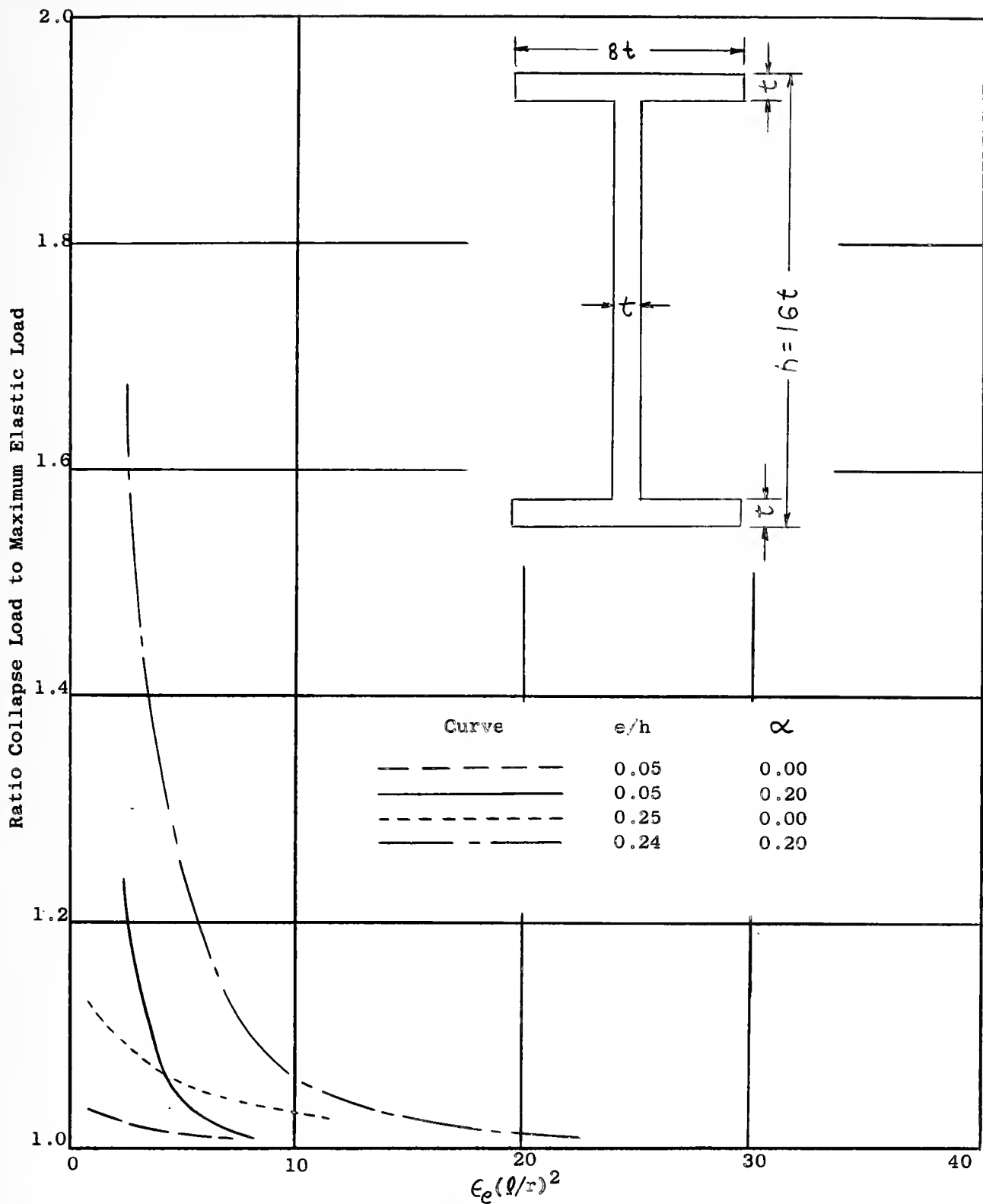


Fig. 11 Ratio of Collapse Load to Maximum Elastic Load for I-Section Eccentrically-Loaded Columns



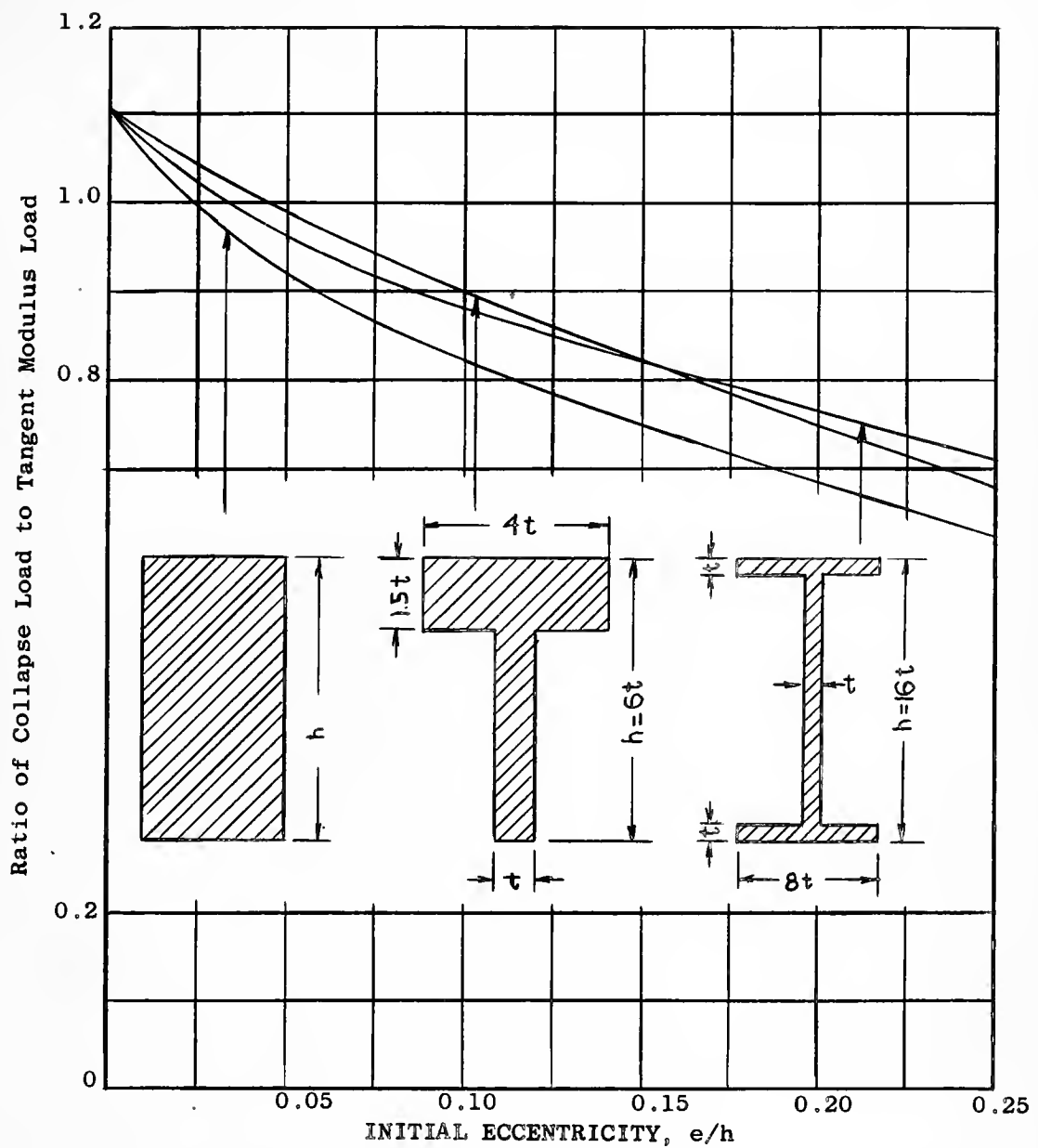


Fig. 12 Ratio of Collapse Load to Tangent Modulus Load for Eccentrically-Loaded Columns Made of a Material that Creeps



WADD TECHNICAL REPORT 60-580  
Part IV

INELASTIC DESIGN OF LOAD CARRYING MEMBERS

Part IV. The Behavior of Beam-Columns in the  
Inelastic Range

B. B. Muvdi  
O. M. Sidebottom

Theoretical and Applied Mechanics Department  
University of Illinois

April, 1961

Materials Central  
Contract No. AF 33 (616)-7600  
Project No. 7351

Wright Air Development Division  
Air Research and Development Command  
United States Air Force  
Wright Patterson Air Force Base, Ohio



WADD TECHNICAL REPORT 60-580  
Part IV

INELASTIC DESIGN OF LOAD CARRYING MEMBERS  
Part IV. The Behavior of Beam-Columns in the  
Inelastic Range

B. B. Muvdi  
O. M. Sidebottom

Theoretical and Applied Mechanics  
University of Illinois

April, 1961

WRIGHT AIR DEVELOPMENT DIVISION



620.1123

IL 59 i

14

copy 2

FOREWORD

This report was prepared by the University of Illinois under USAF Contract No. AF 33(616)-7600. This Contract was initiated under Project No. 7351, "Metallic Materials", Task No. 73521, "Behavior of Metals". It was administered under the direction of the Materials Central, Directorate of Advanced Systems Technology, Wright Air Development Division with Mr. R. F. Klinger acting as the Project Engineer.

This report covers work conducted from October 1, 1960 to Setpember 31, 1961.

The work was conducted in the Department of Theoretical and Applied Mechanics in the Engineering Experiment Station, University of Illinois, Urbana, Illinois. Professor O. M. Sidebottom was the Project Supervisor.



## ABSTRACT

Two theories were presented for constructing either moment-load or load-deflection relations as well as the collapse loads for beam-columns. In each case, trial and error solutions were required which used constant depth of yielding interaction curves. A "so called" exact theory was presented which gave results as accurate as desired; however, the theory was not practical because of the excessive time required. An approximate theory was presented which gave results in close agreement with the exact theory and with experimental data. This theory required the elastic solution for maximum elastic conditions.

The experimental part of the investigation included tests of rectangular - and T-section columns made of 2024-T4 aluminum alloy, SAE 1020 steel, and 17-7PH stainless steel. Several slenderness ratios were considered. In addition to the variable axial load, the columns were subjected to a constant transverse load either at midspan or at quarter span which produced a bending stress of 0.25, 0.50, or 0.75  $\sigma_e$ .

## PUBLICATION REVIEW

This report has been reviewed and is approved.

### FOR THE COMMANDER:

W. J. Trapp  
Chief, Strength and Dynamics Branch  
Metals and Ceramics Laboratory  
Materials Central



## TABLE OF CONTENTS

	Page
I. INTRODUCTION	1
1. Preliminary Statement	1
2. Purpose and Scope	2
II. ANALYSIS	4
1. Interaction Curves	4
2. Elastic Solution for the Beam-Column	7
3. Method of Solution	11
4. Sample Problem	12
III. MATERIALS AND TEST PROCEDURE	15
1. Materials and Specimens	15
2. Apparatus and Test Procedure	16
IV. RESULTS AND DISCUSSION	18
1. Symmetrically Loaded Beam-Columns	18
2. Unsymmetrically Loaded Beam-Columns	20
V. SUMMARY AND CONCLUSIONS	23
VI. BIBLIOGRAPHY	25
VII. APPENDIX A	27



## LIST OF ILLUSTRATIONS

Figure		Page
1	T-Section Member Subjected to Combined Loading. The Sketch Shows the Stress Distribution When the Member is Partly Elastic and Partly Inelastic.	34
2	A Schematic Representation of Stress-Strain Relations in Tension and Compression.	35
3	A Schematic Representation of Interaction Curves for Constant Depth of Yielding .	36
4	A Sketch Showing the Beam-Column Studied in this Program.	37
5	Dimensionless Interaction Curves for Rectangular Sections Made of 2024-T4 Aluminum.	38
6	Dimensionless Interaction Curves for T-Sections Made of 2024-T4 Aluminum .	39
7	Dimensionless Interaction Curves for Rectangular Sections Made of SAE 1020 Steel.	40
8	Dimensionless Interaction Curves for T-Sections Made of SAE 1020 Steel.	41
9	Dimensionless Interaction Curves for Rectangular Sections Made of 17-7PH Stainless Steel.	42
10	Test Apparatus Used to Apply Transverse and Axial Loads to Beam-Columns.	43
11	Knife-Edge Fixtures Used to Apply Axial Load to Beam Columns.	44
12	Comparison of Moment Load Curves for Symmetrically Loaded 2024-T4 and SAE 1020 Steel Beam-Columns Determined by Two Theoretical Methods and by Test.	45
13	Moment-Load Curves for Symmetrically Loaded, Rectangular 2024-T4 Aluminum Beam-Columns. ( $M_Q/M_e = 0.25$ , $e_1 = e_2 = 0$ )	46
14	Moment-Load Curves for Symmetrically Loaded, Rectangular 2024-T4 Aluminum Beam-Columns. ( $M_Q/M_e = 0.50$ ; $e_1 = e_2 = 0$ )	47



## LIST OF ILLUSTRATIONS

Figure		Page
15	Moment-Load Curves for Symmetrically Loaded, Rectangular 2024-T4 Aluminum Beam-Columns. $(M_Q/M_e = 0.25; e_1 = e_2 = 0.15h)$	48
16	Moment-Load Curves for Symmetrically Loaded T-Section Beam Columns of 2024-T4 Aluminum.	49
17	Moment-Load Curves for Symmetrically Loaded, Rectangular SAE 1020 Steel Beam-Columns. $(M_Q/M_e = 0.50; e_1 = e_2 = 0)$	50
18	Moment-Load Curves for Symmetrically Loaded, Rectangular SAE 1020 Steel Beam Columns. $(M_Q/M_e = 0.75; e_1 = e_2 = 0)$	51
19	Moment-Load Curves for Symmetrically Loaded T-Section Beam-Columns of SAE 1020 Steel.	52
20	Moment-Load Curves for Symmetrically Loaded Rectangular 17-7PH Stainless Steel Beam-Columns. $(e_1 = e_2 = 0)$	53
21	Moment-Load Curves for Symmetrically Loaded, Rectangular 17-7PH Stainless Steel Beam-Columns. $(e_1 = e_2 = 0.15h)$	54
22	Moment-Load Curves for Unsymmetrically Loaded, Rectangular 2024-T4 Aluminum Beam-Columns. $(M_Q/M_e = 0.50; e_1 = e_2 = 0)$	55
23	Moment-Load Curve for an Unsymmetric -Loaded T-Section Beam-Column of 2024-T4 Aluminum. $(M_Q/M_e = 0.50; e_1 = e_2 = 0)$	56
24	Moment-Load Curves for Unsymmetrically Loaded, Rectangular SAE 1020 Steel Beam-Columns. $(M_Q/M_e = 0.50; e_1 = e_2 = 0)$	57
25	Moment-Load Curves for Unsymmetrically Loaded, Rectangular SAE 1020 Steel Beam-Columns, with Equal and Unequal End Eccentricities	58
26	Moment-Load Curve for an Unsymmetrically Loaded T-Section Beam-Columns of SAE 1020 Steel. $(M_Q/M_e = 0.75; e_1 = e_2 = 0)$	59
27	Moment-Load Curve for Unsymmetrically Loaded Rectangular 17-7PH Stainless Steel Beam Columns. $(M_Q/M_e = 0.25; e_1 = e_2 = 0)$	60



## I. INTRODUCTION

### 1. Preliminary Statement

In modern design, particularly in the aircraft and missile fields, load carrying members are, in general, used to the limit of their capacity. This stipulation requires that the design of many load carrying members be based on an inelastic analysis. If inelastic action is allowed to penetrate only a small depth into the member, the resulting deformations will not, in general, become excessive and an inelastic analysis can be used in design for either strength or deformation. Small amounts of inelastic action have been found to impart to a member an appreciable increase in the load-carrying capacity above that associated with initiation of yielding (1-3)<sup>1</sup>.

This investigation was undertaken to examine the behavior of a certain class of members known as beam-columns, when subjected to loads higher than those necessary to initiate yielding in the member. The term beam-column is applied to long, slender members which are subjected to transverse as well as axial loads, i. e., members that simultaneously perform the functions of beams and columns.

While the problem of column behavior beyond the elastic range has been examined extensively in recent years (4-15), that of beam-columns has received very little attention. Aside from the well-known solutions for the behavior of beam columns in the elastic range (16), only two-published papers were found that treat the subject of beam-columns in the inelastic range. The first and the oldest of the two papers was published by Osgood (17) in 1947. In his paper, Osgood proposed an approximate method which essentially consisted of replacing the given beam-column by an equivalent eccentrically loaded column. Available methods were then applied to the resulting eccentrically loaded column. Theoretical solutions were presented for several cases, but no test data were given. The second paper was published in 1955 by Ketter (18) who presented a solution based on the principal of virtual displacements. Ketter's method is essentially based on the premise that instability in the beam-column will set in when the rate of increase of the internal resisting moment ( $M_{int}$ ) with respect to the curvature

---

1. Numbers in parentheses refer to corresponding entries in the bibliography.



( $\psi$ ) becomes equal to the rate of increase of externally applied moment ( $M_{ext}$ ) with respect to curvature. Symbolically, this instability condition may be expressed as follows:

$$\frac{\Delta M_{int}}{\Delta \psi} = \frac{\Delta M_{ext}}{\Delta \psi}$$

By assuming ideal plasticity (i. e. non-strain hardening material) and a given configuration for the deflection curve, Ketter determined the combination of axial load and bending moment that would cause instability in members subjected to constant axial load with increasing bending moment. However, all cases considered involved members that were symmetrically loaded.

In the present paper, a new method is proposed that would make it possible to analyse beam-columns made of materials with any strain hardening characteristics. The approach is sufficiently general to consider symmetrically and unsymmetrically loaded members, as well as concentrically and eccentrically applied axial loads. Furthermore, the shape of cross-section of the member does not influence the case with which the solution can be performed.

## 2. Purpose and Scope

The purpose of this investigation was to develop a procedure that would predict the moment-load curve, or the load-deflection curve as well as the collapse load for beam-columns which are subjected to constant transverse loads. While the analysis was applied only to the case of a single concentrated transverse load, it is believed that the theory is equally valid for cases in which the transverse loading is made up of several concentrated loads, distributed loads, or any combination of the two.

Two theories are presented for predicting the load-deflection curves for beam-columns. An exact numerical procedure is outlined in Appendix A. Although this procedure will yield results as accurate as desired, several hours of computations are required for a beam-column that is symmetrically-loaded. The amount of time is increased many folds for an unsymmetrically loaded beam-column. Since the exact theory was found to be impractical, an approximate theory was developed. In this theory the configuration of the inelastic beam-column was based on the elastic configuration of the member when yielding was impending.

The experimental part of the investigation included tests on 46 beam-columns. These tests covered several variables as follows:



(a) Material: Three different materials were investigated, namely, 2024-T4 aluminum alloy, SAE 1020 mild steel and 17-7PH stainless steel.

(b) Cross-section: The two shapes of cross sections that were examined were the rectangular and the T-sections.

(c) Slenderness ratio: In the case of the rectangular section, slenderness ratios of 50, 75, and 100 were used. A slenderness ratio of 60 was used in the case of the T-section.

(d) Position of transverse load: The transverse load was either applied at midspan or at the quarter point of the member.

(e) Magnitude of transverse load: The transverse load was maintained constant throughout a given test. The magnitude of this load was selected so as to produce maximum bending stresses in the member equal to 25, 50, and 75 per cent of the yield strength of the material.

(f) Eccentricity: The axial load was applied either concentrically or with initial eccentricity of 15 per cent of the section depth. Furthermore, equal and unequal eccentricities at the two ends of the beam-column were examined.



## II. ANALYSIS

Two methods will be presented for constructing either moment-load or load-deflection curves for beam-columns. The collapse load is defined as the maximum load obtained from either the moment-load or load-deflection curve. In order to construct these curves, two independent relations between the variables axial load, moment and curvature are developed.

The first axial load-moment-curvature relation is obtained by considering the equilibrium of internal forces and moments, and is represented graphically by dimensionless interaction curves together with a moment-curvature equation. In this investigation, interaction curves for constant depth of yielding are used. The second axial load-moment-curvature relation is established by equating the interval and external moments, and by considering the deformation characteristics of the beam-columns.

Using the interaction curves and a numerical procedure described by Chwalla (6), the configuration of the inelastically deformed member can be derived as accurately as desired. This so-called exact method is described in Appendix A; however, the method is considered impractical because of the time required to obtain a solution for even the simplest problem.

A theory based on certain approximations regarding the configuration of the inelastically deformed beam-column was found to compare favorably with both the exact theory and test results. This approximate theory requires that the elastic solution to the beam-column be known, so that the magnitude of the axial load, maximum moment, deflection and curvature at the critical section<sup>1</sup> can be determined for maximum elastic conditions.

### 1. Interaction Curves

Consider the T-section member shown in Fig. 1 which is subjected to an axial load,  $P$ , at the centroid and to a moment,  $M$ . In order to construct interaction curves for the given T-section, it is necessary to obtain expressions for  $P$  and  $M$  for any given strain distribution. These expressions were previously developed by Sidebottom and Clark (2) using the following assumptions:

---

1. The term "critical section" is used in its ordinary sense to signify the section of the member at which the bending moment has its maximum value.



(a) Plane sections remain plane in both the elastic and inelastic ranges. This assumption has been shown to be reasonably accurate (19).

(b) The stresses and strains in the beam-column are related in the same fashion as they are in simple tension and compression. Experimental evidence exists to justify this assumption (19, 20).

(c) The stress-strain diagram for the material can be approximated by two straight lines intersecting at a value of stress considered to be the yield stress of the material as shown schematically in Fig. 2.

(d) The modulus of elasticity in tension is the same as that in compression.

Let the member shown in Fig. 1 be subjected to a load,  $P$ , and moment,  $M$ , of such magnitude that yielding has penetrated to a depth,  $a_1$ , on the compression side and to a depth,  $a_2$ , on the tension side. The remaining depth,  $a$ , is elastic. The expressions for  $P$  and  $M$  as developed by Sidebottom and Clark (2), are given below without derivation.

$$\text{For } a_1 \leq t_2 : \quad \frac{P}{P_e} = 1 - \frac{2}{a} (c_1 - a_1) \frac{\sigma_e}{\sigma_{e_1}} - \frac{a_1^2 b}{a A} (1 - a_1) \frac{\sigma_e}{\sigma_{e_1}} + \frac{a_2^2 t_1}{a A} (1 - a_2) \frac{\sigma_e}{\sigma_{e_1}} . \quad (1)$$

$$\frac{M}{M_e} = \frac{2c_2}{a} \frac{\sigma_e}{\sigma_{e_2}} - \frac{a_1^2 b c_2}{a I} (1 - a_1) (c_1 - \frac{a_1}{3}) \frac{\sigma_e}{\sigma_{e_2}} - \frac{a_2^2 t_1 c_2}{a I} (1 - a_2) (c_2 - \frac{a_2}{3}) \frac{\sigma_e}{\sigma_{e_2}} . \quad (2)$$

$$\text{For } a_1 \geq t_2 : \quad \frac{P}{P_e} = 1 - \frac{2}{a} (c_1 - a_1) \frac{\sigma_e}{\sigma_{e_1}} + \frac{a_2^2 t_1}{a A} (1 - a_2) \frac{\sigma_e}{\sigma_{e_1}} - \frac{(1 - a_1)}{a A} \left[ b a_1^2 - (b - t_1)(a_1 - t_2)^2 \right] \frac{\sigma_e}{\sigma_{e_1}} . \quad (3)$$



$$\frac{M}{M_e} = \frac{2c_2}{a} \frac{\sigma_e}{\sigma_{e_2}} - \frac{a_2^2 t_1 c_2}{a I} (1 - a_2)(c_2 - \frac{a_2}{3}) \frac{\sigma_e}{\sigma_{e_2}}$$

$$- (1 - a_1) \left[ \frac{2c_2}{a} - \frac{c_2 t_1}{a I} (a + a_2)^2 (c_2 - \frac{a + a_2}{3}) \right] \frac{\sigma_e}{\sigma_{e_2}} . \quad (4)$$

In the above expressions  $P_e$  is the axial load required to initiate yielding when acting alone;  $M_e$  is the moment required to initiate yielding when acting above;  $A$  is the cross-sectional area of the member;  $I$  is the moment of inertia of the section; and  $2\sigma_e = \sigma_{e_1} + \sigma_{e_2}$ . The remaining symbols are as defined in Figs. 1 and 2.

By making the thickness of the web  $t_1$  equal to the width of the flange  $b$ , the above equations become applicable to rectangular sections. In this case, however, only Eqs. 1 and 2 are needed in which  $c_1$  becomes equal to  $c_2$ . Furthermore, since for the materials considered  $\sigma_{e_2}$  was equal to or greater than  $\sigma_{e_1}$ , it is replaced by  $\sigma_{e_1}$  in Eq. 2.

While expressions for the dimensionless quantities  $P/P_e$  and  $M/M_e$  can be obtained separately in terms of the properties of the section and those of the material, there is no simple way of directly relating  $P/P_e$  to  $M/M_e$  analytically. Resort is, therefore, made to a graphical representation of the above relations in the form of dimensionless interaction curves for constant depth of yielding as shown schematically in Fig. 3. The procedure consists of assuming a given depth of inelastic penetration (or a given value for  $a$ ). Then values of  $a_1$  and  $a_2$  are assumed such that their sum is always equal to the depth of plastic penetration. Equations 1 through 4 are then evaluated to compute the values of  $P/P_e$  and  $M/M_e$ . This process is repeated as many times as is necessary to obtain a smooth curve for the specified depth of yielding. The same procedure is used for other depths of inelastic penetration.

A study of Fig. 3 indicates that, with the exception of the straight line defining initiation of yielding (i.e.,  $a = h$ ), all curves consist of two parts, a straight line and a curve. The combinations of  $P/P_e$  and  $M/M_e$  represented by the straight line portion are those necessary to cause yielding on one side of the member only, while the other side is still elastically strained. The point of intersection between the two portions of the interaction curve defines the combination of  $P/P_e$  and  $M/M_e$  that produce the specified depth of yielding on one side of the member and incipient yielding on the other side. The curved portion, however, defines the various combinations of  $P/P_e$  and



$M/M_e$  that would cause inelastic action on both sides such that the total depth of inelastic penetration is equal to the specified depth of yielding.

Once the interaction curves for constant depth of yielding are known (see Fig. 3), they may be used to obtain a relation between axial load, moment, and curvature. It has been shown by Sidebottom and Clark (2) that the curvature of the member for any point on any one of the interaction curves shown in Fig. 3 is given by the relation

$$\psi = \frac{\epsilon_{e_1} + \epsilon_{e_2}}{a} \frac{M/M_e}{M_u/M_e} = \frac{\epsilon_{e_1} + \epsilon_{e_2}}{k h} \frac{M/M_e}{M_u/M_e} \quad (5)$$

where  $\epsilon_{e_1}$  and  $\epsilon_{e_2}$  define the strains corresponding to the compressive and tensile yield stresses, respectively, as shown in Fig. 2. The quantity  $k$  is a proportionality constant which may vary from zero to unity.  $M/M_e$  is the dimensionless moment that exists at the given section of the member and  $M_u/M_e$  is the dimensionless moment at the upper end of the straight line portion of the interaction curve. The ratio  $M/M_u$  assumes a constant value of unity in the curved portion of the interaction curve.

A solution for the beam-column cannot be obtained using only the interaction curves and Eq. 5 since the point on the interaction curve which is valid for a given section of the beam-column is not known. Another relation between axial load, moment, and curvature for the inelastically deformed beam-column will be obtained by considering the equality between internal and external moments as well as the deflection characteristics of the member. The deflection characteristics of the inelastically deformed member are developed from the elastic solution of the given beam-column.

## 2. Elastic Solution for the Beam-Column

For the beam-column shown in Fig. 4, the bending moment at any section a distance  $x$  from the origin is given by the equation

$$M = P \left[ y + e_1 - \frac{x}{l} (e_1 - e_2) \right] + M_Q \quad (a)$$

which applies to sections on either side of the transverse load  $Q$ . The symbols  $e_1$  and  $e_2$  are the eccentricities of the load  $P$  at the left and right ends, respectively,  $y$  is the deflection of the centroidal axis of the member at the point considered,  $l$  is the length of the member and  $M_Q$  is the moment at the section in question due to the transverse load  $Q$  acting alone. Equation a may be written in dimensionless form by dividing both sides by the quantity  $M_e = P_e/\gamma$ , in which  $\gamma$  is a constant that



depends on the properties of the cross-section.<sup>2</sup> Thus

$$\frac{M}{M_e} = \gamma \left( \frac{P}{P_e} \right) \left[ y + e_1 - \frac{x}{l} (e_1 - e_2) \right] + M_Q/M_e. \quad (b)$$

It should be noted that Eqs. a and b are valid for either elastic or inelastic conditions.

The differential equations of the elastic deflection curve for the beam-column shown in Fig. 4 may be expressed as

$$EI \frac{dy^2}{dx^2} = - \left[ \frac{Qd}{l} - \frac{P(e_1 - e_2)}{l} \right] x - P(e_1 + y) \dots \dots$$

$$x \leq (l - d) \quad (c)$$

$$EI \frac{dy^2}{dx^2} = \left[ \frac{Q(l - d)}{l} + \frac{P(e_1 - e_2)}{l} \right] x - P(e_1 + y)$$

$$- Q(l - d) \dots \dots x \geq (l - d) \quad (d)$$

where E is the modulus of elasticity and the remaining symbols are as defined previously. Using the notation  $\beta^2 = P/EI$  and rearranging terms, the above equations may be written as

$$\frac{dy^2}{dx^2} + \beta^2 y = - \frac{1}{EI} \left[ \frac{Qd}{l} - \frac{P(e_1 - e_2)}{l} \right] x - \frac{Pe_1}{EI}$$

$$\dots \dots x \leq (l - d) \quad (e)$$

$$\frac{dy^2}{dx^2} + \beta^2 y = \frac{1}{EI} \left[ \frac{Q(l - d)}{l} + \frac{P(e_1 - e_2)}{l} \right] x - \frac{Pe_1}{EI}$$

$$- \frac{Q(l - d)}{EI} \dots \dots x \geq (l - d). \quad (f)$$

2. In the case of a rectangular section, for example,  $M_e = \frac{\sigma e_1 I}{c_1} = \frac{P_e}{c_1 A/I}$   
 $= \frac{P_e}{6/h}$  so that  $\gamma$  is equal to  $6/h$ .



The general solutions of Eqs. e and f are given by the following equations

$$y = C_1 \cos \beta x + C_2 \sin \beta x - \left[ \frac{Qd}{P\ell} - \frac{(e_1 - e_2)}{\ell} \right] x - e_1 \quad \dots \quad x \leq (\ell - d) \quad (g)$$

$$y = C_3 \cos \beta x + C_4 \sin \beta x + \left[ \frac{Q(\ell - d)}{P\ell} + \frac{(e_1 - e_2)}{\ell} \right] x - e_1 - \frac{Q(\ell - d)}{P} \quad \dots \quad x \geq (\ell - d). \quad (h)$$

From the conditions at the ends of the beam-column (i.e.,  $y = 0$  for  $x = 0$  and  $x = \ell$ ), the constants of integration  $C_1$  and  $C_3$  are found to be

$$C_1 = e_1; \quad C_3 = -C_4 \tan \beta \ell + e_2 / \cos \beta \ell. \quad (i)$$

The constants of integration  $C_2$  and  $C_4$  are determined from the conditions at the point of application of the transverse load  $Q$ . At this point, the two portions of the elastic deflection curve, as defined by Eqs. g and h possess the same values of deflection and slope. From these conditions, the values of  $C_2$  and  $C_4$  are found to be

$$C_2 = \frac{e_2 - e_1 \cos \beta \ell}{\sin \beta \ell} - \frac{Q}{P\beta} \left[ \frac{\sin \beta(\ell - d)}{\tan \beta \ell} - \cos \beta(\ell - d) \right] \quad (j)$$

$$C_4 = \frac{e_2 - e_1 \cos \beta \ell}{\sin \beta \ell} - \frac{Q}{P\beta} \frac{\sin \beta(\ell - d)}{\tan \beta \ell}$$

Substitution of the values of the constants  $C_1 \dots C_4$  into Eqs. g and h, rearranging terms and simplifying leads to the following equations defining the elastic deflection curve of the beam-column shown in Fig. 4,

$$y = e_1 \left[ \frac{\sin \beta(\ell - x)}{\sin \beta \ell} - \frac{\ell - x}{\ell} \right] + e_2 \left( \frac{\sin \beta x}{\sin \beta \ell} - \frac{x}{\ell} \right) + \frac{Q \sin \beta d}{P\beta \sin \beta \ell} \sin \beta x - \frac{Qd}{P\ell} x \quad \dots \quad x \leq (\ell - d) \quad (6a)$$



$$y = e_1 \left[ \frac{\sin \beta(\ell - x)}{\sin \beta \ell} - \frac{\ell - x}{\beta} \right] + e_2 \left( \frac{\sin \beta x}{\sin \beta \ell} - \frac{x}{\ell} \right) \quad (6b)$$

$$+ \frac{Q \sin \beta(\ell - d)}{P \beta \sin \beta \ell} \sin \beta(\ell - x) - \frac{Q(\ell - d)(\ell - x)}{P \ell} \dots x \geq (\ell - d)$$

The elastic curvatures may be obtained by differentiating Eqs. 6 twice, thus

$$\psi = y'' = -e_1 \beta^2 \frac{\sin \beta(\ell - x)}{\sin \beta \ell} - e_2 \beta^2 \frac{\sin \beta x}{\sin \beta \ell}$$

$$- \frac{Q \beta \sin \beta d}{P \sin \beta \ell} \sin \beta x \dots x \leq (\ell - d) \quad (7)$$

$$\psi = y'' = -e_1 \beta^2 \frac{\sin \beta(\ell - x)}{\sin \beta \ell} - e_2 \beta^2 \frac{\sin \beta x}{\sin \beta \ell}$$

$$- \frac{Q \beta \sin \beta(\ell - d)}{P \sin \beta \ell} \sin \beta(\ell - x) \dots x \geq (\ell - d).$$

The bending moment at any section along the span of the member is then given by the equation

$$M = -EI(\psi). \quad (8)$$

For a given member, the deflection,  $y_c$ , and curvature,  $\psi_c$ , at the critical section may be determined for any value of  $P$  from Eqs. 6 and 7, respectively. Examination of the ratio  $\psi_c/y_c$  revealed that, in general, this ratio did not vary greatly as the axial load  $P$  increased from zero to its maximum elastic value. This behavior led to the assumption that the ratio  $\psi_c/y_c$  remains constant as the beam-column is strained inelastically. Essentially, then, a relation between curvature and deflection at the critical section in the inelastic range is assumed to be of the form

$$\psi_c = C y_c \quad (9)$$

where the constant  $C$  is determined as the ratio of curvature to deflection at the critical section when yielding is impending.

Eliminating the deflection,  $y_c$ , between Eqs. 9 and 9, and solving for  $P/P_e$ , the required relation between axial load, moment, and curvature is obtained, namely



$$\frac{P}{P_e} = \frac{\frac{M/M_e - (M_Q/M_{e_c})}{\gamma [\psi_c/C + e_1 - x_c/\ell(e_1 - e_2)]}}{(10)}$$

where the subscript c designates conditions at the critical section.

### 3. Method of Solution

The purpose of this article is to show how the various relations established in the preceding article may be used to determine the moment-load curve or the load-deflection curve as well as the load P that causes complete collapse of a beam-column when it is subjected to a constant value of the transverse load Q.

The value of the axial load P that would initiate yielding in the member may be determined, by trial and error, using Eqs. 7 and 8. The procedure consists of first assuming a value for P and determining the quantity  $\beta = \sqrt{P/EI}$ . The value of  $x_c$  locating the critical section is now determined by maximizing Eq. 7. The maximum moment is then given by Eq. 8 and the maximum stress at the critical section by the equation

$$\sigma_{\max.} = \frac{(M_{\max.})_{c_1}}{I} + \frac{P}{A}. \quad (11)$$

This process is repeated until the stress determined by Eq. 11 becomes equal to the compressive yield stress of the material,  $\sigma_{e_1}$ .

With the value of P that initiates yielding known, the constant C may be easily found from Eq. 9, in which, the values of  $y_c$  and  $\psi_c$  are determined by the use of Eqs. 6 and 7, respectively. Furthermore, this value of P may be used to locate the intersection of the moment-load curve and the interaction curve defining the beginning of yielding ( $k = 1$ ), see point B in Fig. 3.

The solution is then carried into the inelastic range by means of the interaction curves along with Eqs. 5 and 10.

In applying Eq. 10, the assumption is made that the critical section does not move as the member deforms inelastically. This is equivalent to saying that  $x_c$  and  $(M_Q/M_{e_c})$  retain the same values they assumed at initiation of yielding. With members which are symmetrically loaded (i.e.,  $d = \ell/2$  and  $e_1 = e_2$ ),  $x_c$  does retain the same value, namely  $\ell/2$ , in the inelastic as well as in the elastic range. However, with members which are not symmetrically loaded (i.e.,  $d \neq \ell/2$  and/or  $e_1 \neq e_2$ ),  $x_c$  does not, in general, retain the same value throughout the loading process. Test data indicated that the above assumption did not introduce a serious error into the theory.



Now consider the problem of determining the value of  $P/P_e$  that would produce a given depth of inelastic penetration (i.e.,  $k = k_1 = \text{const}$ ), see Fig. 3. The condition that has to be satisfied is that  $M/M_e$  be of such magnitude that the value of  $P/P_e$  given by Eq. 10 be equal to that given by the relation  $P/P_e = f(M/M_e)$  as expressed by the interaction curves. To this end some value of  $M/M_e$  is assumed and the curvature  $\psi_c$  is determined by Eq. 5. Equation 10 is then used to obtain a value of  $P/P_e$  which is compared to that given by the interaction curve corresponding to  $k = k_1$ . This process is repeated until the two values of  $P/P_e$  are the same or very nearly so. This usually requires not more than three trials. Thus the problem is reduced to the solution of two simultaneous equations in the unknowns  $M/M_e$  and  $P/P_e$ . The deflection  $y_c$ , if needed, may now be obtained from Eq. 9.

Once the correct value of  $P/P_e$  is established for  $k = k_1$ , a point is located on the appropriate interaction curve. Other values of  $k$  are then considered and the same process repeated to establish a set of points such as C, D, E, F, and G in the inelastic domain, see Fig. 3. The location of point A on the  $M/M_e$  axis is dictated by the value of the transverse load  $Q$ . A smooth curve is then constructed through the points A, B, . . . , G to give the moment-load curve. The collapse load for the beam-column may be obtained from the moment load curve and in dimensionless form, is the maximum value of  $P/P_e$ .

If additional points are needed in the elastic range (i.e., between points A and B in Fig. 3) they may be easily determined from the elastic solution, using Eq. 6 and the equilibrium condition expressed by Eq. b.

#### 4. Sample Problem

In this article, a sample problem is solved to illustrate the method used in deriving the moment-load curve for a given beam-column.

(a) Given Data For a Rectangular SAE 1020 Steel Beam-Column:

$$A = b \times h = 0.500 \times 0.625 = 0.3125 \text{ in}^2; I = 0.01017 \text{ in}^4; l = 13.52 \text{ in} (\ell/r = 75)$$

$$M_Q = 0.5 M_e; d = 0.25 \ell; e_1 = 0.15h = 0.09375 \text{ in}$$

$$e_2 = 0; \sigma_{e_1} = \sigma_{e_2} = 30,300 \text{ psi}; P_e = 9470 \text{ lb.}$$

$$\epsilon_{e_1} = \epsilon_{e_2} = 10.1 \times 10^{-4} \text{ in/in.}$$

(b) Problem: To determine the moment-load curve for the beam-column specified above.



$$(c) \quad \text{Solution:} \\ M_Q = \frac{3}{16} Q \ell = 0.5 M_e = 0.5 \frac{\sigma_e I}{c_1}$$

$$Q = \frac{8 I \sigma_e}{3 \ell c_1} = 194.49 \text{ lb.}$$

From the given conditions it is evident that the critical section occurs either under the load  $Q$  or slightly to the left of this position. Maximizing Eq. 7 for  $x \leq (\ell - d)$  leads to the condition that the location of the critical section is defined by the equation

$$\tan \beta x_c = \frac{Q \sin \beta d - e_1 \beta P \cos \beta \ell + e_2 \beta P}{e_1 \beta P \sin \beta \ell} . \quad (k)$$

Since in this problem  $e_2 = 0$ , Eq. k becomes

$$\tan \beta x_c = \frac{Q \sin \beta d - e_1 \beta P \cos \beta \ell}{e_1 \beta P \sin \beta \ell} . \quad (l)$$

By Eqs. 7 and 8 and using the condition  $e_2 = 0$ , the maximum moment,  $M_{\max}$ , is given by the equation

$$M_{\max} = \frac{EI e_1 \beta^2}{\sin \beta \ell} \sin \beta(\ell - x_c) + \frac{EI Q \beta \sin \beta d}{P \sin \beta \ell} \sin \beta x_c \quad (m)$$

The maximum stress,  $\sigma_{\max}$ , will then be given by Eq. 11.

The computations for the axial load that would initiate yielding are given in the following table.

Trial	P - lb	$\beta - 1/\text{in}$	$x_c - \text{in.}$	$M_{\max} - \text{lb-in.}$	$\sigma_{\max} - \text{psi}$
1	3000	0.0992	10.14	654.12	29,700
2	3200	0.1024	10.14	668.03	30,770
3	3100	0.1008	10.14	661.17	30,240
4	3110	0.1010	10.14	661.93	30,290



Thus, to initiate yielding  $P/P_e = 3110/9470 = 0.328$ .

By Eq. 8 for  $x \leq (\ell - d)$ ,  $y_c = 0.0308$  in, for  $P = 3110$  lb.

By Eq. 9 for  $x \leq (\ell - d)$ ,  $\psi_c = 21.69 \times 10^{-4}$  1/in, for  $P = 3110$  lb.

$$C = \psi_c/y_c = 0.0704 \text{ 1/in}^2$$

$$\gamma = 6/h = 9.6 \text{ 1/in}$$

$$\text{At } x_c = 10.14 = \frac{10.14}{13.52} \ell = 0.75 \ell, \quad (M_Q/M_e)_c = 0.50$$

Therefore, the equations that apply in the inelastic range are

$$\psi_c = \frac{32.32 \times 10^{-4}}{k} \cdot \frac{M/M_e}{M_u/M_e}, \quad (5)$$

$$P/P_e = \frac{M/M_e - 0.50}{9.6(14.2\psi_c + 0.0234)}. \quad (10)$$

and the functional relation  $P/P_e = f(M/M_e)$  as expressed by the interaction curves shown in Fig. 7.

A sample calculation is shown for  $k = 0.7$  in the following table.

Trial	$M/M_e$ (Assumed)	$\psi_c$ Eq. 5	$P/P_e$ Eq. 10	$P/P_e$ Fig. 7	$y_c$ Eq. 9
1	0.830	$34.21 \times 10^{-4}$	0.478	0.480	
2	0.832	$34.30 \times 10^{-4}$	0.480	0.478	
3	0.831	$34.25 \times 10^{-4}$	0.479	0.479	0.0487

Thus to produce 0.3 depth of inelastic penetration ( $k = 0.7$ ),  $P/P_e = 0.479$ , which locates a point on the moment-load curve. Other points, corresponding to other values of  $k$  may be similarly located.



### III. MATERIALS AND TEST PROCEDURE

#### I. Materials and Specimens

In order to examine the validity of the analysis discussed in Section II, tests were performed on beam-columns made of three materials, namely 2024-T4 aluminum alloy, SAE 1020 steel and 17-7PH stainless steel. The 2024-T4 aluminum samples were tested in the as-received condition. The SAE 1020 steel was annealed, prior to machining, by soaking at  $1600^{\circ}$  F for 3 hours and furnace cooling. The 17-7PH stainless specimens were precipitation hardened<sup>1</sup> after machining. The SAE 1020 steel samples were machined from a 3 1/2 in. diameter bar, while the 2024-T4 aluminum and the 17-7PH stainless steel specimens were machined from 1/2 in. plates. The various beam-columns tested in this program with their physical characteristics are shown in Table I. Either one or two beam-columns per condition were tested in this study.

Standard tensile and compressive tests were performed on the aluminum alloy to determine the various properties needed for the analysis. However, only compressive tests were performed on the mild and stainless steels. Results of previous tests by Sidebottom and associates (21) on the last two materials have indicated that the difference between tensile and compressive properties was negligible for all practical purposes. The various properties used in the present analysis are shown, for the three materials, in Table II. These values represent an average of at least six tests.

Using the various properties indicated in Table II, and Eqs. 1 through 4, interaction curves for the three materials and the two types of cross-section were developed. These interaction curves are shown in Figs. 5 to 9. Figures 5 and 6 represent the 2024-T4 aluminum interaction curves for rectangular and T-sections, respectively. Figures 7 and 8 show the SAE 1020 steel interaction curves for rectangular and T-sections, respectively. And Fig. 9 illustrates the interaction curves for rectangular sections made of 17-7PH stainless steel. In all instances, k decreased in increments of one tenth to a minimum value of 0.4.

---

1. This heat treatment consisted of soaking at  $1400^{\circ}$  F for 90 minutes, cooling to  $60^{\circ}$  F in 60 minutes, soaking at  $60^{\circ}$  F for 30 minutes, soaking at  $1050^{\circ}$  F for 90 minutes and finally air cooling.



## 2. Apparatus and Test Procedure

The testing apparatus used in this program is shown in the photograph of Fig. 10. A Riehle testing machine having a capacity of 120,000 lb. was used to apply the axial load through fixtures<sup>2</sup> provided with knife edges as illustrated in Fig. 11. The position of the knife edges may be adjusted with respect to the centroid of the specimen by means of set screws. The transverse load was applied by means of dead weights through the pulley system shown in the photograph of Fig. 10. The deflection of the specimen was measured by means of a 1/1000 in. dial indicator which may also be seen in the photograph as well as in Fig. 11.

The specimen was properly placed in the test apparatus and a small value of axial load was applied to maintain the specimen in the proper position. The pulley system was then raised or lowered so as to apply the transverse load at the desired position along the span of the beam-column. The dial indicator was subsequently placed in positon and the desired transverse load applied. This transverse load was maintained at a constant value throughout the test.

The axial load was subsequently increased and readings of this load and the corresponding deflection were taken at predetermined intervals of load until the predicted value of the collapse load was approached. Beyond this point, judgment was exercised in spacing the readings at reasonable intervals of deflection. Sufficient readings were taken to make it possible to construct the moment-load curve well beyond the collapse load.

Once the member was loaded beyond the elastic limit, sufficient time was allowed for equilibrium conditions to be reached (i.e., for the axial load to reach a steady value). In the case of the aluminum and the stainless steel samples, a period of approximately two minutes was sufficient for the axial load to stabilize. In the case of the mild steel specimens, due to the presence of an upper yield point, appreciably more time was required for steady state conditions to be reached. In most instances, up to 20 minutes elapsed before a reading could be taken.<sup>3</sup> It was discovered, however, that this delay time could be shortened, without appreciably

- 
2. A complete description of these fixtures may be found in a paper by Sidebottom et al (22). The two end fixtures added a total of 1.20 in. to the machined length of the specimen.
  3. This time-sensitivity of mild steels was investigated previously by Clark, Corten, and Sidebottom (20).



influencing the load-carrying capacity, by prick punching one row of shallow indentations along the span of the member. These indentations were spaced approximately one-half inch apart. In a few instances, two tests were performed for the same conditions, one with and one without indentations. The results indicated the difference between the load-carrying capacities of the two specimens to be insignificant.



#### IV. RESULTS AND DISCUSSION

In this section, a comparison is made between the results of the proposed approximate theory, and those of the experiments. The comparison is made on the basis of moment-load curves (i.e.,  $M/M_e$  vs.  $P/P_e$ ). This method of presentation was selected over the more conventional load-deflection plots because it conveniently indicates the value of  $M_Q/M_e$  to which the beam-column was initially subjected before the axial load was applied. The various tests that were performed in this program may be conveniently classified into two types as follows:

##### 1. Symmetrically Loaded Beam-Columns

This class of members include those subjected to end loads with zero or equal eccentricities and to a transverse load at midspan. They are characterized by the fact that the maximum moment is located at midspan and possess symmetrical deflection curves throughout the loading process.

In order to examine the degree of accuracy attainable by the approximate method, a comparison was made between moment-load curves obtained by this method and those developed by the so-called exact method (see Appendix A). In view of the fact that the latter method involves rather lengthy computations, particularly with unsymmetrically loaded members as indicated in Appendix A, the comparison was limited to two cases only, namely one 2024-T4 aluminum member and one SAE 1020 steel member. Both members were symmetrically loaded with zero end eccentricities, had a slenderness ratio of 75 and were subjected to transverse loads at midspan such that  $M_Q/M_e$  was equal to 0.50. The results of both methods are illustrated in Fig. 12 together with the values exhibited by test. In the case of 2024-T4 aluminum, the two theoretical moment-load curves were nearly identical and were found to compare very well with the test values. In the case of SAE 1020 steel, however, a slight difference of about 5 per cent is observed between the collapse loads as predicted by the two methods. While this difference was in favor of the exact method, it is too small to justify the added labor required by this method. Furthermore, the approximate theory was conservative.

The actual moment-load curves for symmetrically loaded members are presented in Figs. 13 to 21 in comparison to curves developed by the approximate method. Figures 13 to 16 illustrate the moment-load curves for members made of 2024-T4 aluminum alloy; Figs. 17 to 19 show the moment-load curves for members made of SAE 1020 steel; and Figs. 20 and 21 indicate the moment-load curves for members made of



17-7PH stainless steel. In the case of the 2024-T4 aluminum and SAE 1020 steel, both rectangular and T-sections were examined. Furthermore, four different slenderness ratios ranging between 50 and 100 were investigated. In addition, for each of these two materials, two different values of  $M_Q/M_e$  were analyzed, namely 0.25 and 0.50 for 2024-T4 aluminum, and 0.50 and 0.75 for SAE 1020 steel. In the case of 17-7PH stainless steel, however, testing was limited to members with rectangular-sections, having slenderness ratios of 50 and 75, and subjected to values of  $M_Q/M_e$  equal to 0.25 and 0.50.

Examination of Figs. 13 to 21 leads to several interesting conclusions. It is observed that, in all instances, the predicted curves compare very well with the test data. In general, the discrepancy between the predicted collapse load and that exhibited by test is less than about 7 per cent, as shown in Table III by the ratio of actual collapse load,  $P_{ca}$ , to theoretical collapse load  $P_{ct}$ . This discrepancy is not excessive when considered with respect to the scatter that is normally encountered in materials testing.

In general, when the beam column is symmetrically loaded, the theory always predicts values of collapse load which are either equal to, or slightly lower than those exhibited by test. In other words, the theory tends to predict values which are conservative, as may be seen from Table III by the ratio  $P_{ca}/P_{ct}$ .

It is also observed that, in every instance, there is a considerable increase in the load carrying-capacity above that associated with the beginning of yielding. This increase in the load carrying capacity is represented in Table III by the ratio of actual collapse load,  $P_{ca}$ , to the actual load that initiates yielding,  $P_{ya}$ . Evidently, the increase in the load carrying-capacity (i.e.,  $P_{ca}/P_{ya} - 1$ ) depends upon several factors which include, among other things, the slenderness ratio, magnitude of the transverse load, end eccentricities, material and type of cross-section. While the tests that were performed are insufficient to evaluate the influence of all pertinent factors, it is possible to determine qualitative trends regarding the effects of the slenderness ratio, magnitude of transverse load, material and end eccentricities on the ratio  $P_{ca}/P_{ya}$ .

Examination of Table III indicates that for a given material and for zero eccentricities the ratio  $P_{ca}/P_{ya}$  increases with increase in the magnitude of the transverse load (i.e., with increase in the ratio  $M_Q/M_e$ ), and with decrease in the slenderness ratio. Furthermore, a comparison of the data corresponding to  $M_Q/M_e = 0.50$  and zero end eccentricities indicates that  $P_{ca}/P_{ya}$  is slightly, but consistently, higher



for SAE 1020 steel than for 2024-T4 aluminum. In addition, based on the two tests that were performed on 17-7PH stainless steel with zero end eccentricities, the ratio  $P_{ca}/P_{ya}$  for this material was found to be considerably less than that for the aluminum and mild steel alloys. These trends lead to the conclusion that one of the factors influencing the ratio  $P_{ca}/P_{ya}$  is the strain at yielding, namely  $\epsilon_e$ . Apparently, the larger the value of  $\epsilon_e$  the less is the ratio  $P_{ca}/P_{ya}$  for a given slenderness ratio.

The influence of end eccentricities on the increase in the load-carrying capacity may also be seen from Table III. A comparison of the values corresponding to  $M_Q/M_e$  in the case of 2024-T4 aluminum, indicates that  $P_{ca}/P_{ya}$  attain higher values for members provided with end eccentricities than for members subjected to concentric axial loads.

## 2. Unsymmetrically Loaded Beam-Columns

This type of members include those subjected to unequal end eccentricities and/or to a transverse load not at midspan. They are characterized by the fact that the maximum moment may not occur at the same section of the member throughout the loading process, and the deflection curve is, therefore, unsymmetrical.

The actual moment-load curves for beam-columns of the type described above are presented in Figs. 22 to 27 in comparison to theoretical curves. Figures 22 and 23 illustrate the moment-load curves for members made of 2024-T4 aluminum; Figs. 24 to 26 show the moment-load curves for members made of SAE 1020 steel; and Fig. 27 indicates the moment-load curve for a member made of 17-7PH stainless steel. In the case of 2024-T4 aluminum and SAE 1020 steel, testing was performed to include both rectangular and T-sections, four different values of slenderness ratio ranging between 50 and 100, and two different values of the ratio  $M_Q/M_e$ , namely 0.50 and 0.75. In the case of 17-7PH stainless steel, only one test was performed on a member of rectangular cross-section having a slenderness ratio of 75 and subjected to a transverse load such that  $M_Q/M_e$  was equal to 0.25.

In this series of tests, as in the previous series, very good agreement is observed between the predicted and the actual test values. The discrepancy between the theoretical collapse load and that given by test, was found not to exceed about 5 per cent, as shown in Table IV by the ratio  $P_{ca}/P_{ct}$ .

However, in this series, unlike the previous series, the tests did not consistently yield values of collapse load which were either equal to, or slightly higher than that predicted by theory. This lack of consistency may be seen in Table IV as the ratio



$P_{ca}/P_{ct}$  varied from a minimum of 0.95 to a maximum of 1.05 depending upon the material, slenderness ratio and loading conditions. This inconsistency in the observed trends may be explained as follows:

At the beginning of loading (i. e., when only the transverse load,  $Q$ , is acting and the axial load,  $P$ , is zero or very nearly so), the maximum moment occurs at the point of application of the transverse load. When the axial load  $P$  reaches a certain value that depends upon the material, the slenderness ratio and the cross-sectional area, the position of the maximum moment (critical section) begins to move away from the point of application of the transverse load,  $Q^1$ . The axial load,  $P$ , at which movement of the critical section begins, may occur either within the elastic or within the inelastic range of the material depending upon the conditions stated previously. The conditions investigated in this program were such that movement of the critical section was always from the point of application of the transverse load  $Q$  towards midspan. In the elastic range, the influence of the migration of the critical section can be easily included in the analyses. However, there is no simple method known by means of which the position of the critical section may be determined at any stage of inelastic action. This difficulty was circumvented in the present analyses by making the assumption that the critical section, during inelastic deformation, retains the same position it assumed at initiation of yielding, as explained previously. Obviously, this assumption cannot be expected to be equally approached by members made of different materials, possessing different physical characteristics and subjected to different loading conditions; hence, the lack of a consistent trend observed in the actual behavior of members when compared to theoretical predictions. However, this lack of consistency does not appear to be detrimental, since for all cases examined in this program, the theory predicted values of collapse load which were in close agreement with those exhibited by test.

As in the previous series of tests, an appreciable increase was observed in the load-carrying capacity beyond that corresponding to initiation of yielding. This increase may be seen in Table IV by the ratio  $P_{ca}/P_{ya}$ . Unfortunately, not all the parameters that may influence the increase in the load-carrying capacity can be examined on the basis of the few tests that were performed. However, the remarks made

---

1. The dependence of the position of the critical section on the axial load,  $P$ , in the elastic range may be seen from Eq. k.



previously with regards to the influence of slenderness ratio, material and end eccentricities on the ratio  $P_{ca}/P_{ya}$  apply equally well in the case of unsymmetrically loaded beam-columns.



## V. SUMMARY AND CONCLUSIONS

In order to examine the inelastic behavior of beam-columns, two theories were developed. An exact numerical procedure as outlined in Appendix A, would yield results as accurate as desired. However, in view of the fact that this method may become rather lengthy and sometimes prohibitive, an approximate, but relatively simple method was developed. Essentially, the approximate method requires a trial-and-error solution of two independent relations between the variables axial load, moment and curvature. The first of the two  $P$ - $M$ - $\psi$  relations is established from considerations of the equilibrium of internal forces and moments, and is represented graphically by dimensionless interaction curves along with a moment-curvature equation. The second  $P$ - $M$ - $\psi$  relation is developed by considering the equality between the internal and external moments, as well as the deflection characteristics of the member. The proposed method makes it possible to determine the magnitude of the axial load (concentric or eccentric) at any stage of inelastic deformation including that at which collapse takes place, for a beam-column which is initially subjected to a constant transverse load.

To examine the validity of the various assumptions made in developing the approximate theory, tests were performed on members made of three different materials, namely 2024-T4 aluminum, SAE 1020 steel and 17-7PH stainless steel. Several parameters were investigated within each material. These included the type of cross section, slenderness ratio, position and magnitude of transverse load, and eccentricity of the axial load. Dimensionless moment-load curves were constructed from the test data and compared to those obtained analytically. Furthermore, in two instances, a comparison was made between the approximate method and the so-called exact method. The various results lead to a number of significant conclusions which may be summarized as follows:

1. The results obtained by the proposed approximate method compared well with those obtained by the exact method. The differences observed between the results of the two methods are too small to justify the added labor required by the exact method.
2. Very good agreement was observed, in all instances, between the moment-load curves predicted by the approximate method and those obtained by test, particularly up to the collapse load. While close agreement was generally encountered beyond the collapse load, there were a few instances in which the discrepancy between the predicted and actual curves became pronounced.



3. The difference between the predicted and actual values of collapse loads was, in general, much less than 7 per cent. Thus the proposed approximate method was found to be sufficiently adequate for all practical purposes.

4. In general, inelastic action was found to induce a considerable increase in the load-carrying capacity beyond that associated with initiation of yielding. The increase in the load-carrying capacity was observed to range from a maximum of 159 per cent for SAE 1020 steel, to a minimum of about 2 per cent for 17-7PH stainless steel.

5. The increase in the load-carrying capacity was found to vary directly with  $M_Q/M_e$ , and inversely with  $\ell/r$  and  $\epsilon_e$ .

6. Members with end eccentricities of 15 per cent of the section depth attained a much higher increase in load-carrying capacity than members with zero end eccentricities.



## VI. BIBLIOGRAPHY

1. Seely, F. B., and Smith, J. O., Advanced Mechanics of Materials, John Wiley and Sons, Inc., New York, 1952, pp. 511-581.
2. Sidebottom, O. M., and Clark, M. E., "The Effects of Inelastic Action on the Resistance to Various Types of Loads of Ductile Members Made From Various Classes of Metals," WADC Technical Report 56-330, Pt. I, 1956.
3. Sidebottom, O. M., and Clark, M. E., "Theoretical and Experimental Analysis of Members Loaded Eccentrically and Inelastically," University of Illinois Engineering Experiment Station, Bulletin No. 447, 1958.
4. Von Kármán, T., "Untersuchungen über Knickfestigkeit," Mitt. über Forschungsarbeiten des V. D. I., H. 81, Berlin, 1910.
5. Chwalla, E., "Die Stabilität zentrisch und exzentrisch gedrückter Stäbe aus Baustahl," Akad. d. Wissenschaften in Wien, math.-naturwiss. Klasse, Sitzungsberichte Abt. II a, Bd. 137, 1928, pp. 469-512.
6. Chwalla, E., "Theorie des aussermittig gedrückten Stabes aus Baustahl," Der Stahlbau, Vol. 7, 1934, pp. 161-165, 173-176, 180-184.
7. Osgood, W. R., "The Double-Modulus Theory of Column Action," Civil Eng., Vol. 5, No. 3, Mar. 1935, pp. 173-175.
8. Shanley, F. R., "Inelastic Column Theory," Jour. of Aero. Sci., Vol. 14, No. 5, May 1947, pp. 261-267.
9. Wang, C. T., "Inelastic Column Theories and an Analysis of Experimental Observations," Jour. of Aero. Sci., Vol. 15, No. 5, May 1948, pp. 283-292.
10. Cicala, P., "Column Buckling in the Elastoplastic Range," Jour. of Aero. Sci., Vol. 17, No. 8, Aug. 1950, pp. 508-512.
11. Jordan, W. D., "Inelastic Behavior of Eccentrically Loaded Columns," Doctor's Thesis, Dept. of Theo. and Appl. Mech., University of Illinois, 1952.
12. Bijlaard, P. P., "Buckling of Columns with Equal and Unequal End Eccentricities and Equal and Unequal Rotational End Strains," Proc. 2nd U.S. National Congress Appl. Mech., 1954, pp. 555-562.
13. Galambos, T. V., and Ketter, R. L., "Columns Under Combined Bending and Thrust," Proc. ASCE, Vol. 85, EM-2, 1959, p. 1990.
14. Costello, G. A., "The Creep Buckling of Columns Made of Canvas Laminate," Doctor's Thesis, Dept. of Theo. and Appl. Mech., University of Illinois, 1959.
15. Sidebottom, O. M., Pocs, E., and Costello, G. A., "The Effect of End Conditions on the Collapse Loads of Columns," Dept. of Theo. and Appl. Mech. Report No. 585, University of Illinois, 1960.



16. Timoshenko, S., Theory of Elastic Stability, McGraw-Hill Book Co., New York, 1936, pp. 1-63.
17. Osgood, W. R., "Beam-Columns," Jour. of Aero. Sci., Vol. 14, No. 3, Mar. 1947, pp 167-170.
18. Ketter, R. C., "Stability of Beam-Columns Above the Elastic Limit," Proc. ASCE, Vol. 81, No. 692, Oct. 1955.
19. Clark, M. E., Corten, H. T., and Sidebottom, O. M., "Inelastic Behavior of Ductile Members Under Dead Loading," University of Illinois Engineering Experiment Station, Bulletin No. 426, 1954.
20. Morkovin, D., and Sidebottom, O. M., "The Effect of Non-uniform Distribution of Stress on the Yield Strength of Steel," University of Illinois Engineering Experiment Station, Bulletin No. 372, 1947.
21. Sidebottom, O. M., Dharmarajan, S., Gubser, J. L., and Leasure, J. D., "The Effects of Inelastic Action on the Resistance to Various Types of Loads of Ductile Members Made From Various Classes of Metals," WADC Technical Report 56-330, Pt. XII, 1959.
22. Sidebottom, O. M., Clark, M. E., and Dharmarajan, S., "The Effects of Inelastic Action on the Resistance to Various Types of Loads of Ductile Members Made From Various Classes of Metals," WADC Technical Report 56-330, Pt. VIII, 1958.



## VII. APPENDIX A

In this appendix, a brief outline is given of another method of approach to the problem of beam-columns. This method is capable of yielding extremely accurate results, and is referred to here as the "exact method". Essentially, the exact method differs from the approximate method described in this paper only in the way of relating curvature to deflection in the inelastic range. For simplicity in presenting this approach, a symmetrically loaded beam-column with zero end eccentricities will be considered, as shown in Fig. 1A.

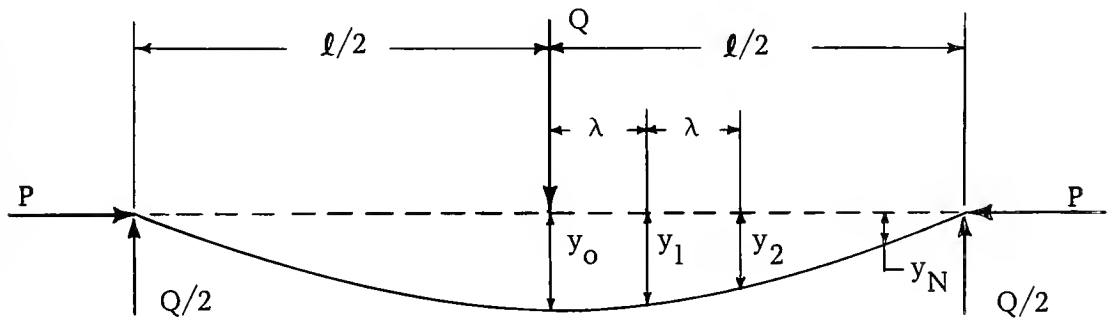


Fig. 1A

The method of relating curvature to deflection in the inelastic range is similar in principle to that used by Chwalla (6) in his solutions of column problems. It consists of subdividing the member into a number of equal segments,  $\lambda$ , as shown in Fig. 1A. The assumption is then made that within each segment, the curvature remains constant (i.e., within each segment, the deflection curve is a circular arc). The deflection at any section of the member may then be found by the relation



$$y_N = y_o - \frac{\lambda^2}{2} \psi_{N-1} - \frac{3\lambda^2}{2} \psi_{N-2} - \dots$$

$$- \frac{(2N-1)\lambda^2}{2} \psi_o, \quad N = 1, 2, 3 \text{ etc.} \dots \quad (1A)$$

where  $\psi_N$  designates the curvature at the Nth section along the member, and  $y_o$  is the deflection at midspan.

For the beam-column shown in Fig. 1A, Eq. b becomes

$$\frac{M}{M_e} = \gamma(\frac{P}{P_e}) y + \mu (\frac{M_Q}{M_e}) \dots \quad (b)$$

where  $\mu$  is a factor varying linearly from unity at the center section to zero at the end of the member. Eqs. 1A and b thus provide one P-M- $\psi$  relation. The second P-M- $\psi$  relation is obtained using Eq. 5 and interaction curves of the type shown in Fig. 3.

The solution of the problem is effected by means of the above relations in the following manner.

As in the previous solution, point A (see Fig. 3) is determined by the magnitude of the transverse load  $Q$ , and point B is determined from the elastic solution. For a given depth of inelastic penetration ( $k = k_1$ ), some value of  $P/P_e$  is assumed and the corresponding value of  $M/M_e$  determined from the appropriate interaction curve. With  $\mu = 1$ , the value of  $y_o$  is then determined from Eq. b. Equation 5 is now used to determine the curvature,  $\psi_o$ , at the center of the member. The deflection  $y_1$  may now be determined by Eq. 1A. Using the value of  $y_o$  and the appropriate value for  $\mu$  in Eq. b, the dimensionless moment,  $M/M_e$ , corresponding to the section of the member at  $y_1$  may be established.<sup>1</sup> Then the curvature  $\psi_1$  is found by Eq. 5. The values of  $M_u/M_e$  and  $k$  for use in Eq. 5 are found from the interaction curves by interpolation. This process is continued until the deflection at the end of the member is determined. The assumed value of  $P/P_e$  is correct if the computed value of deflection at the end of the beam-column is zero or very nearly so. Thus to determine one point on the moment-load curve, this numerical procedure may have to be repeated three or four times until the boundary condition is satisfied.

1. In determining the value of  $M/M_e$  from Eq. b for any given section, the procedure consisted of adding the maximum value due to  $P$ , to the average value due to  $Q$ . Thus for example,  $(M/M_e)_1 = \gamma(P/P_e)y_o + 1/2 [(M_Q/M_e)_o + (M_Q/M_e)_1]$



Theoretically, very accurate results may be obtained by this method of solution if the segments,  $\lambda$ , are made extremely small. This, however, would entail very lengthy if not prohibitive computational work, particularly if conditions other than those shown in Fig. 1A are to be met. For example, when the transverse load  $Q$  is not applied at midspan, one more unknown is introduced into the problem, namely the slope of the deflection curve at the point of application of  $Q$ . Therefore, in applying the method outlined above, it becomes necessary to assume a value for this slope in addition to the value of  $P/P_e$ . The procedure is then applied to both portions of the beam-column until the conditions at both ends of the member are satisfied (i.e., until the determined values of deflection are zero at both ends of the member). Obviously, this method can become very laborious even when the number of segments considered is small. It would appear that this method, compared to the approximate solution presented previously, can become economically feasible only if a technique is developed to program the calculations on a computing machine.



Table I. Materials and Physical Characteristics of Specimens Tested in this Program  
 $\ell/r$  = Slenderness Ratio

Material	Rectangular Sections			T-Sections
	$\ell/r = 50$	$\ell/r = 75$	$\ell/r = 100$	$\ell/r = 60$
2024-T 4 Aluminum Alloy	b = 0.500 h = 0.625	b = 0.500 h = 0.625	b = 0.500 h = 0.500	$t_1 = 0.100$
SAE 1020 Steel	b = 0.500 h = 0.625	b = 0.500 h = 0.625	b = 0.500 h = 0.500	$t_1 = 0.100$
17-7PH Stainless Steel	b = 0.350 b = 0.500	b = 0.400 h = 0.420		



Table II. Properties of the Three Materials Used in this Investigation.

Material	$E$ psi $\times 10^6$	$\sigma_{e_1}$ psi $\times 10^6$	$\sigma_{e_2}$ psi $\times 10^6$	$\epsilon_{e_1}$ in/in $\times 10^{-4}$	$\epsilon_{e_2}$ in/in $\times 10^{-4}$	$a_1$	$a_2$
2024-T4 Aluminum Alloy	10.8	37.5	51.5	34.7	47.7	0.189	0
SAE 1020 Steel	30.0	30.3	30.3	10.1	10.1	0	0
17-7PH Stainless Steel	28.0	170.0	170.0	60.7	60.7	0.111	0.111



Table III. Values of  $P_{ca}$ ,  $P_{ca}/P_{ct}$  and  $P_{ca}/P_{ya}$  for the Various Symmetrically Loaded Beam-Columns Studied in this Program.  $P_{ca}$  = Actual Collapse Load;  $P_{ct}$  = Theoretical Collapse Load; and  $P_{ya}$  = Actual Yield Load.

Material	Shape	$\ell/r$	$M_Q/M_e$	$e_1$	$e_2$	$P_{ca}$ lb.	$P_{ca}/P_{ct}$	$P_{ca}/P_{ya}$
2024-T 4 Aluminum Alloy	Rect.	100	0.25	0	0	2,130	1.04	1.05
		75	0.25	0	0	4,240	1.00	1.09
		50	0.25	0	0	7,750 7,620	1.03 1.01	1.21 1.18
		100	0.50	0	0	1,680 1,680	1.04 1.04	1.37 1.37
		75	0.50	0	0	3,580 3,510	1.05 1.03	1.45 1.43
		50	0.50	0	0	6,360 6,330	1.06 1.05	1.70 1.69
		100	0.25	0.15h	0.15h	1,690	1.03	1.17
		75	0.25	0.15h	0.15h	3,250	1.06	1.28
		50	0.25	0.15h	0.15h	5,130	1.05	1.50
	T- Section	60	0.50	0	0	1,850	1.01	1.27
		60	0.25	0.15h	0.15h	1,550	1.03	1.21
SAE 1020 Steel	Rect.	100	0.50	0	0	3,410 3,400	1.07 1.07	1.44 1.44
		75	0.50	0	0	5,370 5,400	1.05 1.06	1.49 1.50
		50	0.50	0	0	6,400 6,450	1.02 1.03	1.52 1.54
		100	0.75	0	0	2,460	1.06	2.24
		75	0.75	0	0	3,980	1.04	2.36
		50	0.75	0	0	5,260 5,100	1.07 1.04	2.59 2.54
		60	0.50	0	0	2,450	1.02	1.17
		60	0.50	0.15h	0.15h	1,640 1,680	1.00 1.03	1.30 1.33
	Rect.	75	0.50	0	0	4,770	1.00	1.17
		50	0.25	0	0	13,200	1.01	1.10
		75	0.50	0.15h	0.15h	3,890	1.00	1.30
		50	0.25	0.15h	0.15h	9,100	1.04	1.27



Table IV. Values of  $P_{ca}$ ,  $P_{ca}/P_{ct}$  and  $P_{ca}/P_{ya}$  for the Various Unsymmetrically Loaded Beam-Columns Studied in this Program     $P_{ca}$  = Actual Collapse Load;  $P_{ct}$  = Theoretical Collapse Load; and  $P_{ya}$  = Actual Yield Load.

Material	Shape	$\ell/r$	$M_Q/M_e$	$e_1$	$e_2$	$P_{ca}$ lb.	$P_{ca}/P_{ct}$	$P_{ca}/P_{ya}$	
2024-T4 Aluminum Alloy	Rect.	100	0.50	0	0	1,740 1,710	1.00 0.98	1.22 1.20	
		75	0.50	0	0	3,610	0.96	1.32	
		50	0.50	0	0	6,480 6,490	0.96 0.96	1.58 1.58	
	T- Section	60	0.50	0	0	1,840 1,890	0.95 0.97	1.15 1.20	
		100	0.50	0	0	3,660	1.05	1.41	
	Rect.	75	0.50	0	0	5,680	1.04	1.47	
SAE 1020 Steel		50	0.50	0	0	6,530	1.01	1.52	
		75	0.50	0.15h	0.15h	3,590	1.00	1.69	
		75	0.50	0.15h	0	4,400	0.96	1.47	
		60	0.75	0	0	2,210	1.01	1.28	
17-7PH Stainless Steel	Rect.	75	0.25	0	0	6,480	1.00	1.02	



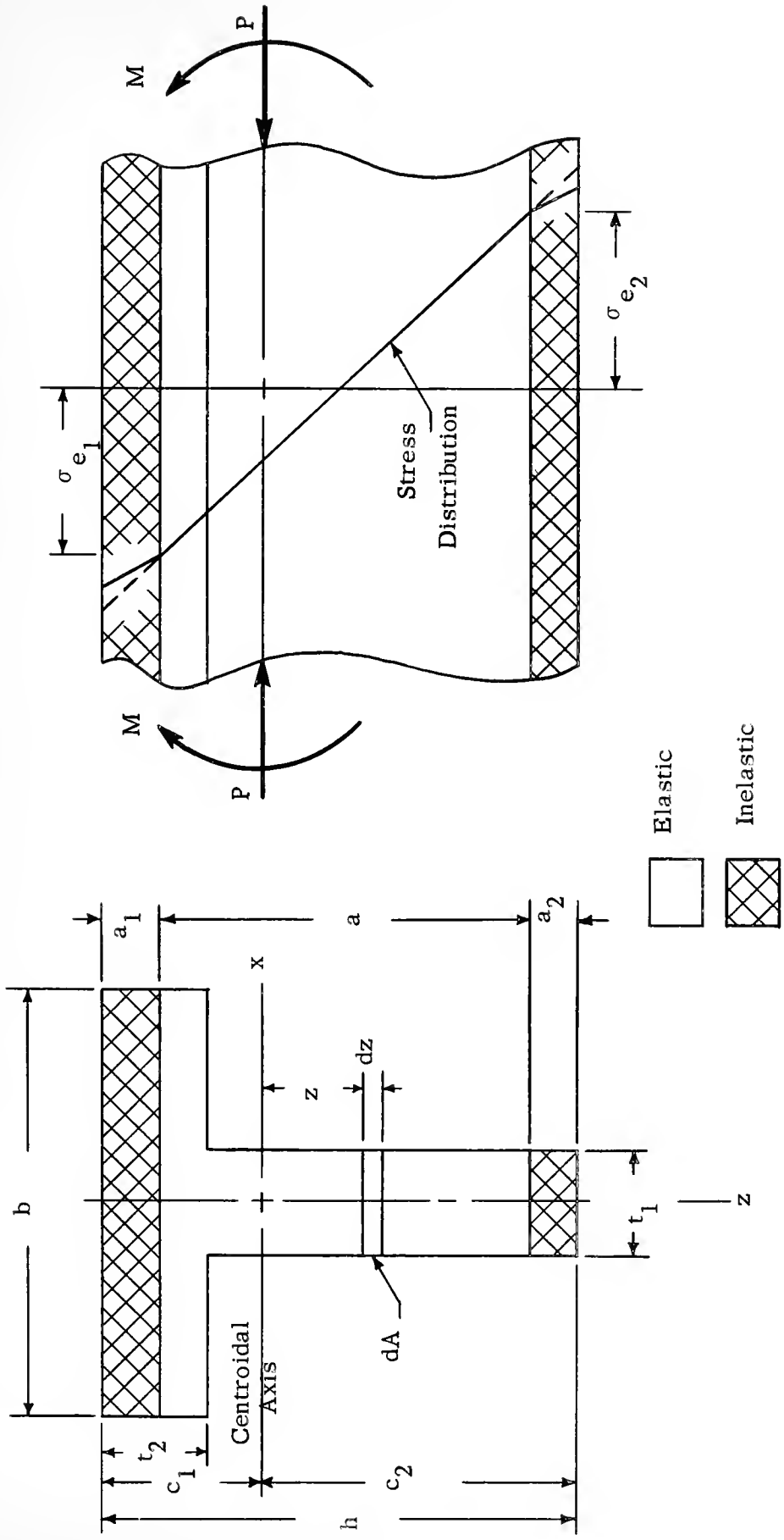


Fig. 1. T-Section Member Subjected to Combined Loading. The Sketch Shows the Stress Distribution When the Member is Partly Elastic and Partly Inelastic.



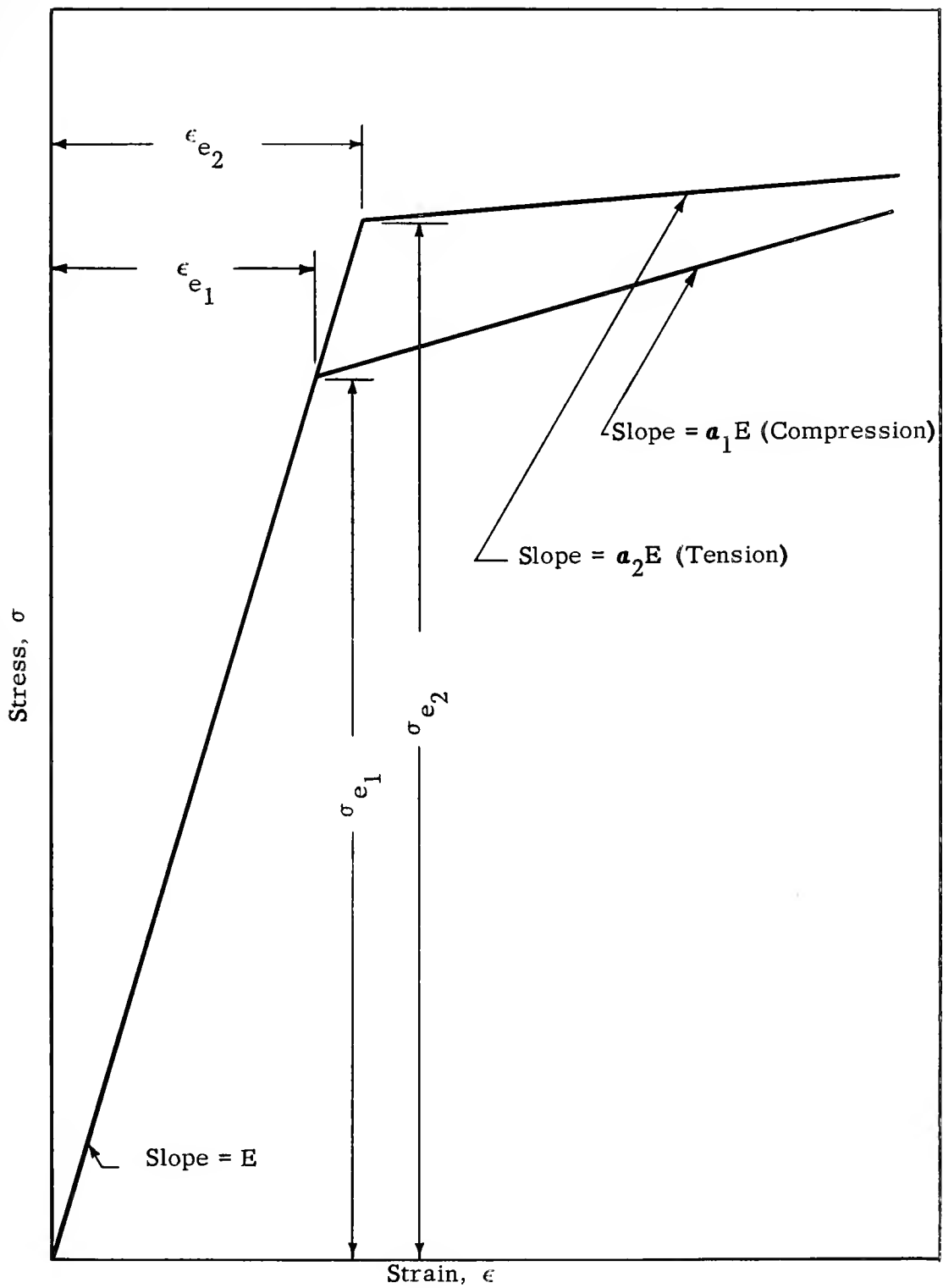


Fig. 2. A Schematic Representation of Stress-Strain Relations in Tension and Compression.



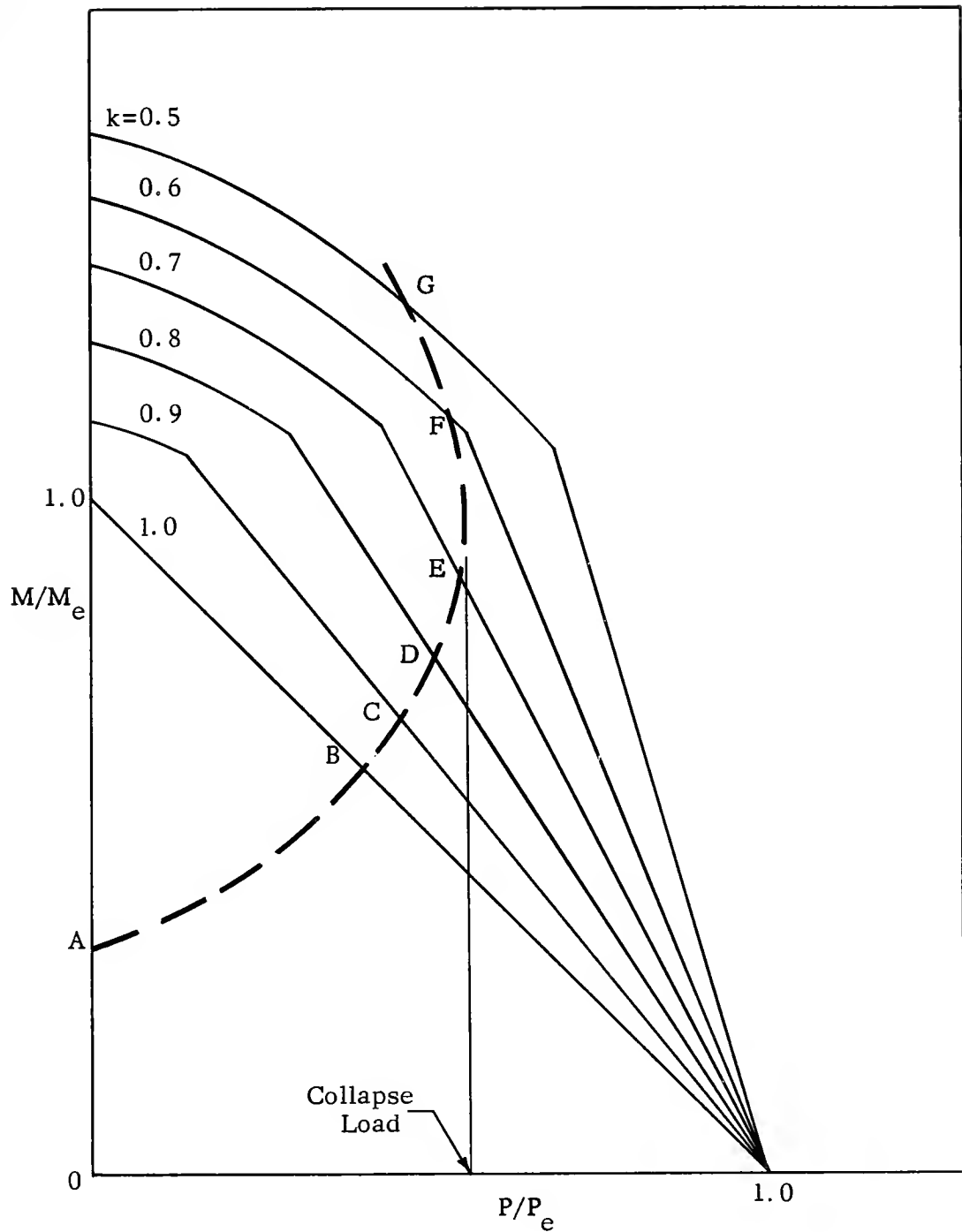


Fig. 3. A Schematic Representation of Interaction Curves for Constant Depth of Yielding.



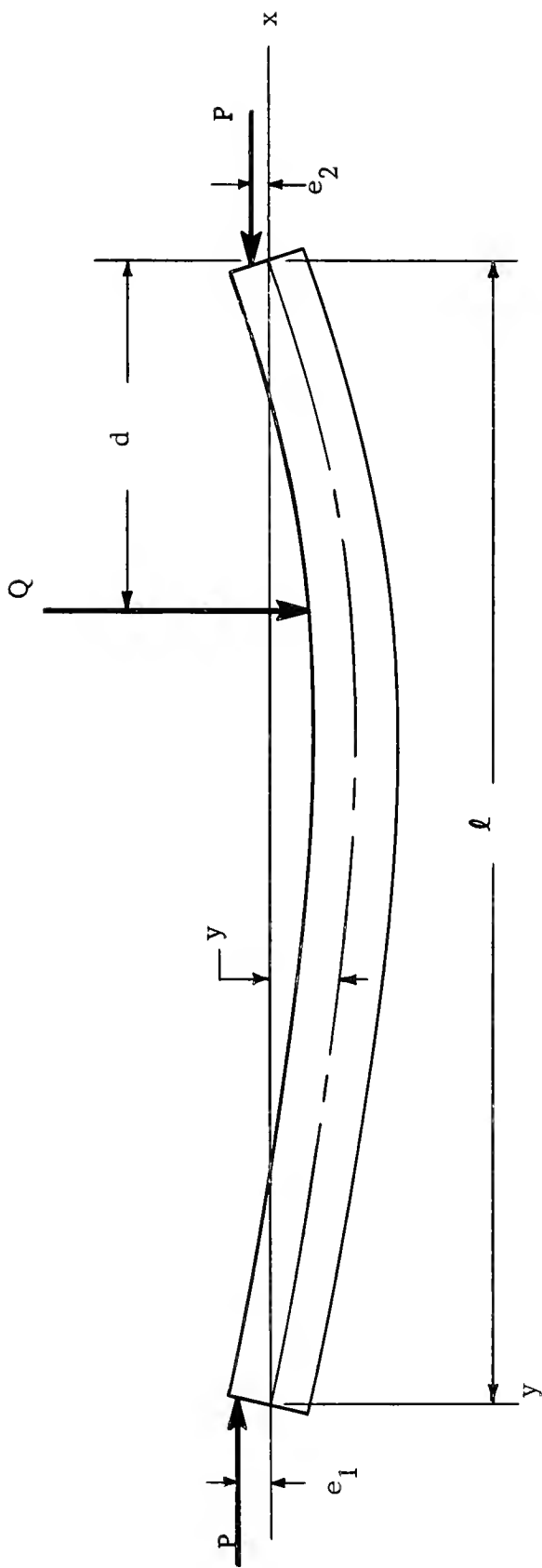
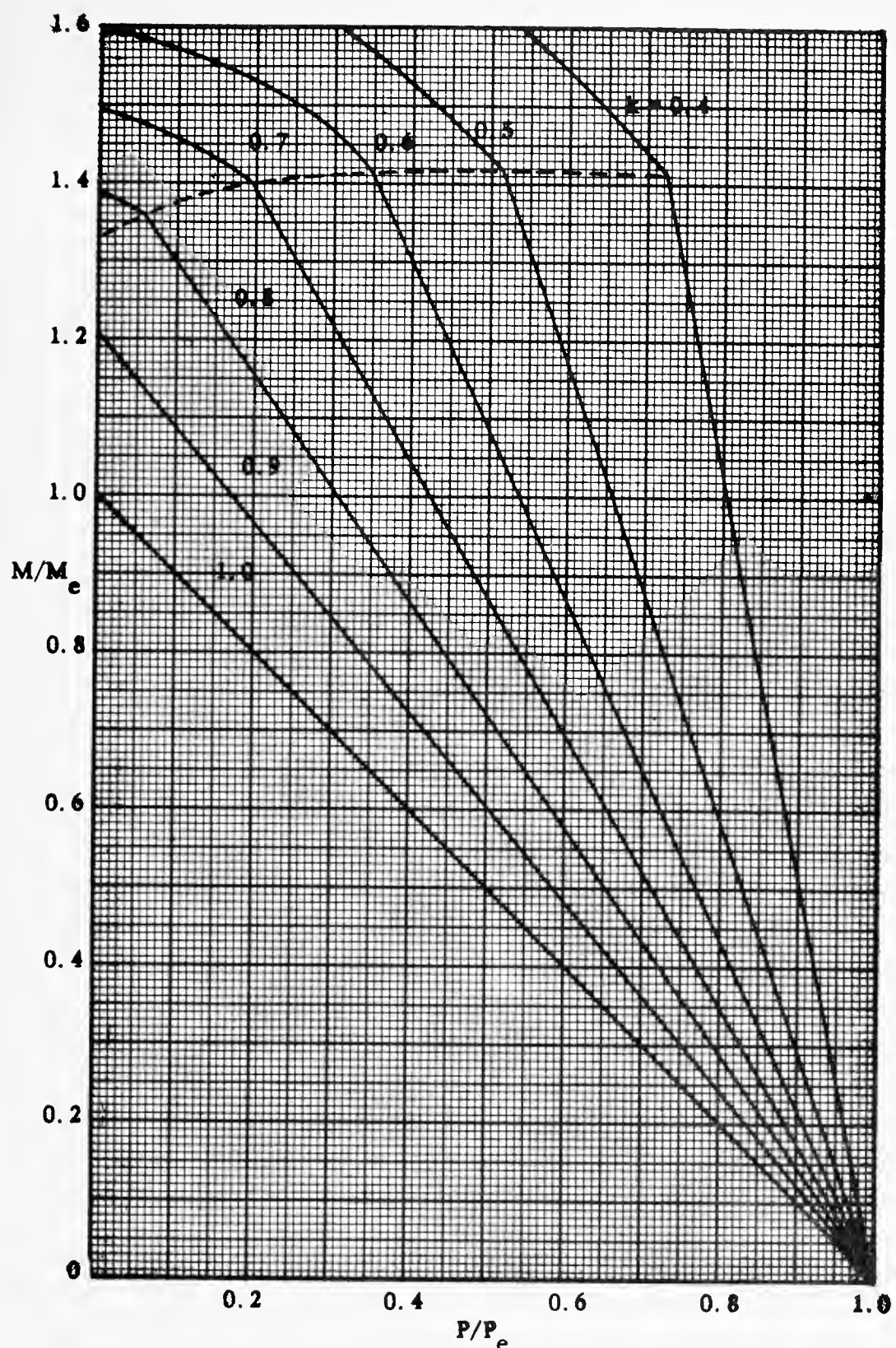


Fig. 4. A Sketch Showing the Beam-Column Studied in this Program.





**Fig 5.** Dimensionless Interaction Curves for Rectangular Sections Made of 2024-T4 Aluminum.



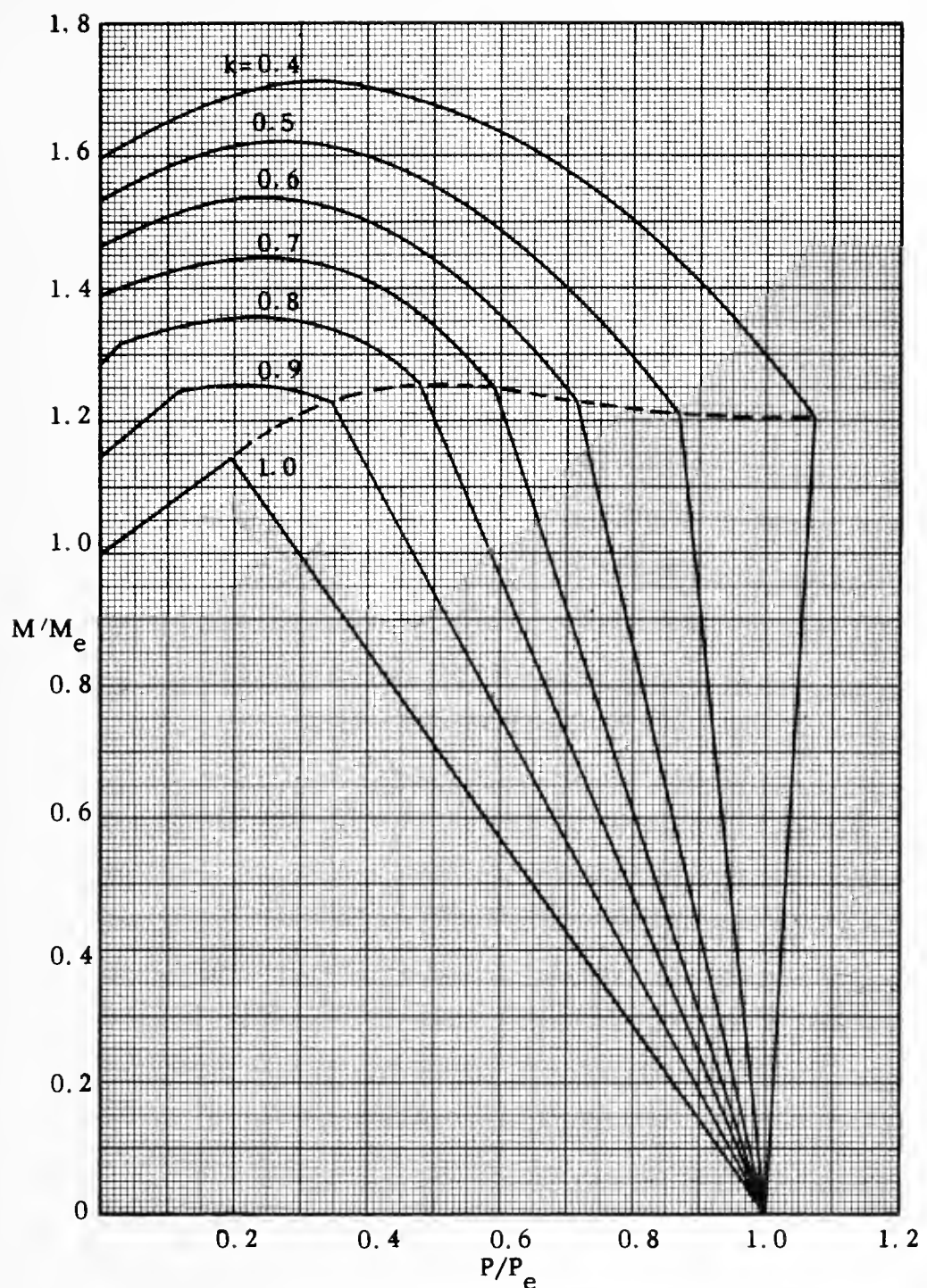


Fig. 6. Dimensionless Interaction Curves for T-Sections Made of 2024-T4 Aluminum.



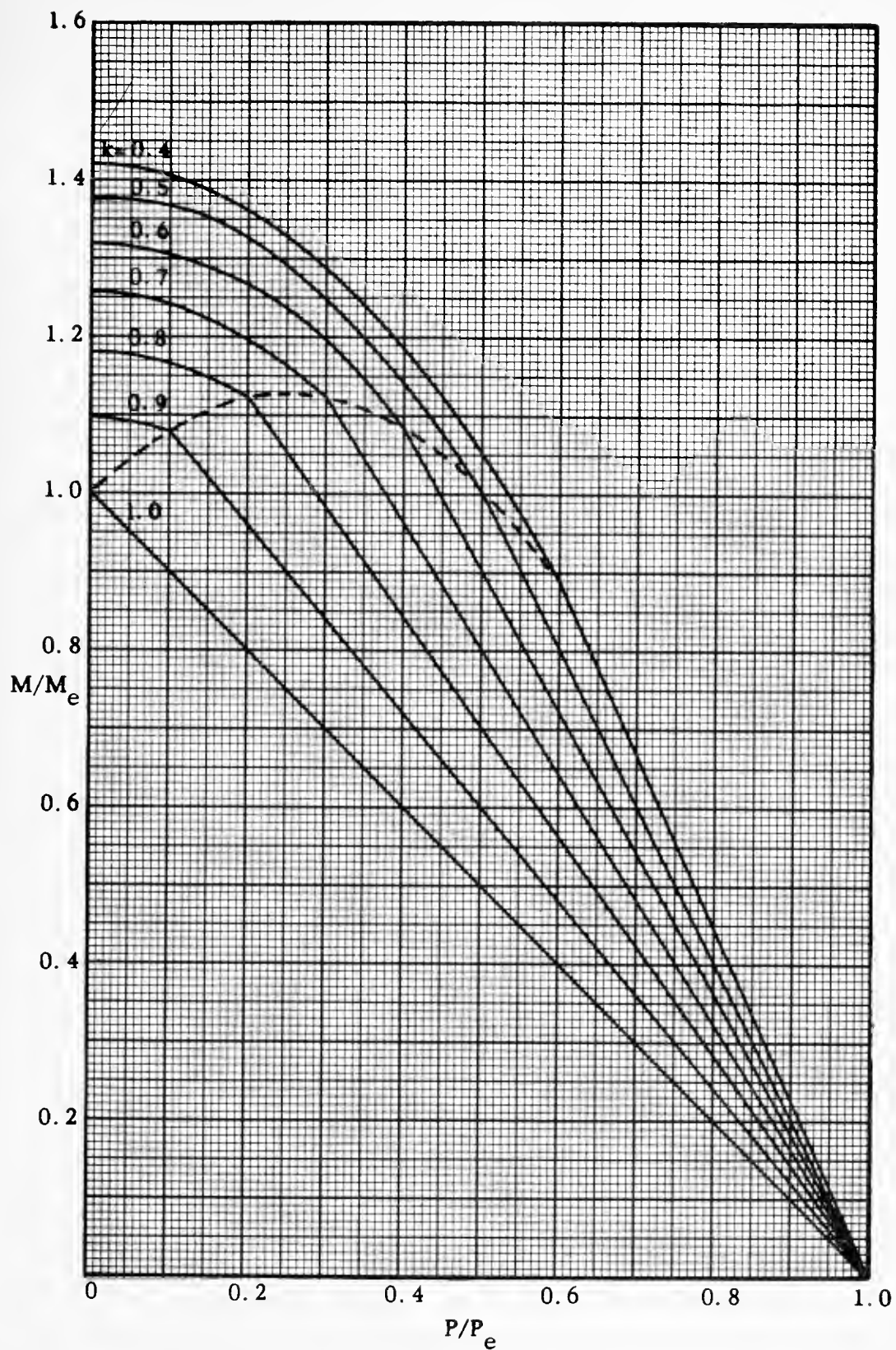


Fig. 7. Dimensionless Interaction Curves for Rectangular Section Made of SAE 1020 Steel.



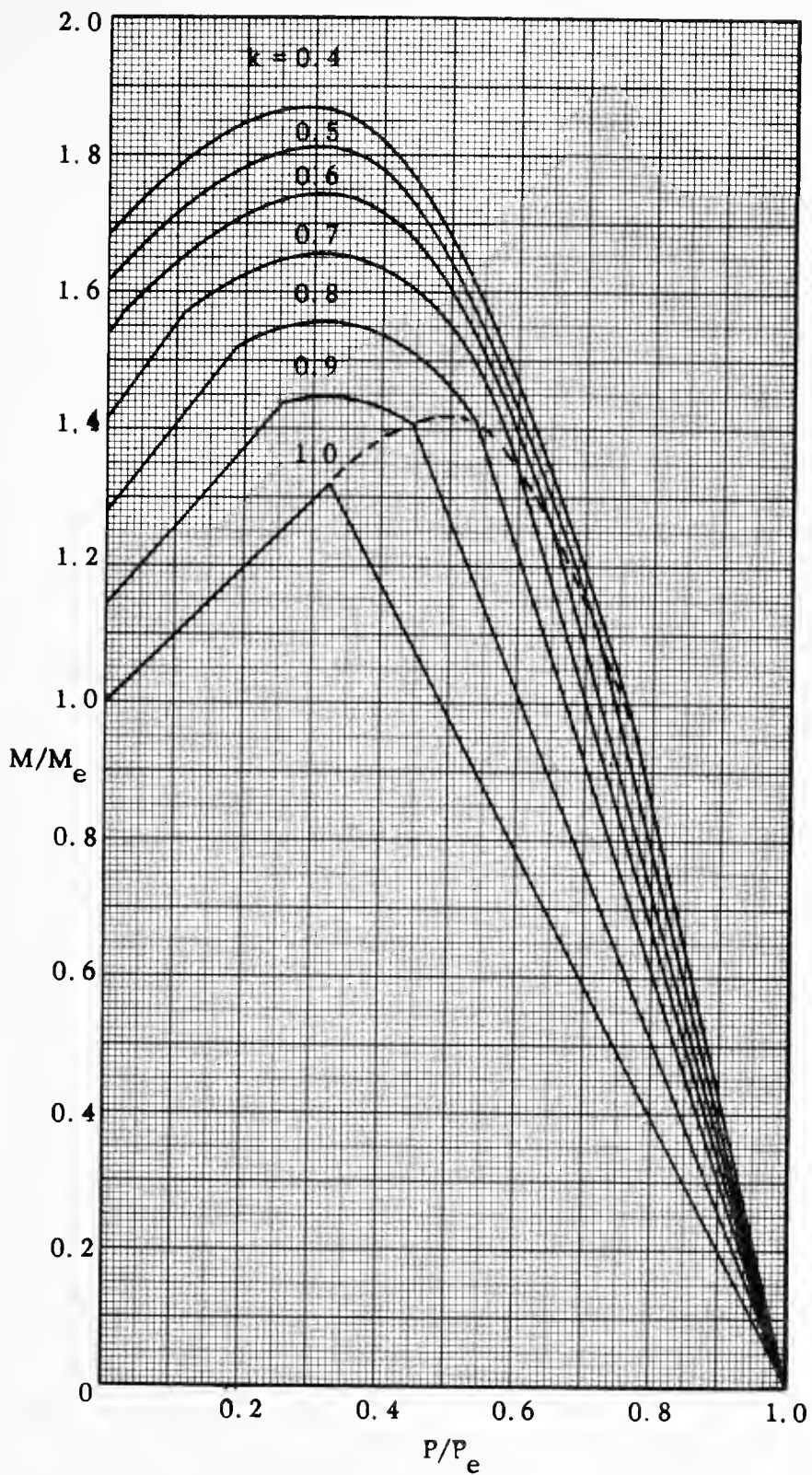


Fig. 8. Dimensionless Interaction Curves for T-Sections Made of SAE 1020 Steel.



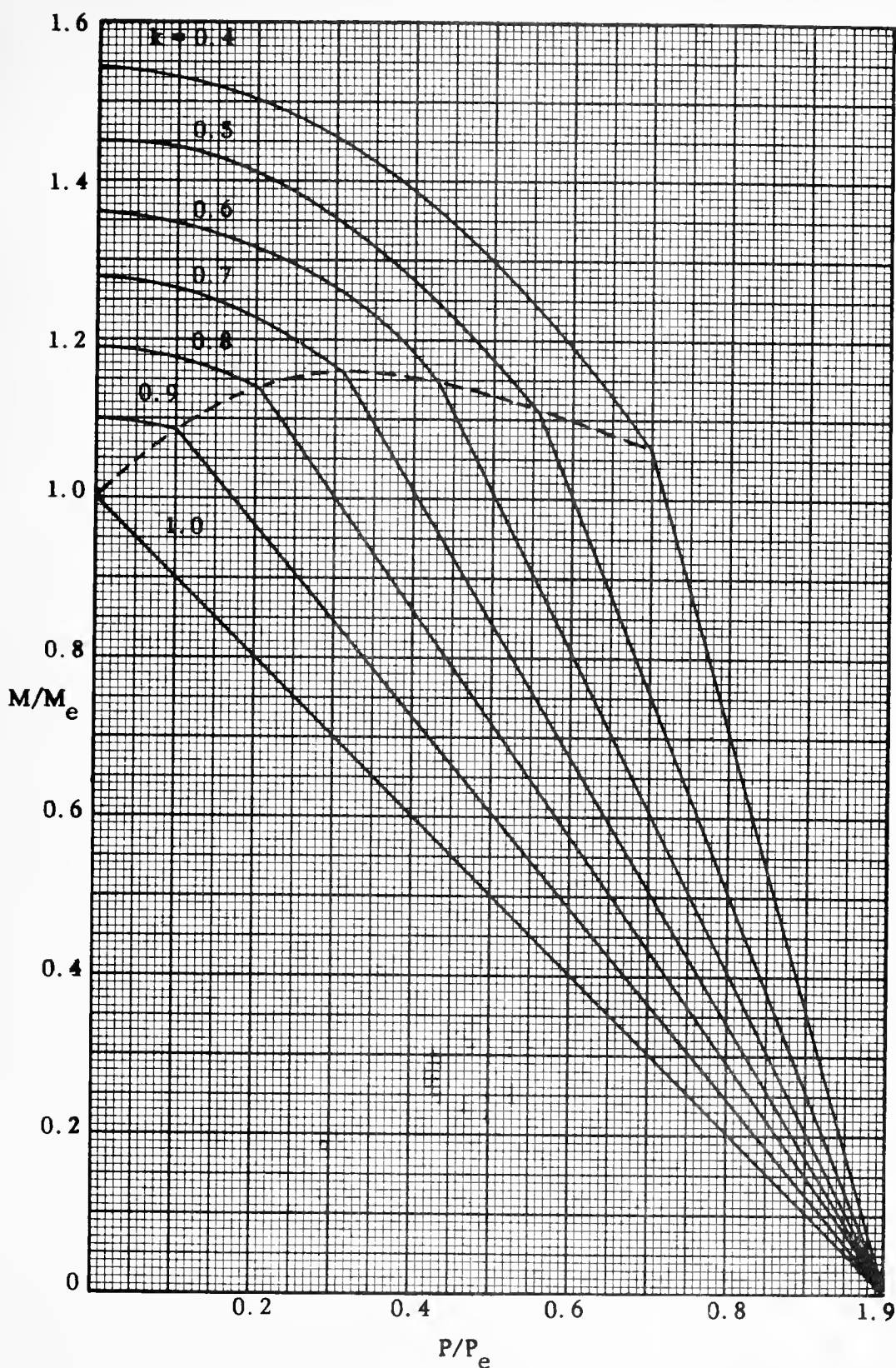


Fig. 9. Dimensionless Interaction Curves for Rectangular Sections Made of 17-7PH Stainless Steel.



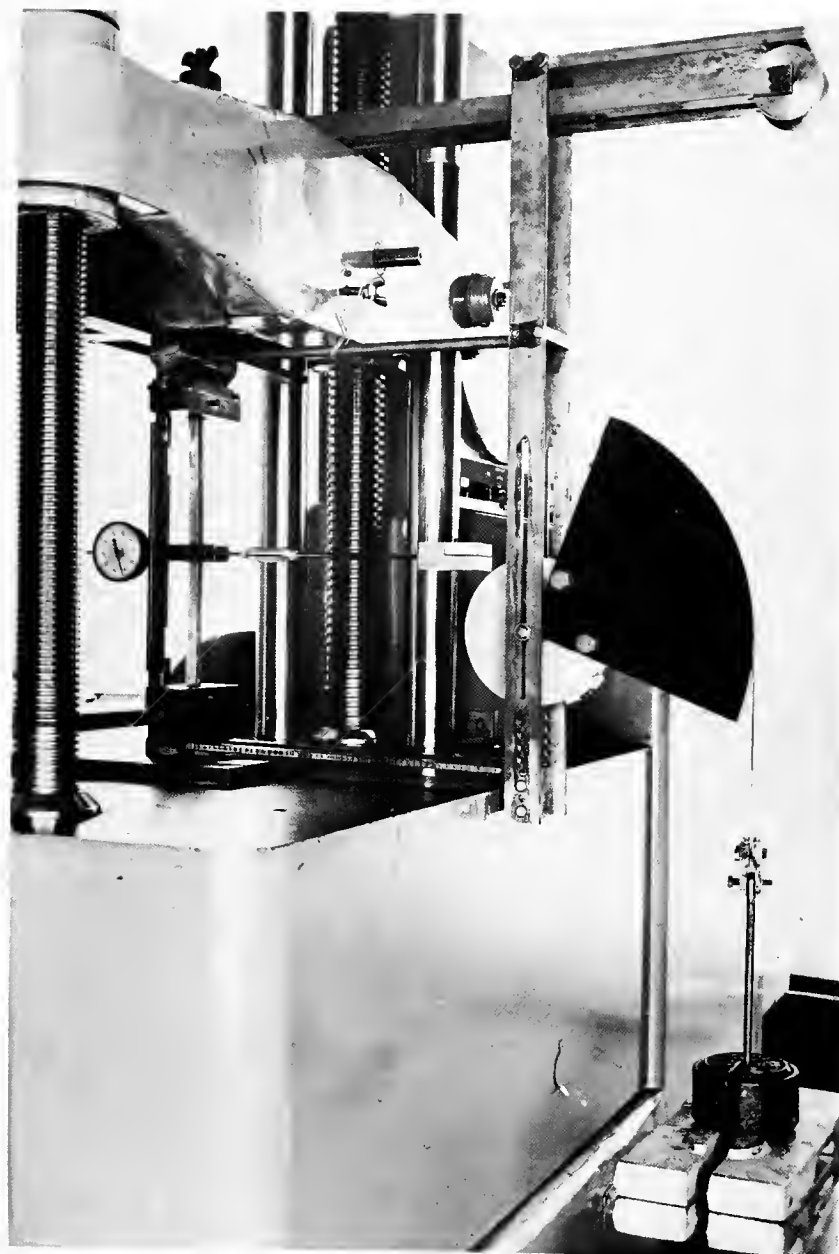


Fig. 10. Test Apparatus Used to Apply Transverse and Axial Loads to Beam-Columns.



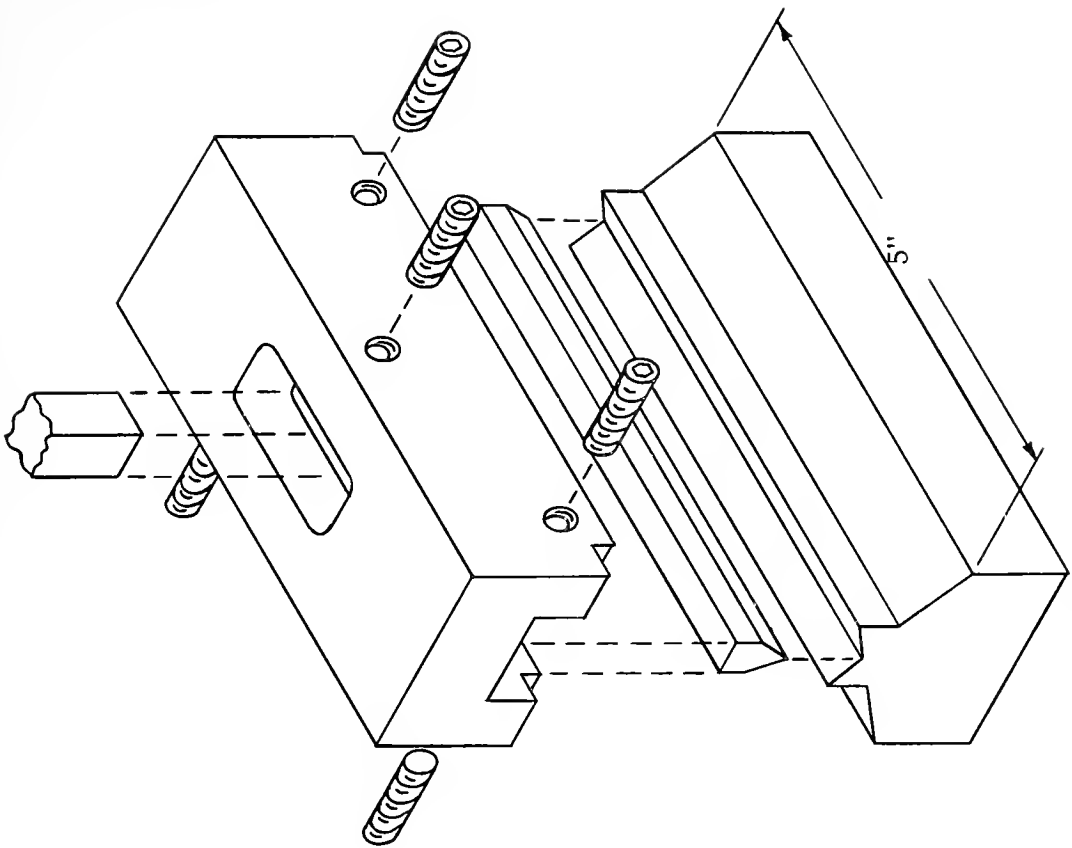
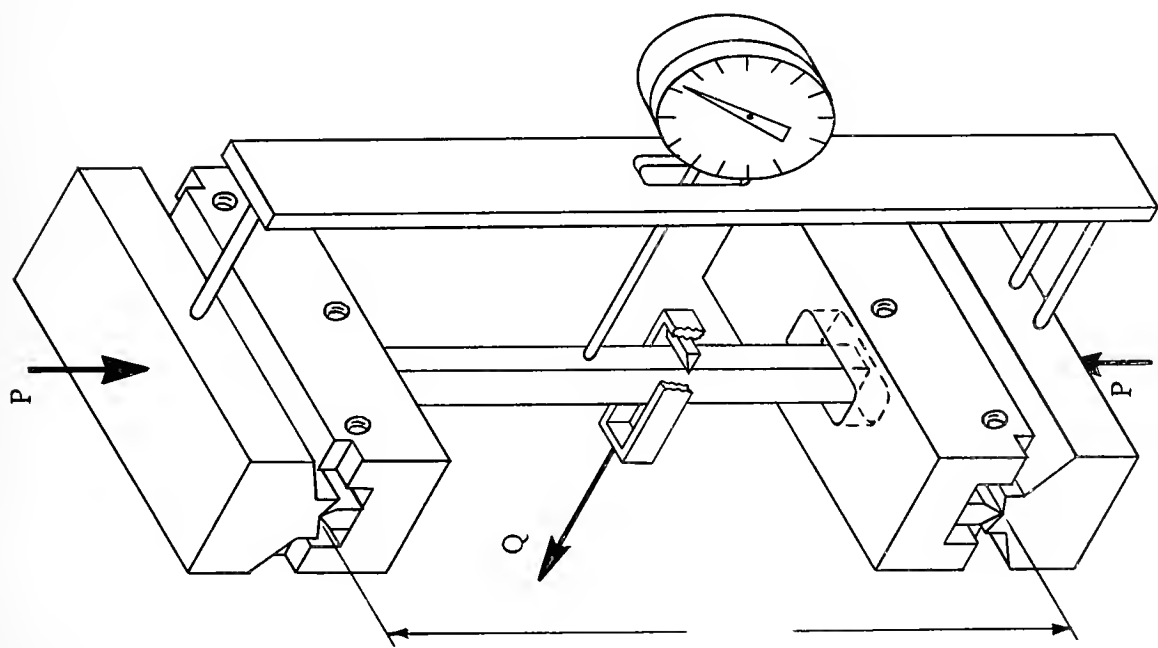


Fig. 11. Knife-Edge Fixtures Used to Apply Axial Load to Beam-Column.





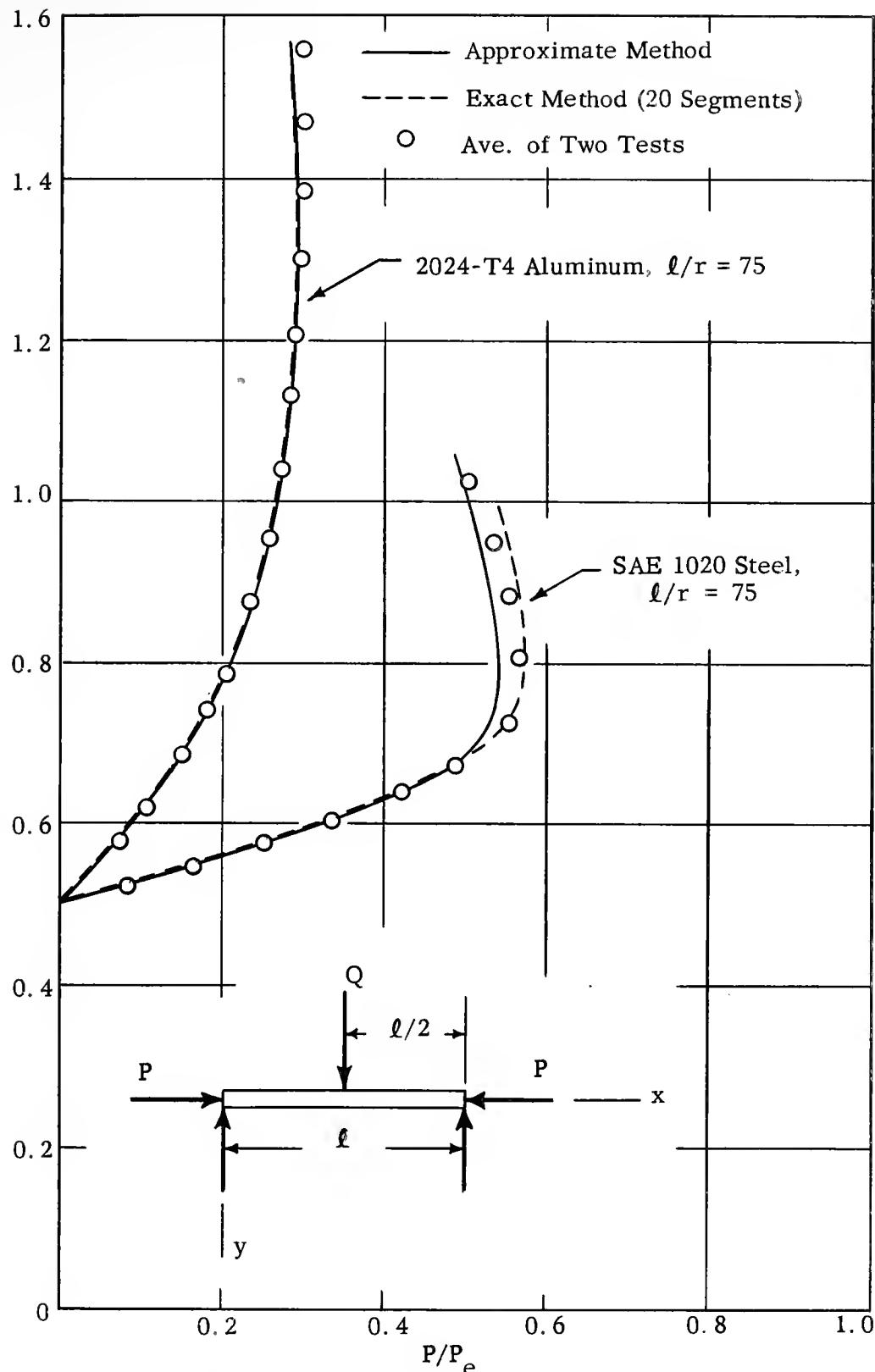


Fig. 12. Comparison of Moment-Load Curves for Symmetrically Loaded 2024-T4 and SAE 1020 Steel Beam-Columns Determined by Two Theoretical Methods and By Test.



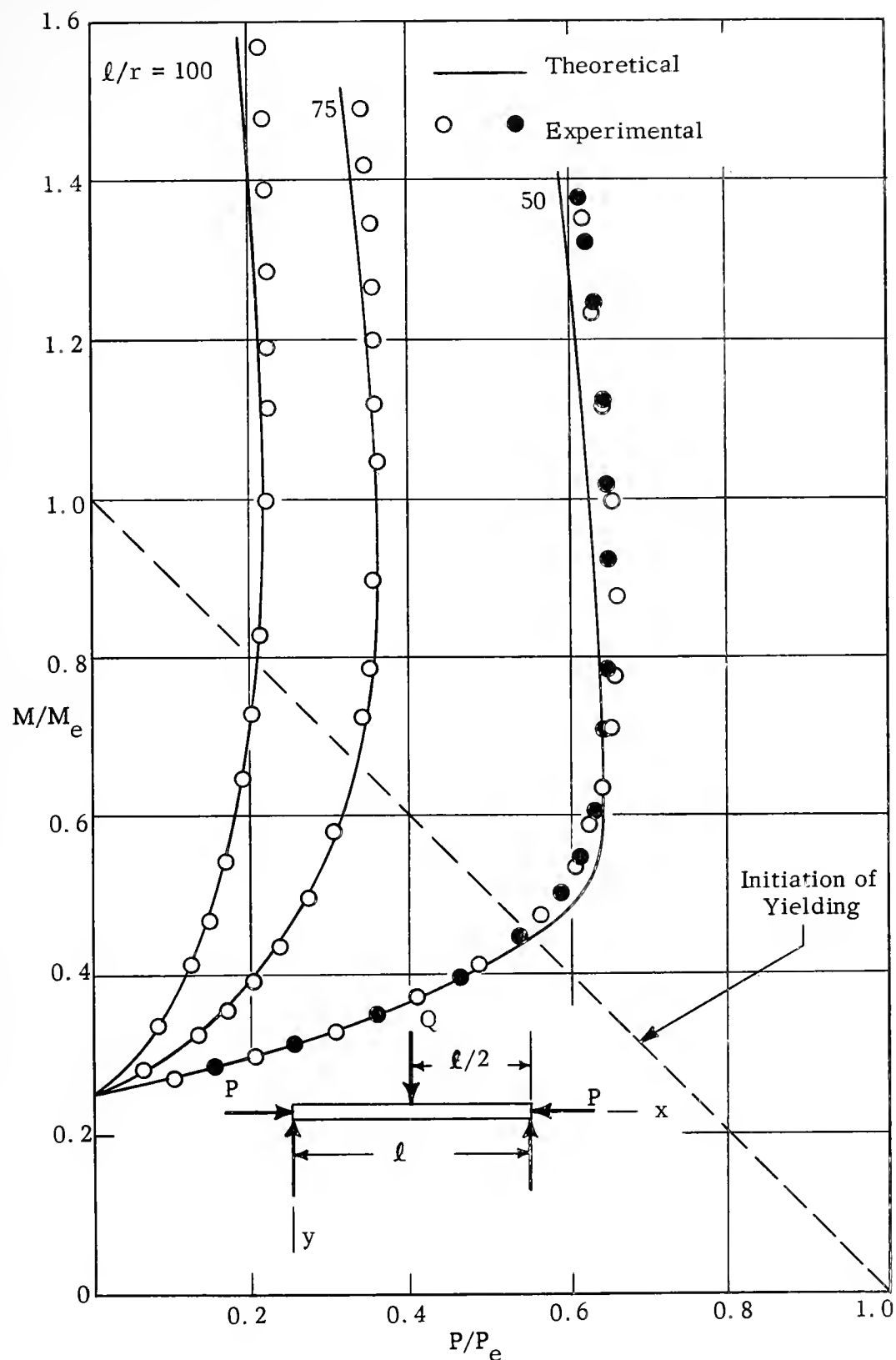


Fig. 13. Moment-Load Curves for Symmetrically Loaded, Rectangular 2024-T4 Aluminum Beam-Columns. ( $M_Q/M_e = 0.25$ ;  $e_1 = e_2 = 0$ )



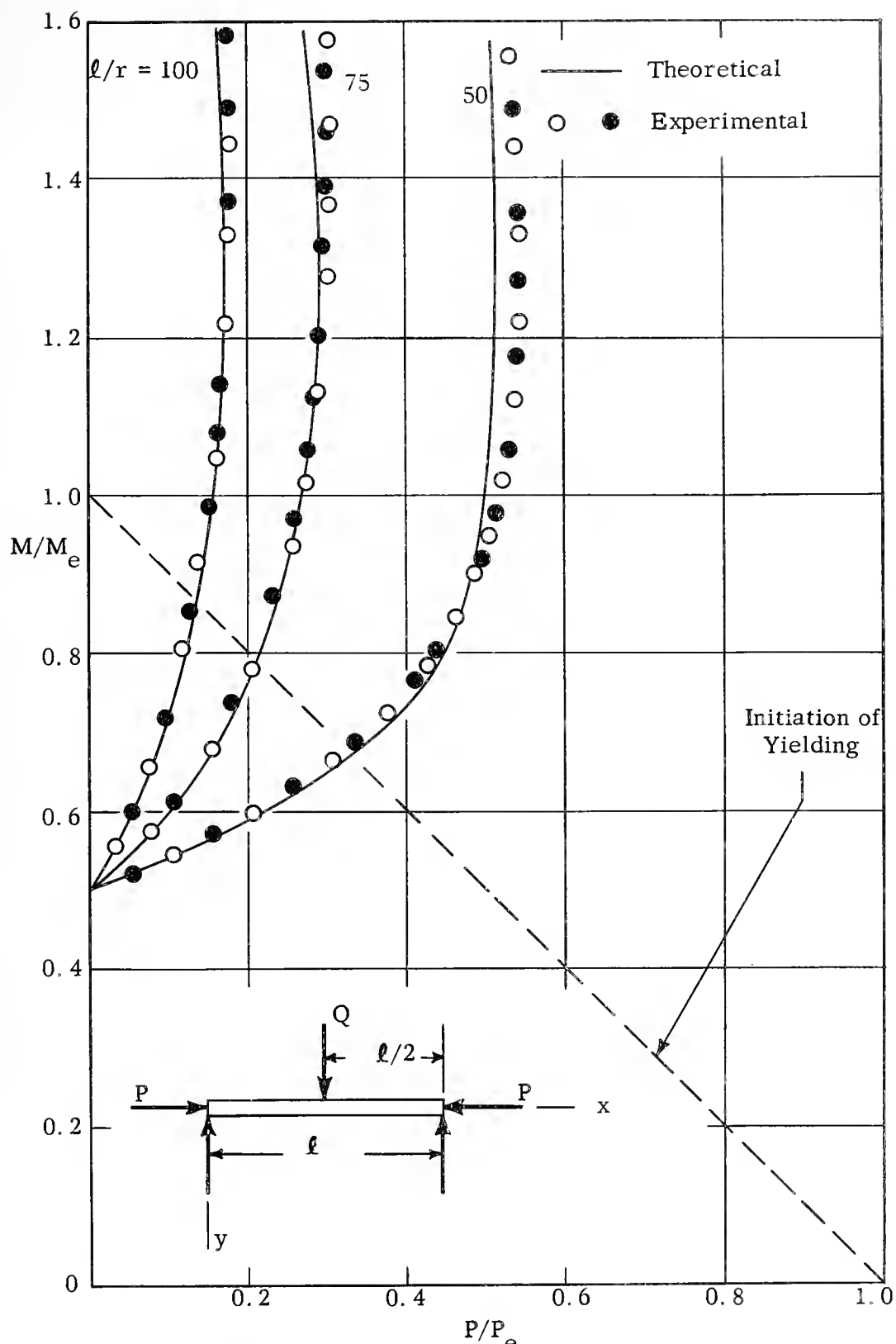


Fig. 14. Moment-Load Curves for Symmetrically Loaded, Rectangular 2024-T4 Aluminum Beam-Columns. ( $M_Q/M_e = 0.50$ ;  $e_1 = e_2 = 0$ )



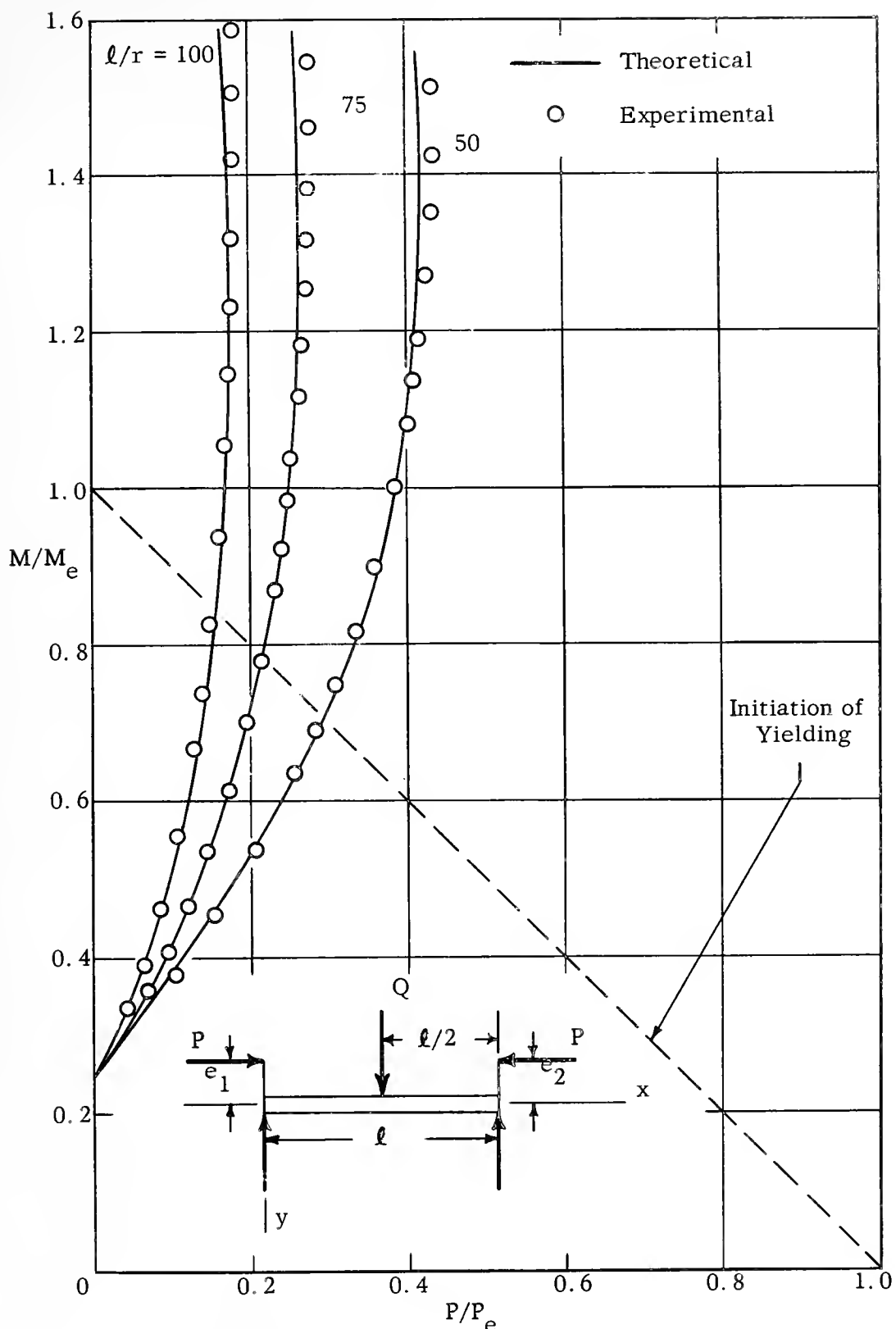


Fig. 15. Moment-Load Curves for Symmetrically Loaded, Rectangular 2024-T4 Aluminum Beam-Columns. ( $M_Q/M_e = 0.25$ ;  $e_1 = e_2 = 0.15h$ )



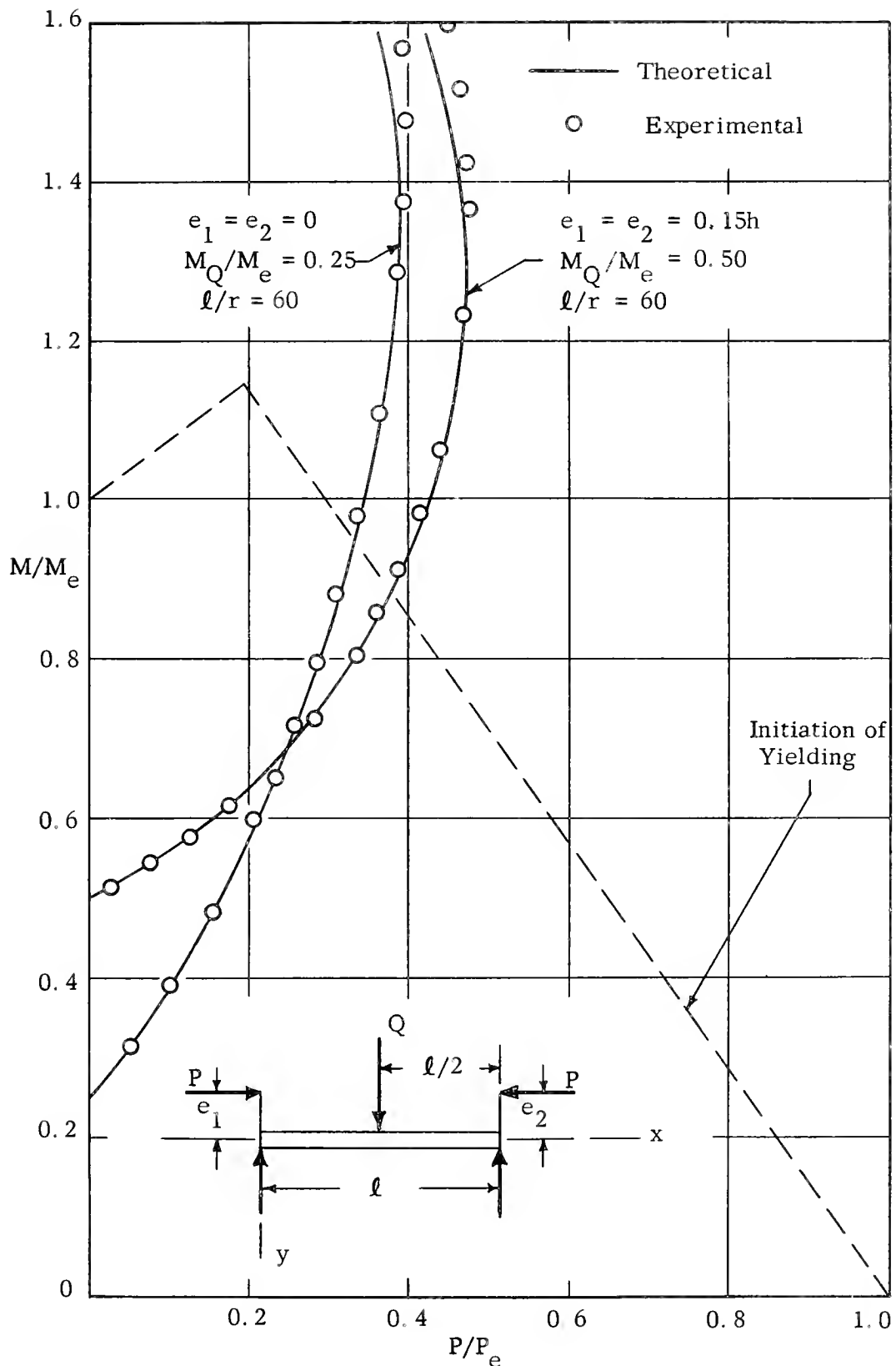


Fig. 16. Moment-Load Curves for Symmetrically Loaded T-Section Beam-Columns of 2024-T4 Aluminum.



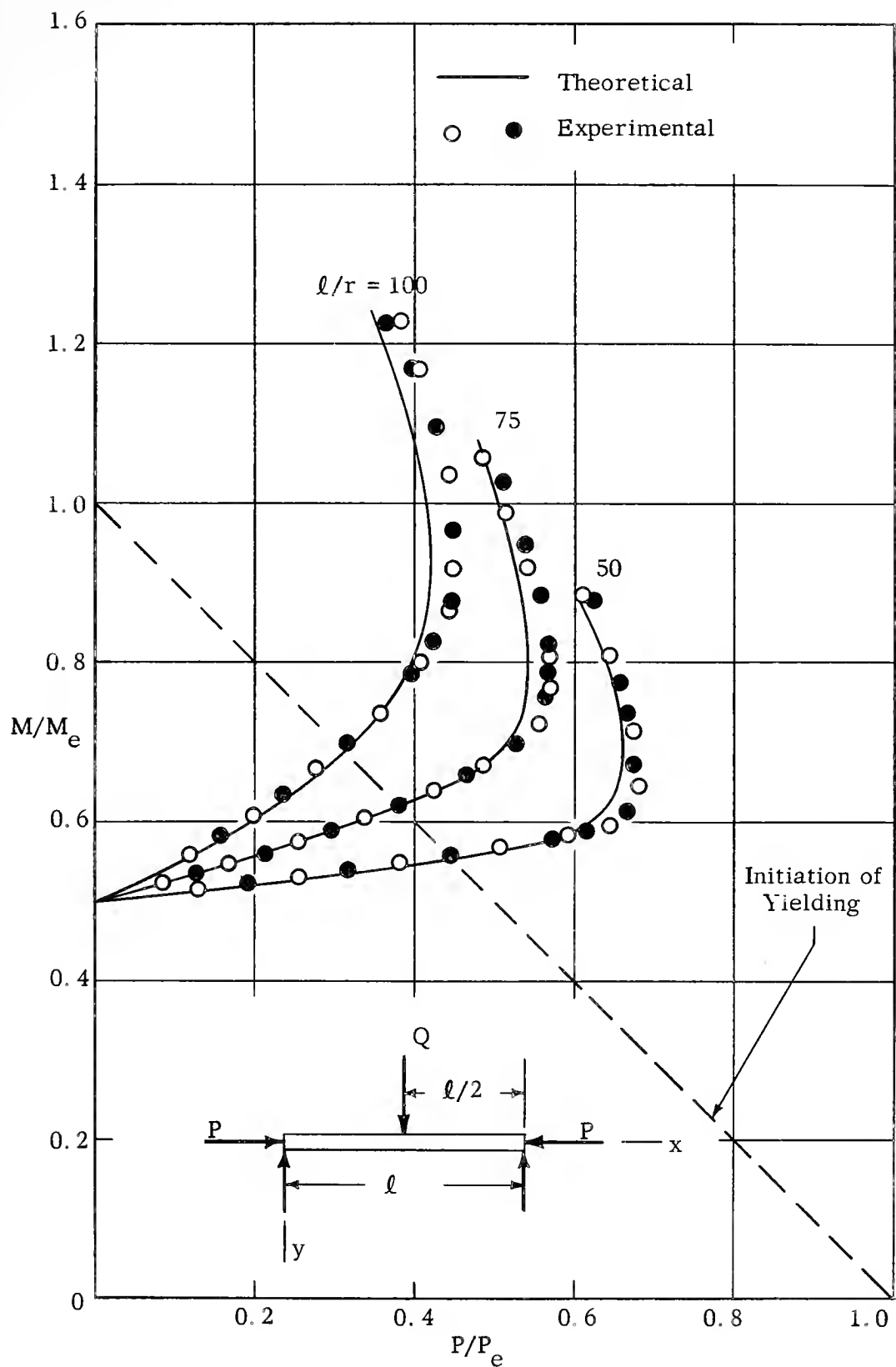


Fig. 17. Moment-Load Curves for Symmetrically Loaded, Rectangular SAE 1020 Steel Beam-Columns. ( $M_Q/M_e = 0.50$ ;  $e_1 = e_2 = 0$ )



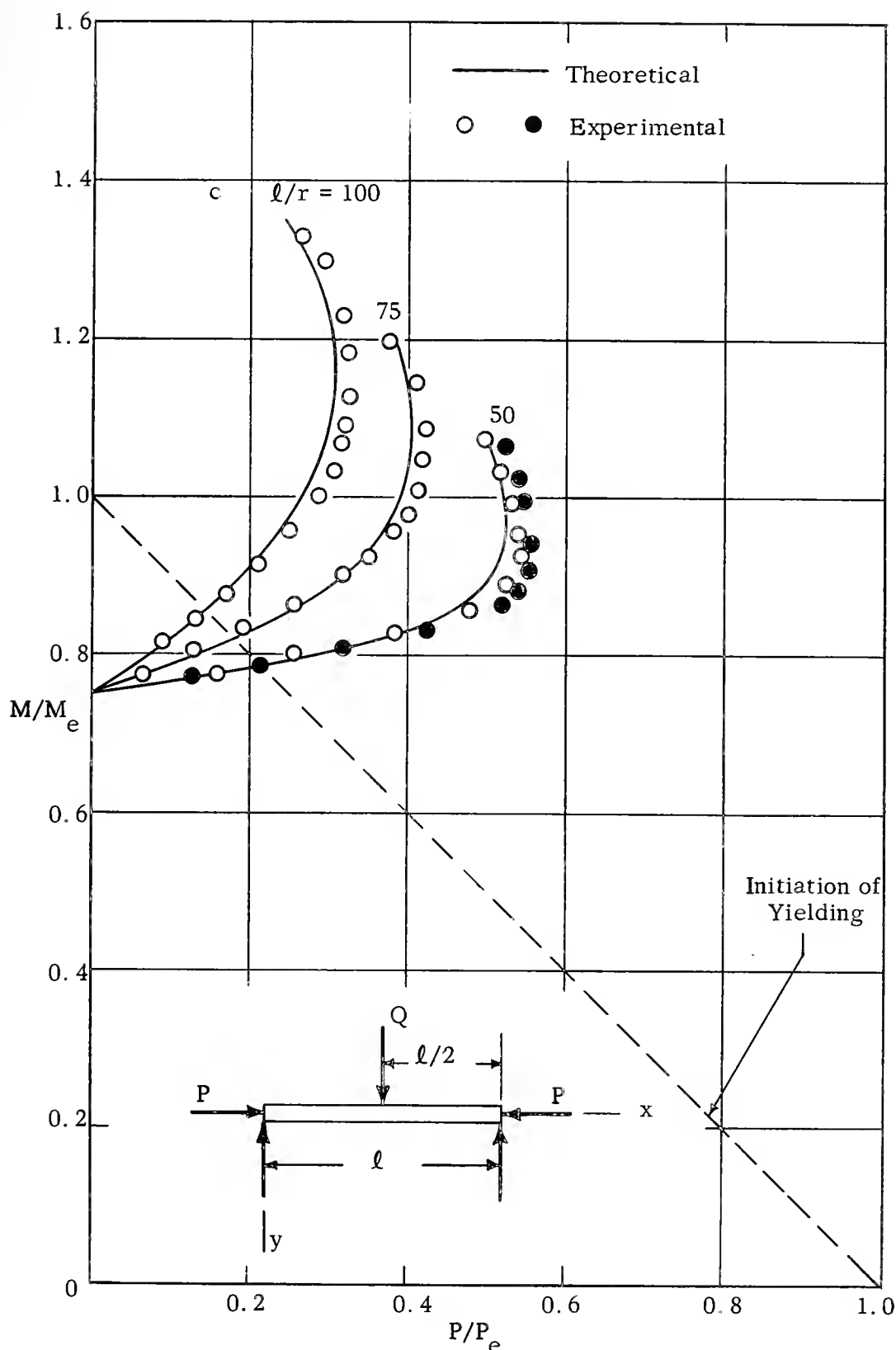


Fig. 18. Moment-Load Curves for Symmetrically Loaded, Rectangular SAE 1020 Steel Beam-Columns. ( $M_Q/M_e = 0.75$ ;  $e_1 = e_2 = 0$ )



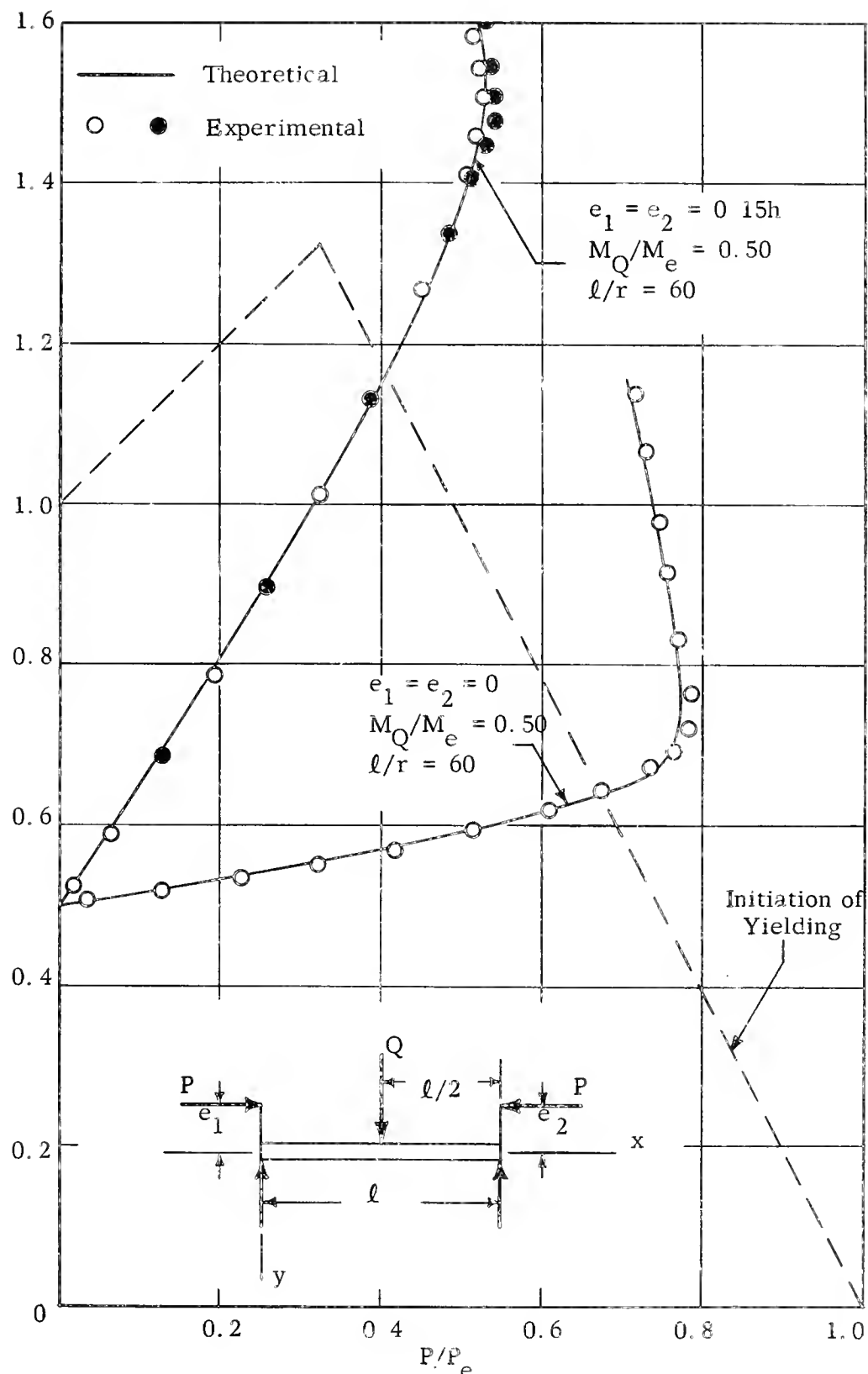


Fig. 19. Moment-Load Curves for Symmetrically Loaded T Section Beam Columns of SAE 1020 Steel.



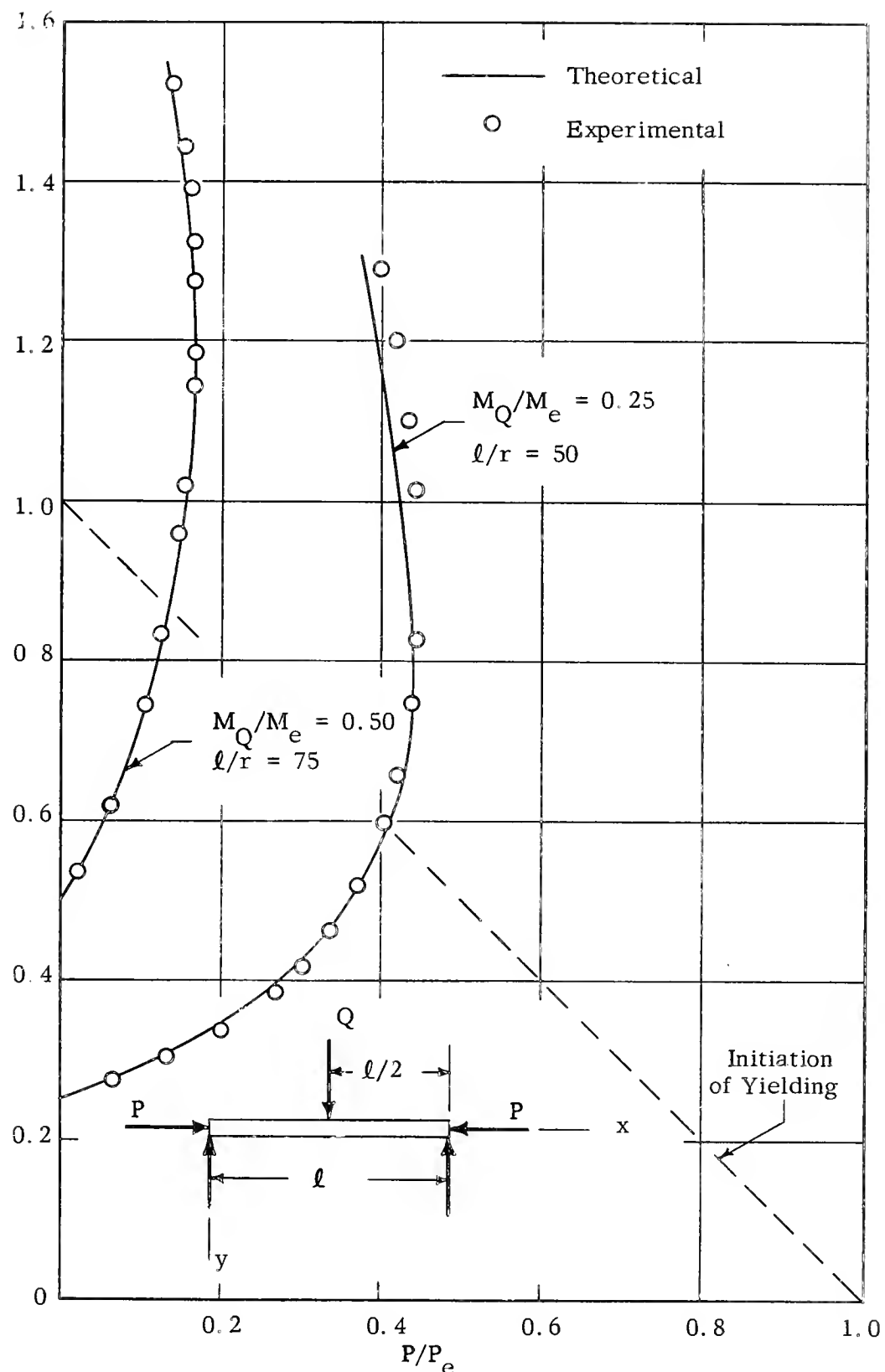


Fig. 20. Moment-Load Curves for Symmetrically Loaded, Rectangular 17-7PH Stainless Steel Beam-Columns. ( $e_1 = e_2 = 0$ )



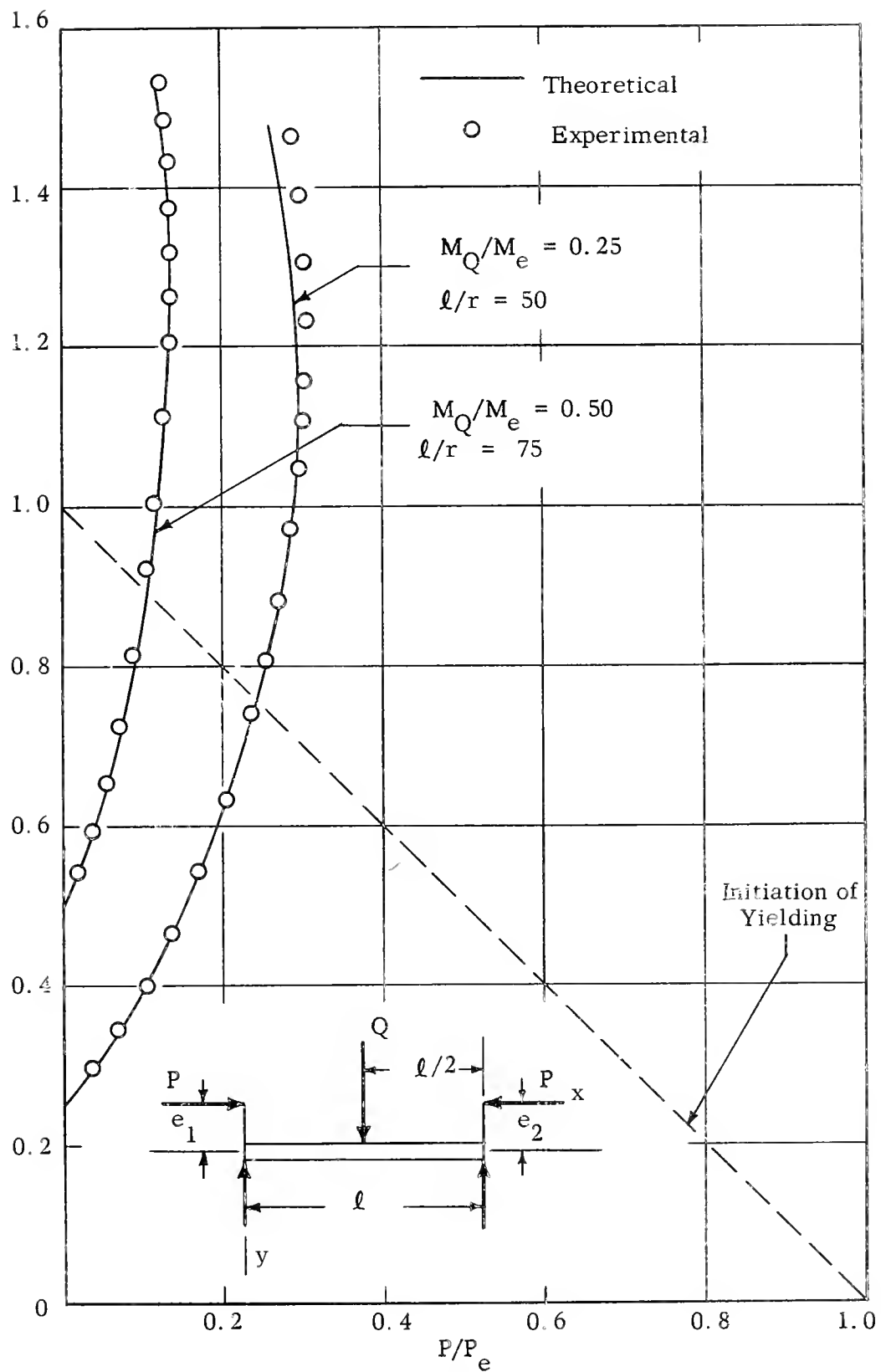


Fig. 21. Moment-Load Curves for Symmetrically Loaded Rectangular 17-7PH Stainless Steel Beam-Columns. ( $e_1 = e_2 = 0.15h$ )



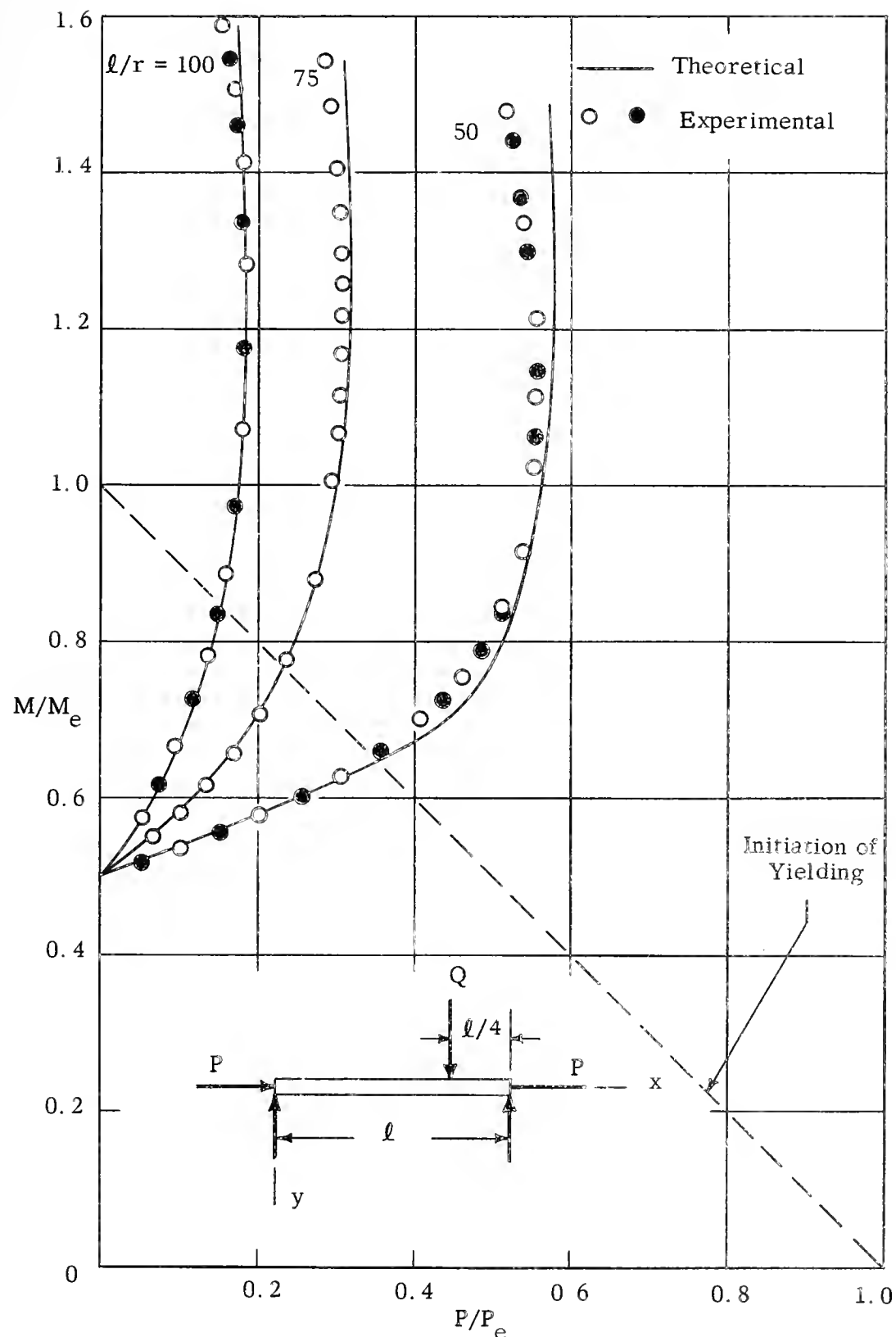


Fig. 22. Moment-Load Curves for Unsymmetrically Loaded, Rectangular 2024-T4 Aluminum Beam-Columns.  
( $M_Q/M_e = 0.50$ ;  $e_1 = e_2 = 0$ )



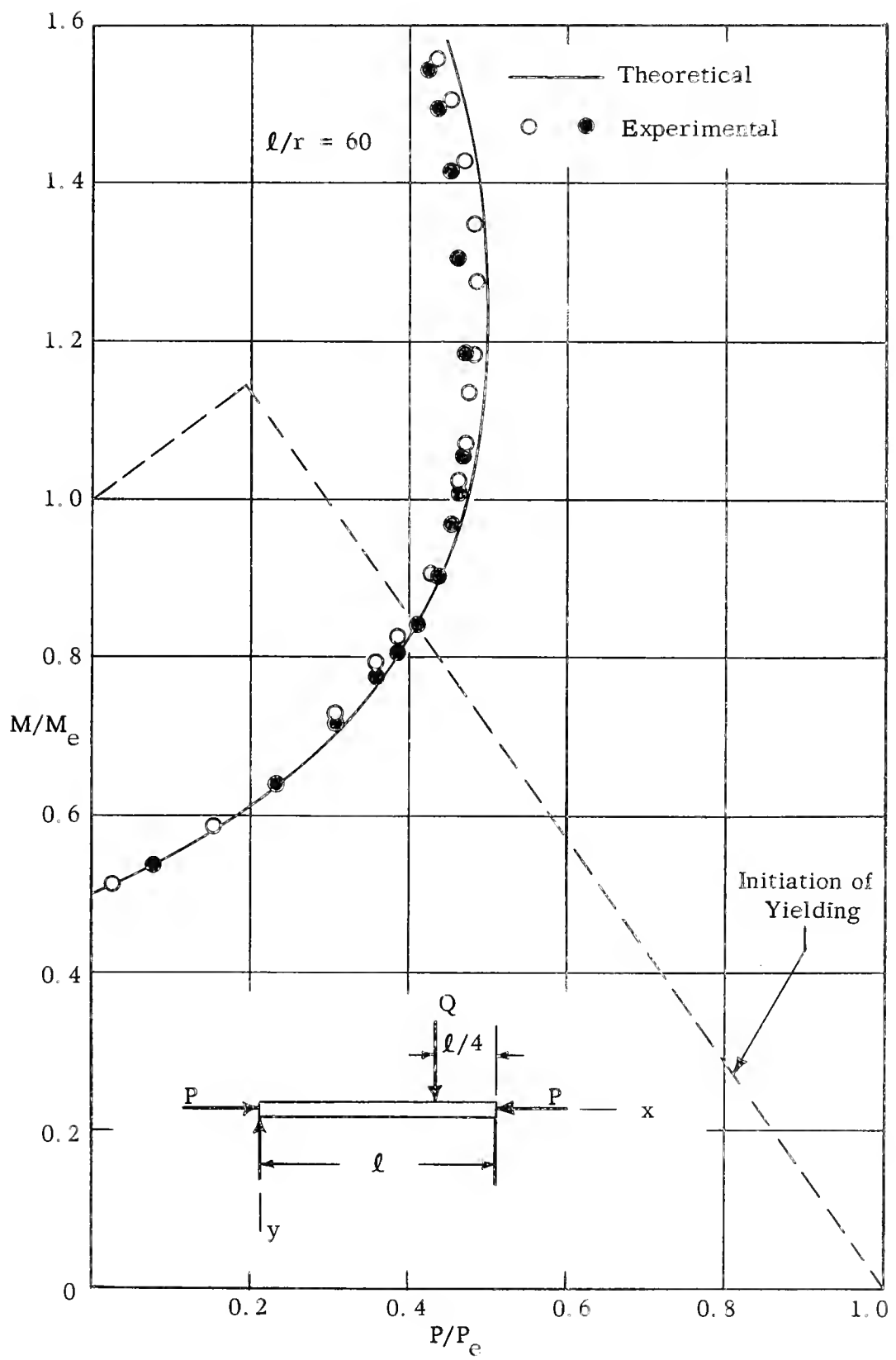


Fig. 23. Moment-Load Curve for an Unsymmetrically Loaded T-Section Beam-Column of 2024-T4 Aluminum. ( $M_Q/M_e = 0.50$ ;  $e_1 = e_2 = 0$ )



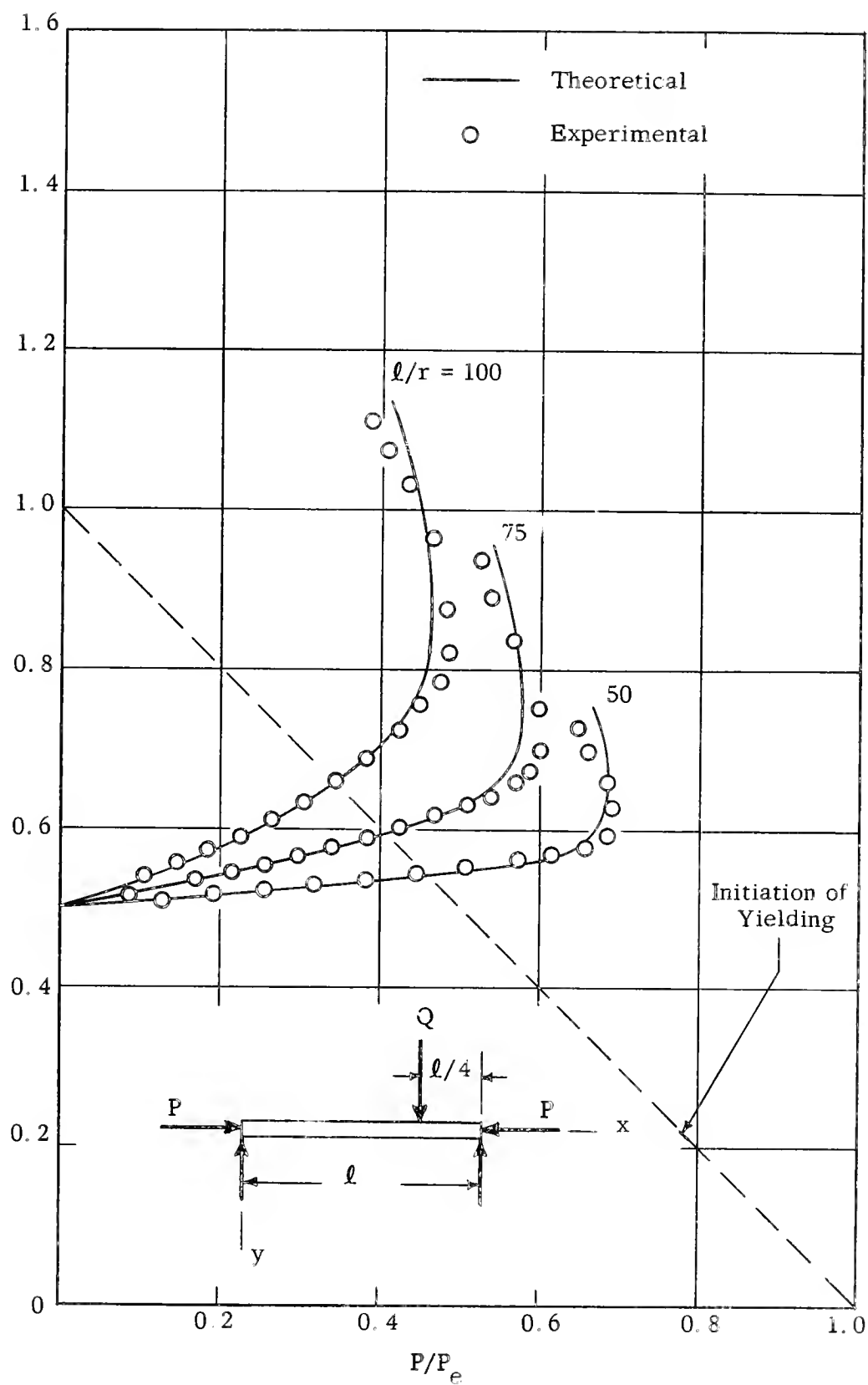


Fig. 24. Moment-Load Curves for Unsymmetrically Loaded, Rectangular SAE 1020 Steel Beam-Columns ( $M_Q/M_e = 0.50$ ;  $e_1 = e_2 = 0$ )



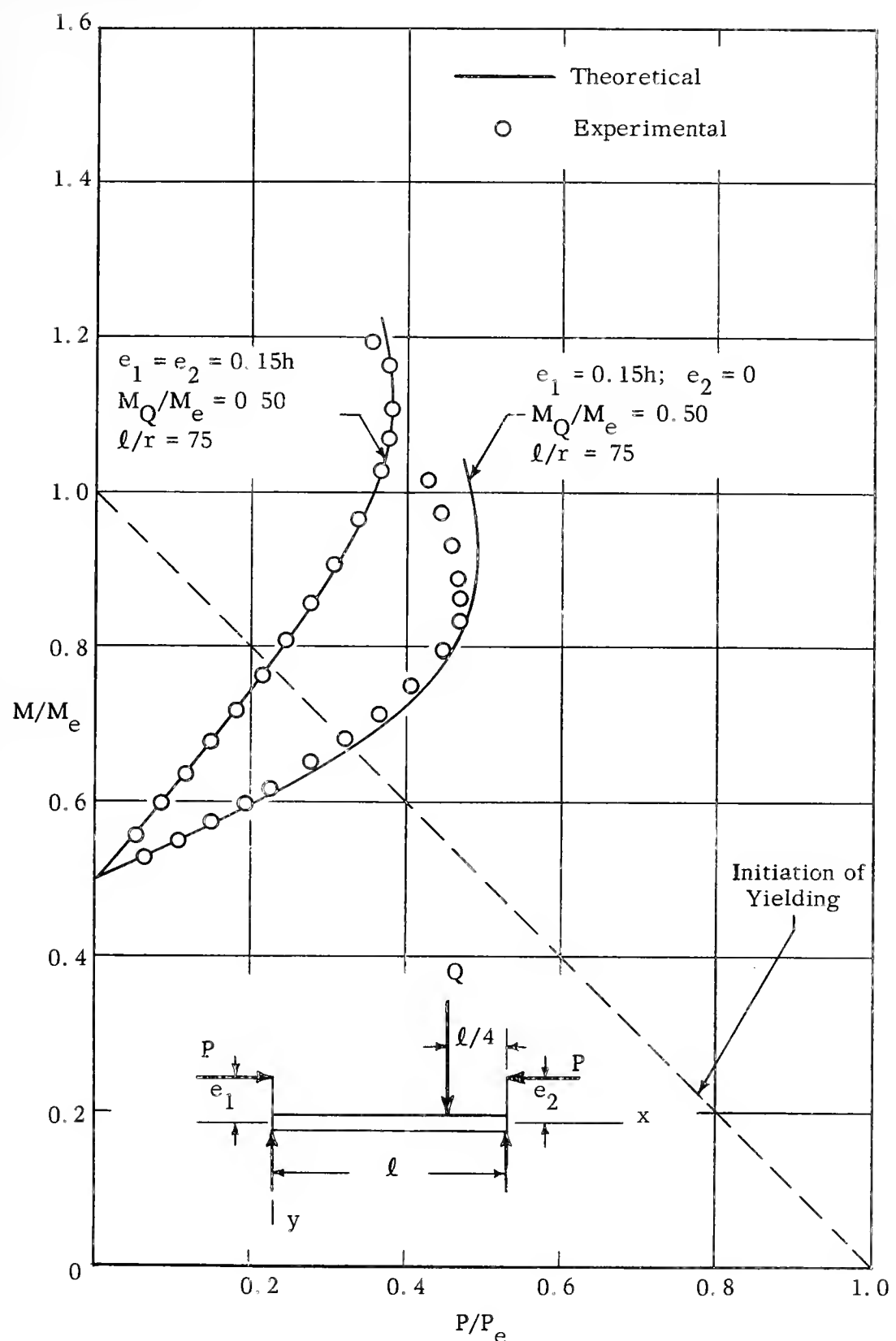


Fig. 25. Moment-Load Curves for Unsymmetrically Loaded, Rectangular SAE 1020 Steel Beam-Columns, with Equal and Unequal End Eccentricities.



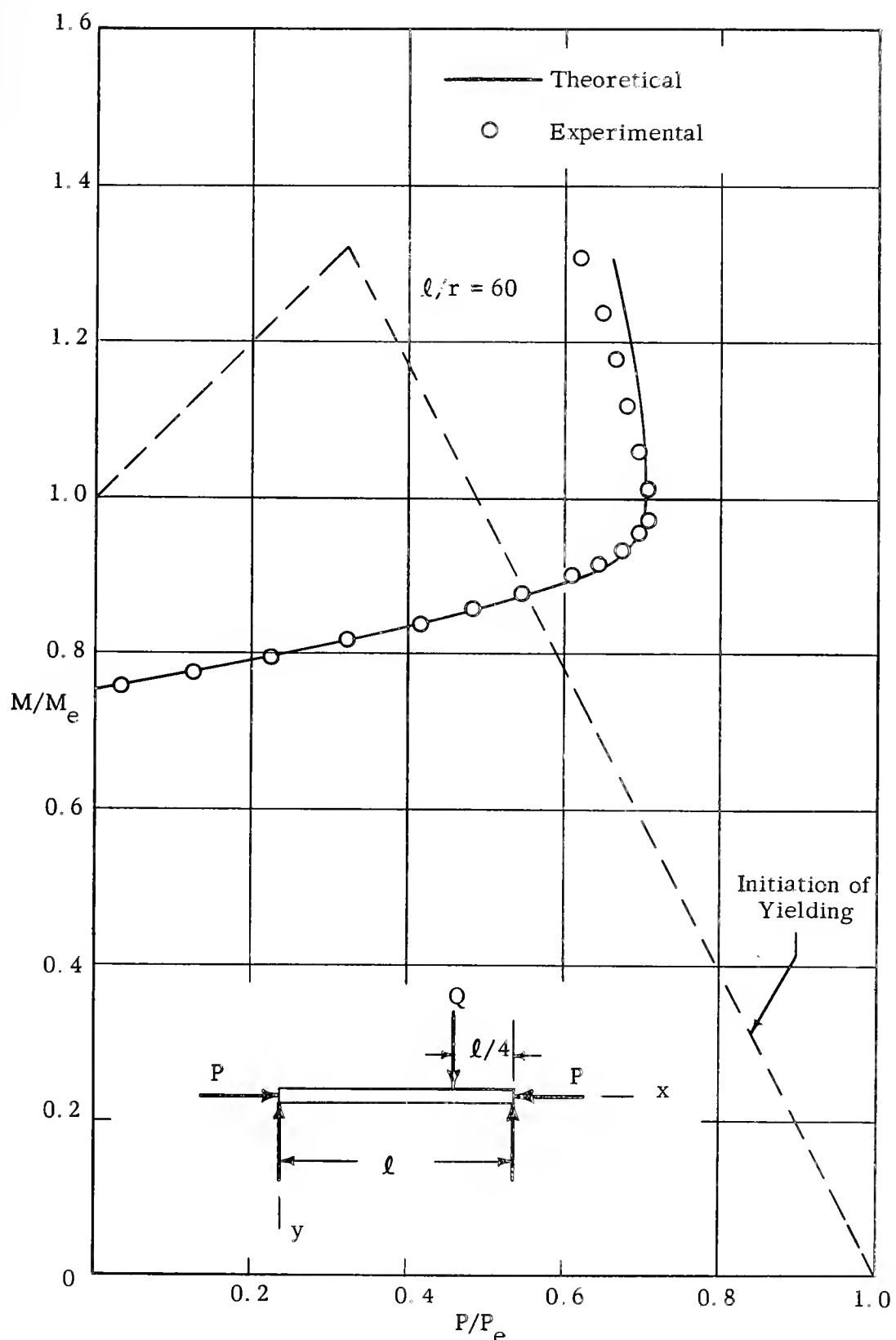


Fig. 26. Moment-Load Curve for an Unsymmetrically Loaded T-Section Beam-Column of SAE 1020 Steel. ( $M_Q/M_e = 0.75$ ;  $e_1 = e_2 = 0$ )



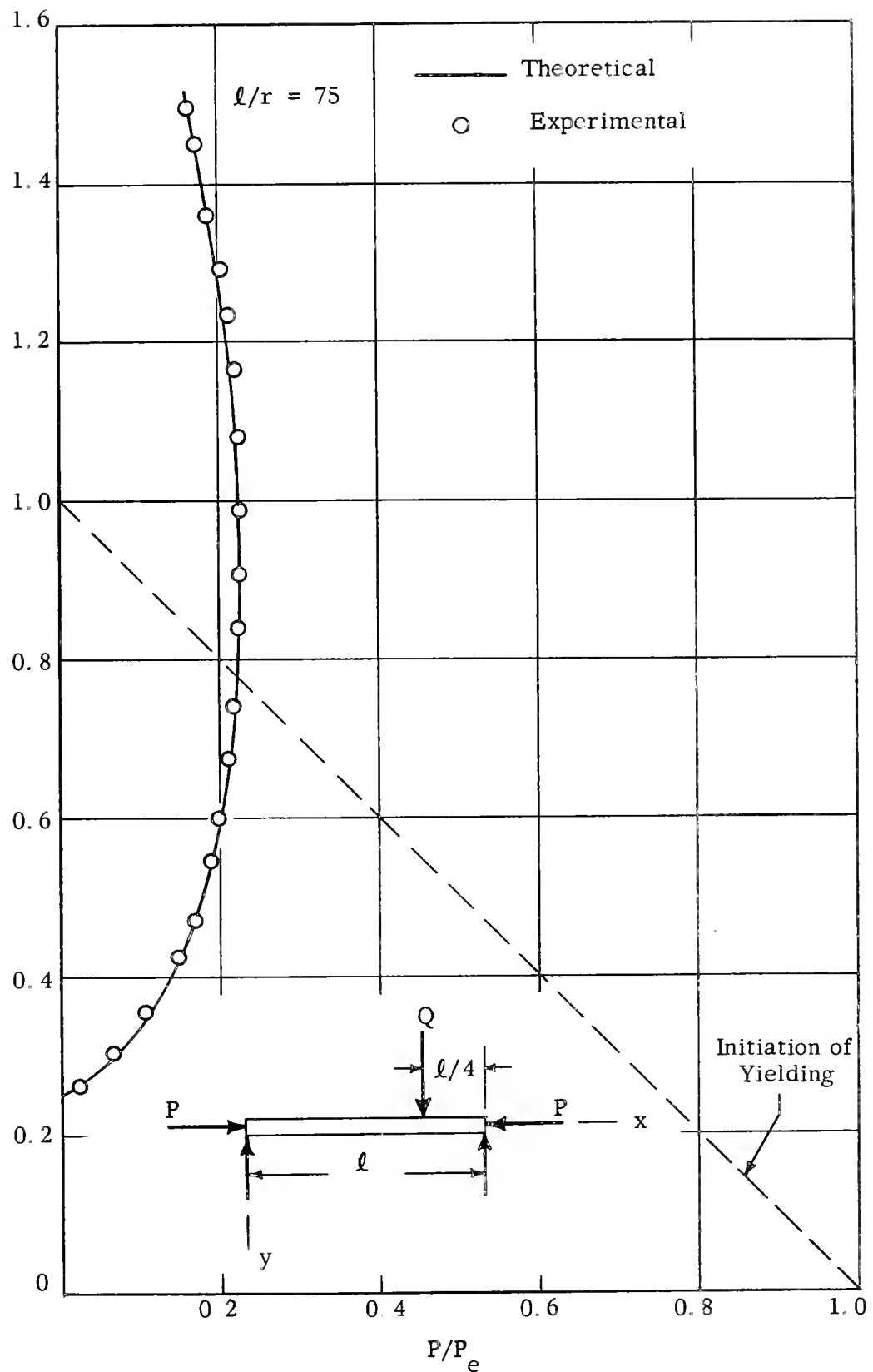


Fig. 27. Moment-Load Curve for Unsymmetrically Loaded, Rectangular 17-7PH Stainless Steel Beam-Columns. ( $M_Q/M_e = 0.25$ ;  $e_1 = e_2 = 0$ )



WADD TECHNICAL REPORT 60-580  
Part V

INELASTIC DESIGN OF LOAD CARRYING MEMBERS  
Part V. Theoretical and Experimental Creep Analyses  
of Beam-Columns

D. L. Dewhirst  
O. M. Sidebottom

Theoretical and Applied Mechanics Department  
University of Illinois

September, 1961

Materials Central  
Contract No. AF 33 (616)-7600  
Project No. 7351

Wright Air Development Division  
Air Research and Development Command  
United States Air Force  
Wright Patterson Air Force Base, Ohio



WADD TECHNICAL REPORT 60-580

Part V

INELASTIC DESIGN OF LOAD CARRYING MEMBERS  
Part V. Theoretical and Experimental Creep Analyses  
of Beam-Columns

D. L. Dewhirst  
O. M. Sidebottom

Theoretical and Applied Mechanics Department

University of Illinois

September 1961

WRIGHT AIR DEVELOPMENT DIVISION



620-1123

22591

v.5

cop.2

Engin  
v

ENGINEERING LIBRARY

## FOREWORD

This report was prepared by the University of Illinois under USAF Contract No. AF 33(616)-7600. This Contract was initiated under Project No. 7351, "Metallic Materials", Task No. 73521, "Behavior of Metals". It was administered under the direction of the Materials Central, Directorate of Advanced Systems Technology, Wright Air Development Division with Mr. R. F. Klinger acting as the Project Engineer.

This is a final report which covers work conducted from October 1, 1960 to September 31, 1961.

The work was conducted in the Department of Theoretical and Applied Mechanics in the Engineering Experiment Station, University of Illinois, Urbana, Illinois. Professor O. M. Sidebottom was the Project Supervisor.



## ABSTRACT

A theory is presented for constructing load-creep deflection curves for beam-columns at any specified time. The stress-strain-time relation for the material is assumed to be represented by an isochronous stress-strain diagram approximated by an arc hyperbolic sine curve (see Equation 16). A program has been written for the IBM 650 digital computer to calculate points on moment-curvature curves for a general I-section. The theory uses these curves and the successive approximations procedure by Newmark (32).

The experimental part of the investigation included tests of rectangular- and T-section beam-columns made of 17-7Ph stainless steel and tested at 972°F. Several slenderness ratios were considered. The beam-columns were subjected to a constant axial load located either at the centroid of the section or at an eccentricity of 15 per cent of its depth and to a constant transverse load at midspan of sufficient magnitude to produce a linear elastic bending stress when acting alone of 0.50  $\sigma_o$ .

## PUBLICATION REVIEW

This report has been reviewed and is approved.

FOR THE COMMANDER:

W. J. Trapp  
Chief, Strength and Dynamics Branch  
Metals and Ceramics Laboratory  
Materials Central



## TABLE OF CONTENTS

	Page
I. INTRODUCTION	1
1. Preliminary Statement	1
2. Purpose and Scope	3
II. THEORY	5
1. Assumptions	5
2. Moment-Curvature Interaction Curves	5
3. Load-Deflection Curves	7
III. MATERIALS AND METHODS OF TESTING	10
1. Materials Used, Test Members, and Testing Procedure	10
2. Properties of Materials	10
3. Method of Loading Beam-Columns	11
IV. ANALYSIS OF RESULTS	12
V. SUMMARY AND CONCLUSIONS	14
1. Summary	14
2. Conclusions	14
BIBLIOGRAPHY	16
APPENDIX A	19



## I. INTRODUCTION

### 1. Preliminary Statement

Since the heating of structural members is unavoidable in many present day engineering applications such as nuclear reactors, missiles, and aircraft, the effect of creep cannot be neglected. One structural element which is important in this respect is the creep behavior of a beam-column. It is the purpose of this paper to present a workable method for the design of beam-columns, whose dimensions and creep properties are known. The term beam-column is applied to a long, slender member which is subjected to transverse as well as axial loads, that is to a member simultaneously performing the function of a beam and column.

The principal difference between the method herein described and the methods used by other authors is the form of the stress-strain-time law adopted. In previous investigations (1-16, 18-22, 24-28)\* including those on beams, columns, and beam-columns, the stress-strain-time law has been represented by one of the following forms:

$$\dot{\epsilon} = B\sigma^n \quad (1)$$

$$\dot{\epsilon} = Ae^{B\sigma} \quad (2)$$

$$\dot{\epsilon} = B \sinh \frac{\sigma}{\sigma_0} \quad (3)$$

$$\dot{\epsilon} = \frac{\dot{\sigma}}{E} + \lambda\sigma^k \quad (4)$$

$$\dot{\epsilon} = A\sigma^m \dot{\sigma} + B\sigma^n \quad (5)$$

$$\dot{\epsilon} = \frac{\dot{\sigma}}{E} + A\sigma^m \dot{\sigma} + B\sigma^n \quad (6)$$

$$\dot{\epsilon} = \frac{\dot{\sigma}}{E} + \frac{\sigma}{\lambda} \quad (7)$$

$$\dot{\epsilon} = \frac{\dot{\sigma}}{E} + \left(\frac{\sigma}{\lambda}\right)^n + \left(\frac{\sigma}{\mu}\right)^m \frac{\dot{\sigma}}{\mu} \quad (8)$$

$$\dot{\epsilon} = \frac{\dot{\sigma}}{E} + \lambda pt^{p-1} \sigma^n \quad (9)$$

$$\dot{\epsilon} = \frac{\dot{\sigma}}{E} + K\sigma^n F(t) \quad (10)$$

---

\*

Numbers in parentheses refer to corresponding entries in the bibliography.

Manuscript released by authors September, 1961, for publication as a WADD Technical Report.



$$\epsilon = \frac{\sigma}{E} + A e^{B\sigma t k} \quad (11)$$

$$\epsilon = (\epsilon_0 + mt^n) \sinh \frac{\sigma}{\sigma_0} \quad (12)$$

$$\epsilon = \epsilon_0 + mt^n \quad (13)$$

$$\epsilon = \frac{\sigma}{E} + K\sigma^a(1-e^{-qt}) + B\sigma^n t \quad (14)$$

$$\sigma = K\epsilon^m \dot{\epsilon}^n \quad (15)$$

In the above,  $\sigma$  denotes stress,  $\epsilon$  denotes strain,  $t$  denotes time and the dot indicates differentiation with respect to time. The remaining symbols are constants, empirically obtained from constant stress creep curves. One of the difficulties in the analysis of the beam column is that no beam fiber is subjected to a constant stress.

In order to overcome this difficulty, several investigators (14, 15, 16, 22, 28) have attempted to follow the stress history of the various fibers of columns or beam columns but have represented the stress-strain-time relation for the material by equation 10 with the experimental constants obtained from constant stress creep curves. Based on a study by Shanley (29), the stress-time curve for a given fiber of the column is represented by infinitesimal steps. Each step consists of a constant stress period of time followed by an instantaneous increment of stress. Libove (14, 15) tested only pin ended columns, and assumed that the inelastic column deformed into a sine curve. Higgins (22) treated only pin ended columns but did not assume a configuration of the inelastic column. His analysis uses an iterative type of numerical solution which requires six or seven 8 hour days on an IBM digital computer. Lin (16, 28) has treated both the column and beam-column. His analysis uses a stepwise method of calculation which is somewhat less involved than Higgins' method. Finnie and Heller (4) have compared creep curves by Lin and Higgins with test data. The agreement was not good.

Instead of predicting the creep curve for a given column, some investigators (30, 33, 34, 35, 38) have considered the problem of predicting the behavior of the column for a specified time. They have represented the stress-strain-time diagram of the material by an isochronous stress-strain diagram of the material obtained by plotting values of stress and strain at a specified time from constant stress creep curves. Carlson and Manning (30) did not represent the isochronous stress-strain diagram by a mathematical function so that a graphical solution is required for each column. Sidebottom, Clark, Costello, Dharmarajan, and Pocs (33, 34, 35, 38) have



assumed that the isochronous stress-strain diagram can be represented by an arc hyperbolic sine curve of the form

$$\sigma = \sigma_0 \operatorname{arc} \sinh \frac{\epsilon}{\epsilon_0} \quad (16)$$

in which  $\sigma_0$  and  $\epsilon_0$  are time dependent as well as temperature dependent constants. It should be noted that Eq. 12 is identical with equation 16 for constant time. Furthermore, equation 16 is an integrated form of equation 3 which has been shown by Kauzmann (31) to have a theoretical basis.

Equation 16 has many advantages. It is readily integrated or differentiated. It is characterized by only two material constants, while most of the equations used in column analyses have three or more. Equation 16 shows extreme versatility. It has been successfully applied to multiaxial state of stress problems (35, 39) in addition to beams and columns. Equation 16 will be adopted in this investigation.

Theories based on equation 16 have the same limitations as all other theories in that the experimental constants are obtained from constant stress creep curves while stresses in columns and beam-columns are not independent of time. The theory must be corrected if the behavior of the column or beam-column is to be predicted. In the case of columns, several different variables have been investigated and the correction needed to predict the collapse load at any specified time has been found to be independent of the type of variable. The only correction needed was to increase  $\sigma_0$  by 10 per cent. It is believed that this correction will be satisfactory for the beam column if the column action is predominant.

## 2. Purpose and Scope

The purpose of this investigation is to develop a theory to predict the load-creep deformation curve and the collapse load at any specified time for columns and beam-columns subjected to any given loading condition. The validity of the theory has been checked by tests of 17-7PH stainless steel beam-columns at 972°F.

A program was written for the IBM 650 digital computer to determine points on the moment-curvature diagram. This program is valid for the general I-section which includes the rectangular and T-sections as special cases. Using the method of successive approximations due to N. M. Newmark (32), the load-deflection curve



for a given column or beam-column with any loading can be constructed as accurately as desired. Furthermore, the resulting load-deflection curve is independent of the properties of the material so that it can be used to predict the deflection at any load and the collapse load at any time for which values of  $\sigma_o$  and  $\epsilon_o$  are known.

The experimental part of the investigation included tests of rectangular- and T-section pivot ended beam-columns of 17-7PH stainless steel tested at an elevated temperature of  $972^{\circ}\text{F}$ . These columns had slenderness ratios of 50.0, 60.2, 75.0, and 100.0. Each column was subjected to a constant transverse load at the center of the column of sufficient magnitude to produce a maximum linear elastic bending stress equal to  $\sigma_o/2$ . The axial load was also held constant and was of sufficient magnitude to cause collapse of each beam-column in 30 minutes. The axial load was applied through the centroid of the cross section or with eccentricity equal to 15 per cent of the depth.

Good agreement was found between theory and experiment.



## II. THEORY

### 1. Assumptions

Theoretical load-deflection curves for columns and beam-columns are constructed using a family of moment-curvature interaction curves for constant values of load. The derivation of these curves are based on the following assumptions:

1. Plane cross-sections remain plane and do not warp with time. The validity of this assumption for pure bending has been shown independently by at least two investigators, MacCollough (17) and Tapsell and Johnson (23). Presumably the assumption is poor only for short deep beams when shear stresses are high.

2. The stress-strain-time relationship for the material is given by the isochronous stress-strain relation represented by Equation 16. Since the beam fibers do not experience a constant stress, this relationship is in error. Previous investigations (34, 38) have shown that use of the arc hyperbolic sine relationship for eccentrically loaded columns predicts a collapse load which is ten per cent too small.

3. The experimental constants  $\sigma_o$  and  $\epsilon_o$  are assumed to be the same for tension and compression. If the creep properties are different for tension and compression, the compression properties should generally be used, since compressive stresses are appreciably greater than the tensile stresses in most columns and beam-columns. If the stresses due to the axial load are small compared to the bending stresses,  $\sigma_o$  and  $\epsilon_o$  can be based on the average isochronous stress-strain diagram.

4. The material is assumed to be isotropic and homogeneous.

### 2. Moment-Curvature Interaction Curves

Consider the general I-section member shown in Figure 1 which is subjected to an axial load  $P$ , and to a bending moment  $M$  locating the neutral axis at a distance  $q_h$  from the most strained fibers. With the strain distribution known, the stress distribution is obtained using equation 16, and the magnitude of  $P$  and  $M$  can be determined from the equations of equilibrium:

$$P = \int \sigma dA \quad (17)$$

$$M = \int (y - d) \sigma dA \quad (18)$$

Equations 17 and 18 integrate into the following equations:

$$P = \frac{\sigma_o q h^2}{K} \left[ b_1 B_K - b_4 \frac{B_{1-q}}{q} K - b_2 \frac{B_{q-u}}{q} K + b_3 \frac{B_{q-v}}{q} K \right] \quad (19)$$

$$M = \frac{\sigma_o q^2 h^3}{K^2} \left[ b_1 C_K - b_4 C_{\frac{1-q}{q} K} - b_2 C_{\frac{q-u}{q} K} + b_3 C_{\frac{q-v}{q} K} \right] - (q - \beta) Ph \quad (20)$$



in which  $K = \epsilon_1/\epsilon_o$ . In these equations, the functions  $B_N$  and  $C_N$  are defined as follows:

$$B_N = N \log_e (N + \sqrt{N^2 + 1}) - \sqrt{N^2 + 1} \quad (21)$$

$$C_N = \frac{1}{4} \left[ (1 + 2N^2) \log_e (N + \sqrt{N^2 + 1}) - N \sqrt{N^2 + 1} \right] \quad (22)$$

$N$  represents the various subscripts for  $B$  and  $C$  in equations 19 and 20.

If the deformations are considered small, the curvature can be written in terms of the strain distribution, shown in Figure 1 to give :

$$\frac{d^2y}{dx^2} = \psi = \frac{1}{R} = \frac{\epsilon_1}{qh} = \frac{K\epsilon_o}{qh} \quad (23)$$

It is convenient to define the cross sectional area  $A$ , by the relation:

$$A = Dh^2 \quad (24)$$

and rewrite equations 19, 20 and 24 in dimensionless form as follows:

$$\frac{P}{A\sigma_o} = \frac{q}{KD} \left[ b_1 B_k - b_2 \frac{B_{q-u}}{q} K + b_3 \frac{B_{q-v}}{q} K - b_4 \frac{B_{q-1}}{q} K \right] \quad (25)$$

$$\frac{M}{A\sigma_o h} = \frac{q^2}{DK^2} \left[ b_1 C_K - b_2 \frac{C_{q-u}}{q} K + b_3 \frac{C_{q-v}}{q} K - b_4 \frac{C_{q-1}}{q} K \right] - \frac{(q-\beta)P}{A\sigma_o} \quad (26)$$

$$\frac{h\psi}{\epsilon_o} = \frac{K}{q} \quad (27)$$

It will be noted that the right sides of equations 25, 26 and 27 are functions of  $q$  and  $K$  and are independent of the properties of the material and of the magnitude of the relative dimensions of the cross-section. A trial and error solution is required if a dimensionless moment-curvature curve for a specified load is required. A program has been written for the IBM 650 digital computer to make the necessary calculations. A description of this program is given in Appendix A.

The dimensionless moment-curvature curves for the rectangular-section ( $b_1=b_4=D, b_2=b_3=0$ ) are shown in Figure 2 and for the T-section ( $b_1=\frac{2}{3}, b_2=\frac{1}{2}, b_3=0, b_4=\frac{1}{6}$ ,  $u=\frac{1}{4}, v=0$ ) are shown in Figure 3.



Although an IBM 650 digital computer program was written for the general I-section, similar programs could be written for any cross-section made up of a finite number or rectangular elements.

### 3. Load-Deflection Curves

The load-deflection curve for a given column or beam-column subjected to any general loading can be computed by a method of successive approximations (32) provided moment-curvature curves for the given column cross-section are known. See Figures 2, 3, and 4. In order to illustrate the procedure, a point on the load-deflection curve will be computed for the T-section beam-column used in this investigation.

Consider the T-section beam-column shown in Figure 4. For convenience in the calculation of the deflection, the depth is assumed to be unity. The magnitudes of the dimensionless coefficients in Figure 1 are  $b_1 = \frac{2}{3}$ ,  $b_2 = \frac{1}{2}$ ,  $b_3 = 0$ ,  $b_4 = \frac{1}{6}$ ,  $u = \frac{1}{4}$ ,  $v = 0$ , and  $\beta = 0.3393$ . For a slenderness ratio of 60.2, its length is 17.46 inches.

The beam-column is subjected to a concentrated load  $Q$  at its midpoint and to an axial load  $P$  at an eccentricity of 15 per cent of its depth. Since the deflections are symmetric about the center, only half of the column need be considered. The beam-column has been arbitrarily divided into eight equal segments  $\lambda = l/8$ , the endpoints of which specify station points a, b, c, d and f. The dimensionless moments due to  $Q$ ,  $M_Q/\sigma_o Ah$ , have been computed for the specified locations and are shown in Figure 4. For this example,  $P$  is taken of sufficient magnitude to make  $P/\sigma_o A = 0.7$ . The moments due to  $P$  depend upon the unknown deflections. The first step in determining the deflections is to assume a reasonable value for the deflection at each station point. The initially assumed deflections shown in Figure 4 are calculated using the deflection formula for a linear elastic beam-column with  $E = \sigma_o/\epsilon_o$ . The dimensionless moments  $M_P/\sigma_o Ah$  are computed and added to  $M_Q/\sigma_o Ah$  to obtain the total moment  $M/\sigma_o Ah$ . For each dimensionless moment, the dimensionless curvature,  $h\psi/\epsilon_o$ , is obtained from the curve for  $P/A\sigma_o = 0.7$ , Figure 3. Since the curvature is equal to the angle change per unit length, the curvature diagram is sometimes called the angle-change diagram. Using the conjugate beam method, deflections are calculated by loading the beam through stringers with the curvature diagram. The number of stringers used corresponds to the number of segments into which the beam is broken, in our case eight. By equations of statics, the concentrated curvature (i.e. finite angle change) at each station point can be calculated. This is analogous to the process of finding a reaction force on a stringer. Assuming the curvature to vary parabolically between any three station points, this gives:



$$\psi_a = \frac{\epsilon_0 \lambda}{24} (7a + 6b - c)$$

and

$$\psi_b = \frac{\epsilon_0 \lambda}{12} (a + 10b + c)$$

where  $\psi$  is the equivalent concentrated curvature, or finite change of angle, at the station point denoted by the subscript.

Since the member is assumed to be made up of infinitely stiff segments of length  $\lambda = \frac{\ell}{8}$  with concentrated angle-changes at each station point, the slope of each segment is easily computed. The slope is zero at the center so that the slope of the segment from a to b is  $22.5 \epsilon_0 \lambda / 12$ . The slope for the adjacent segment is equal to the slope of segment a to b plus the angle change at b. In this way the slope for each segment can be calculated. Beginning at the left hand reaction f where the deflection is zero, the deflection of the adjacent station point d is seen to equal the product of the segment length and slope. The deflection of the next station point is equal to this deflection plus the product of its segment length and slope, i.e.

$$\delta_c = 126.4 \epsilon_0 \lambda^2 / 12 + \lambda (100.0 \epsilon_0 \lambda / 12) = 226.4 \epsilon_0 \lambda^2 / 12$$

Using the material properties listed in Figure 8, the deflections are computed and compared to the assumed deflections.

The calculated deflections do not coincide with the assumed values so that another set of assumptions must be made. The calculated deflections may be used as a closer approximation to the real deflections and the computations repeated. However, the number of trials can be greatly reduced by doubling the correction. For instance the deflection at the center was 0.017 inches greater than that assumed. For the next trial assume the center deflection to be :

$$\delta_A = 0.125 + 2 \times 0.017 = 0.159 \text{ in.}$$

Let the other deflections be increased in the same proportion, i. e.:

$$\delta_b = \frac{0.132}{0.142} \times 0.159 \text{ in.}$$

The calculated deflections for the second trial are nearly identical with the assumed deflections so that only two trials are required. The above calculations locate one point on the dimensionless load-deflection curve shown in Figure 5.

There are some features to be noted for the convergence of the iteration procedure. If the assumed deflection locates a point below the curve, the calculated deflection is



less than the assumed. Above the curve, the calculated deflection is greater than the assumed. Therefore, if the assumed deflection is below or to the left of the actual deflection curve, the numerical procedure will converge to the pre-collapse deflection. The procedure always diverges from the post-collapse deflection.

Since the load-deflection curve can be presented in this dimensionless form, it is independent of the material. It is valid for any material whose isochronous stress-strain diagram is adequately represented by Equation 16. It can be used to determine the collapse load for any magnitude of time for which values of  $\sigma_0$  and  $\epsilon_0$  are known.



### III. MATERIALS AND METHOD OF TESTING

#### 1. Materials Used, Test Members, and Testing Procedure

All test members were machined from a 1/2 inch by 2 inch bar of 17-7PH stainless steel. The compression specimens had square cross sections, 1/2 inch on a side. The columns had rectangular or T-shaped cross sections with lengths and depths as indicated in Table 1.

The T-section beam-columns were machined before being precipitation hardened, while the rectangular section test members were machined after the heat treatment. The specimens were heated to 1400°F. for 90 minutes, cooled to 60°F. in 60 minutes, held at this temperature for 30 minutes, then heated to 1050°F. for 90 minutes, and finally air cooled.

All of the test members were loaded in a Riehle testing machine of 120,000 pound capacity. The machine was equipped with a load holder to maintain any desired load.

Temperatures were measured by vertically spaced thermocouples along the test specimens. Two thermocouples were used on the short compression specimens, while three were used on each of the beam-columns. A piece of asbestos was used to cover each thermocouple as it was attached to the test member. An asbestos shield was placed between the test member and the heating coils, and baffles were placed in the furnace to prevent a chimney effect. Approximately one hour was necessary to bring the furnace up to temperature. The temperature was manually controlled and maintained at 972°F.  $\pm$  2°F. Deformation readings were started as soon as the load was applied, and were taken every minute thereafter.

#### 2. Properties of Materials

Compression creep properties were obtained for the 17-7PH stainless steel at 972°F. The fixtures and furnace used in making the compression tests are shown in Figure 6. The deformations were measured with a Riehle dial-type high temperature creep extensometer with a 2 inch gage length. The compression creep curves for the material are shown in Figure 7. From these creep curves, corresponding values of stress and strain were obtained for zero time, for 30 minutes, and for 60 minutes to give the isochronous stress-strain diagrams shown in Figure 8. An arc hyperbolic sine curve (Equation 16) was fitted to the data for 30 minutes. The pertinent material properties for the material are listed in Figure 8.

The heat treatment of the material used in this investigation was carried out at a temperature 15 to 30°F. higher than in previous investigations (33, 34). This is be-



lieved to account for a slightly higher value of  $\sigma_0$  than before. Also, the data for zero time in Figure 8 indicates that some inelastic deformation occurred before the test load was reached, whereas in the previous tests on eccentrically loaded columns, the load deformation curve remained linear for zero time.

### 3. Method of Loading Beam-Columns

The fixtures used in loading the beam-columns, the furnace and the 1/1000 inch dial indicator are shown in Figure 9. The transverse load was applied by means of dead weights attached to a wire, which passed over the pulley arrangement seen at the right of the figure. The axial load was applied to the beam-columns through the knife edge fixtures illustrated in Figure 10. The length of each knife edge was 2 inches. This fixture added 0.60 inches to each end of the beam-column.

In order to offset the effect of any initial crookedness in the beam column, the eccentricity was measured with respect to its midpoint. The error in measuring the eccentricity is believed to be less than plus or minus 0.002 inches.



#### IV. ANALYSIS OF RESULTS

A total of twenty-one beam-columns were subjected to constant axial and lateral loading at 972°F. Four different slenderness ratios, and two types of cross-section were considered.

Eighteen of the beam-columns had rectangular cross sections. These were split into three groups of six each with slenderness ratios of 50.0, 75.0, and 100.0. Half of each group were tested with the axial load applied through the centroid of the section, zero initial eccentricity, while the other half were subjected to an axial load with 15 per cent initial eccentricity. The deflection-time curves for these beam-columns are shown in Figures 11 and 12.

The deflection-time curves for the three T-section beam-columns are shown in Figure 13. Each T-section beam-column had a slenderness ratio of 60.2. As noted in Figure 15, two of these had zero initial eccentricity, and the other had an initial eccentricity of 15 per cent of its depth.

The deflection of each beam-column is shown in dimensionless form in Figures 14 through 17. The initial deflection, the maximum deflection, and one half maximum deflection are given. The theoretical load-deflection curves for zero time shown in these figures are based on the assumption that the material behaves elastically with  $E = \sigma_0 / \epsilon_0$  (37). The actual test data falls to the right of these curves since the material did not behave elastically while coming up to test load.

The theoretical load-deflection curves for 30 minutes, shown in Figures 14 through 17 were constructed using the arc hyperbolic sine theory presented in Section II. Since the creep curves in Figures 11, 12 and 13 indicate that the deflection of the beam-column immediately prior to collapse was independent of the time to collapse, the experimental deflection may be compared with the theory for 30 minutes. It will be noted that the deflections of the beam-columns corresponding to one half the maximum deflections are approximately equal to the deflections at the peaks of the theoretical load-deflection curves. The theoretical deflection at the collapse load is not highly accurate while for loads appreciably below the collapse load the theoretical creep deflections are small and quite close to the experimental values. This discrepancy between the predicted and experimental values of the deflection at the collapse load is not considered significant, since it is the buckling load which is of primary importance.

Experimental values of  $P/A$  are listed in Table 1 for all of the beam-columns along with the time to collapse. Also listed in Table 1 are computed values of  $P/A$  necessary to cause each beam-column to collapse in 30 minutes. The per cent difference between the theoretical collapse load at 30 minutes and the theoretical collapse



load at other values of time was plotted as a function of time. The appropriate per cent difference was applied to the test load to obtain the adjusted load.

Ratios of the theoretical to experimental collapse loads for 30 minutes are listed in Table 1 for each beam-column. The theory ranged from 6 per cent conservative to 12 per cent nonconservative, with an average of 2.6 per cent nonconservative. None of the variables considered indicated any particular trend. The scatter was no more pronounced for the beam-columns than for the creep specimens. (See Figure 7).



## V. SUMMARY AND CONCLUSIONS

### 1. Summary

A method is presented for predicting the load-deflection relationship and the collapse load for beam-columns subject to creep. This method makes use of:

- a) a stress-strain-time relation which is obtained by fitting the arc hyperbolic sine equation to the isochronous stress-strain data.
- b) a set of dimensionless moment-curvature interaction curves. The IBM 650 digital computer was used to facilitate the construction of these curves.
- c) a method of successive approximations (32) for obtaining the load-deflection relationship.

To check the accuracy of the method developed, several tests were made on beam-columns at elevated temperature. In all, twenty-one 17-7PH stainless steel beam-columns were tested to collapse, at a constant temperature of 972°F. T-section beam-columns having a slenderness ratio of 60.2 and rectangular-section beam-columns having slenderness ratios of 50.0, 75.0, or 100.0 were used. Each beam-column was subjected to a concentrated load at midspan and a constant axial load having an initial eccentricity of zero or 15 per cent of its depth.

### 2. Conclusions

1. The arc hyperbolic sine function (Equation 16) adequately represents the isochronous stress-strain diagram for 17-7PH stainless steel at 972°F for a time duration of thirty minutes.

2. Since the effect of stress redistribution with time is not directly considered in the theory, it is recommended that the experimental constant  $\sigma_0$  be increased by ten per cent when calculating the collapse load or the load-deflection relationship. This empirical correction is in agreement with the results of previous investigations on eccentrically loaded columns (34, 36).

3. The IBM 650 digital computer can be conveniently used to calculate points for dimensionless moment-curvature interaction curves. A program is included in the appendix, which is valid for a general I-section. This includes the T-section and rectangular-section as special cases. Approximately five to fifteen minutes was required for the machine to make the computations for the particular cross-sections considered in this investigation.

4. Since the dimensionless load-deflection relationship is independent of the numerical values of  $\sigma_0$  and  $\epsilon_0$ , these theoretical dimensionless load-deflection curves are independent of both time and material.



5. Test data from the twenty-one beam-columns indicated that the theory ranged from 6 per cent conservative to 12 per cent nonconservative in predicting the collapse load for thirty minutes. The theory averaged 2.6 per cent nonconservative. No trend was noted for any of the variables investigated. The scatter was of approximately the same magnitude as that exhibited by the compression creep data.



## BIBLIOGRAPHY

1. Bleich, H. H. & Dillon, D. W. Jr., "Deformation of Columns of Rectangular Cross Section", Journal of Applied Mechanics, December 1959, pages 517-525.
2. Davis, E. A., "Creep of Metals at High Temperatures in Bending", Journal of Applied Mechanics 5, A-29. (1938).
3. Findley, W. N. and Pocztak, J. J., "Prediction of Creep Deflection and Stress Distribution in Beams from Creep in Tension", Journal of Applied Mechanics, Vol. 77, 1955, pages 165-171.
4. Finnie, I. and Heller, W. R., "Creep of Engineering Materials", McGraw-Hill Book Company, 1959.
5. Freudenthal, A. M., "The Inelastic Behavior of Engineering Materials and Structure", John Wiley & Sons, 1950, First Edition, page 516.
6. Gerard, G., "A Creep Buckling Hypothesis", Journal Aeronautical Science, Vol. 23, September 1956, page 879.
7. Hilton, H. H., "Creep Collapse of Columns With Initial Curvature", Journal Aeronautical Science, Vol. 19, December 1952, pages 844-846.
8. Hoff, N. J., "A Survey of the Theories of Creep Buckling", Proceedings of the Third U. S. National Congress of Applied Mechanics, pages 29-49.
9. Hoff, N. J., "Rapid Creep in Structures", Journal Aeronautical Science, October 1955.
10. Hu, L. W. and Triner, N. H., "Bending Creep and Its Applications to Beam Columns", Journal Applied Mechanics, Transactions A.S.M.E., Vol. 78, pages 35-42.
11. Kempner, J., "Creep Bending and Buckling of Nonlinearly Viscoelastic Columns", N.A.C.A. Technical Note 3137, January 1954.
12. Kempner and Patel, "Creep Buckling of Columns", N.A.C.A. Technical Note 3138, 1954.
13. Kempner, J., "Creep Bending and Buckling of Linearly Viscoelastic Columns", N.A.C.A. Technical Note 3136, 1954.
14. Libove, C., "Creep Buckling of Columns", Journal Aeronautical Science, July 1952, Vol. 19, No. 7.
15. Libove, C., "Creep Buckling Analysis of Rectangular Section Columns", N.A.C.A. Technical Note 2956, June 1953.
16. Lin, T. H., "Creep Deflections and Stresses of Beam Columns", Journal Applied Mechanics, March 1958, pages 75-77.



17. MacCullough, G. H., "An Experimental and Analytical Investigation of Creep in Bending", Transactions A.S.M.E., Vol. 55, APM-55-9, 1933.
18. Marin, Joseph, "Creep Deflections in Columns", Journal of Applied Physics, Vol. 18, No. 1, January 1947, pages 103-109.
19. Marin and Hu, "Deflection of Members Subjected to Bending Accompanied by Creep", Proceedings of First National Congress of Applied Mechanics, 1952, pages 613-618.
20. Pao, Yoh-Han and Marin, J., "Deflections and Stresses in Beams Subject to Bending and Creep", Journal Applied Mechanics, Vol. 74, 1952, pages 478-484.
21. Sanders, J. L. Jr., "A Variational Theorem for Creep with Applications to Plates and Columns", N.A.C.A. Technical Note 4003, 1957.
22. Shanley, F. R., "Weight-Strength Analysis of Aircraft Structures", Dover Book 1960, pages 369-384.
23. Tapsell, H. J. and Johnson, A. E., "An Investigation of the Nature of Creep Under Stress Produced by Pure Flexure", Institute of Metals Journal, Vol. 57, August 1935, page 121.
24. Johnson, A. E., Mathur, V. D. and Henderson, J., "The Creep Deflexion of Magnesium Alloy Struts", Aircraft Eng., 28: 419, 1956.
25. Odqvist, F. K. G., "Influence of Primary Creep on Column Buckling", Journal Applied Mechanics, 22: 295, 1954.
26. Hult, J. A. H., "Critical Time in Creep Buckling", Journal Applied Mechanics, 22: 432, 1955.
27. Hoff, N. J., "Creep Buckling", Aeronautical Quarterly, 7:1, 1956.
28. Lin, T. H., "Creep Stresses and Deflections in Columns", Journal of Applied Mechanics, Transactions A.S.M.E., Vol. 78, 1956, pages 214-218.
29. Shanley, F. R., "Weight-Strength Analysis of Aircraft Structures", Dover Book 1960, pages 263-305.
30. Carlson, R. L. and Manning, G. K., "A Summary of Compressive-Creep Characteristics of Metal Columns at Elevated Temperatures", WADC Technical Report 57-96, 1958.
31. Kauzmann, W., "Flow of Solid Metals from the Standpoint of the Chemical Rate Theory", Transactions American Institute of Mining and Metallurgical Engineering, Institute of Metals Division, Vol. 143, 1941, page 57.
32. Newmark, N. M. "Numerical Procedure for Computing Deflection, Moments and Buckling Loads", Proceedings of A.S.C.E., Vol. 68, 1942, pages 691-718.
33. Sidebottom, O. M., Costello, G. A., Dharmarajan, S., "Theoretical and Experimental Analyses of Members Made of Materials that Creep", University of Illinois Experiment Station Bulletin No. 460.



34. Costello, G. A., Sidebottom, O. M. and Pocs, E., "Inelastic Design of Load Carrying Members", Theoretical and Applied Mechanics Report 178, "Effect of End Conditions on the Collapse of Load Carrying Members".
35. Dharmarajan, S. and Sidebottom, O. M., "Inelastic Design of Load Carrying Members", Theoretical and Applied Mechanics Report 174, "Theoretical and Experimental Analyses of Circular Cross-Section Torsion-Tension Members Made of Materials that Creep".
36. Gubser, J. L., "Theoretical and Experimental Analysis of Eccentrically Loaded 17-7PH Stainless Steel Columns at 1000<sup>o</sup>F", Unpublished Master's Thesis, University of Illinois, 1959.
37. Timoshenko, S. P. and Gere, J. M., "Theory of Elastic Stability", Second Edition, McGraw Hill Book Co., 1961.
38. Sidebottom, O. M., Clark, M. E. and Dharmarajan, S., "The Effects of Inelastic Action on the Resistance to Various Types of Loads of Ductile Members Made from Various Classes of Metals -- Part VIII Eccentrically-Loaded Tension Members Made of Two Stainless Steels Tested at Elevated Temperatures", WADC Technical Report 56-330, April 1958.
39. Schweiker, J. W., "Creep of Thick-Walled Cylinders Under Internal Pressure and Axial Load", Unpublished Ph.D. Thesis, University of Illinois, 1961.



## APPENDIX A

The purpose of this appendix is to present a program for the IBM 650 digital computer for computing points on constant load moment-curvature interaction curves. Relations expressing dimensionless load, dimensionless moment, and dimensionless curvature as functions of the cross section (see Figure 1) and of the variables  $K$  and  $q$  are given by equations 25, 26 and 27. Before starting the program it was necessary to decide on limits for  $K$  and  $q$  and the dimensionless load  $P/A\sigma_0$ . Dimensionless moment-curvature interaction curves were constructed for dimensionless load increments of 0.1 as the dimensionless load varied from 0.2 to 2.0. At each load, a moment and curvature were computed for each value of  $K$  which was applicable; the values considered were 1, 1.5, 2, 2.5, 3, 4, 5, 7, 9, 12, and 15. The magnitude of  $q$  was limited by considering only those values which would make  $1/q$  greater than 0.60.

Figure 18 shows the flow diagram for the IBM 650 digital computer program. It will be noted that there are three different dimensionless loads listed.  $P_b/A\sigma_0$  is the dimensionless load for which values of dimensionless moment and curvature are desired;  $P_a/A\sigma_0$  is the dimensionless load calculated for assumed values of  $K$  and  $1/q$ ;  $P_c/A\sigma_0$  is the dimensionless load calculated for previously assumed values of  $K$  and  $1/q$ .

The procedure followed in the computations can best be illustrated by considering Figure 19 which is a plot of  $P/A\sigma_0$  versus  $1/q$  for a rectangular-section. Consider the problem of calculating the first point on the moment-curvature interaction curve for  $P_b/A\sigma_0 = 0.7$ . The load  $P_1/A\sigma_0$  is computed for initial values of  $K$  and  $1/q$  of 1 and 0.6 respectively. Since this load is below the desired load, the next value of  $K$  is considered. This determines  $P_2/A\sigma_0$ . This load is above the desired load so that increments of 0.12 are added to  $1/q$  to calculate  $P_3/A\sigma_0$ ,  $P_4/A\sigma_0$ , and  $P_5/A\sigma_0$  which is below the desired load. This value of load is placed in the location of  $P_c/A\sigma_0$  and an increment of 0.04 is subtracted from  $1/q$  to compute  $P_6/A\sigma_0$ . Since this load is above the desired load, a linear interpolation between  $P_5$  &  $P_6$  is used to calculate the desired  $1/q$ . With  $K$  and  $1/q$  known, the dimensionless moment and curvature are calculated.

Table 2 lists the entire program except for the square root (FLSQR) and  $\log_e$  (FLLNX) subroutines. To describe important steps in the program, notes have been placed on the printed program. These notes correspond to the following commentary:

NOTE 1. Three cards are read into the immediate access storage to locate constants



which are valid for all the cross sections.

Card 1		Card 2		Card 3	
Location	Constant	Location	Constant	Location	Constant
9000	K = 1	9008	K = 9	9010	K = 15
9001	K = 1.5	9009	K = 12	9011	1/q = 0.6
9002	K = 2			9012	$\Delta 1/q = 0.12$
9003	K = 2.5			9013	$\Delta 1/q = 0.04$
9004	K = 3			9014	$P/A\sigma_o = 0.2$
9005	K = 4			9015	$\Delta P/A\sigma_o = 0.1$
9006	K = 5				
9007	K = 7				

NOTE 2. One card is read into the immediate access storage to locate constants which are peculiar to a given cross section.

#### Card 4

Location	Constant
9020	-u
9021	-v
9022	b <sub>1</sub>
9023	b <sub>2</sub>
9024	b <sub>3</sub>
9025	b <sub>4</sub>
9026	D
9027	$\beta$

NOTE 3. Initial values for load, 1/q and index registers A, B and C are set. Index register A is used to keep track of the four values of  $B_N$  and  $C_N$  in Equations 25 and 26. Index register B specifies the particular value of K being used in the calculations. Index register C is set to zero after each interpolation to indicate final calculations.

NOTE 4. This is a subroutine to solve Equations 21 and 22 for the four values of N in Equations 25 and 26.



NOTE 5. Absolute values of N (except for  $N = K$ ) are calculated and sent to the subroutine to solve Equations 21 and 22. (See NOTE 4.).

NOTE 6. Equation 25 is solved. Calculations were made for the rectangular section at the first location in the program and for the I-section at the second location.

NOTE 7. Index register C is checked for zero. If zero, go to NOTE 11. If not zero, the difference between  $P_a/A\sigma_o$  and  $P_b/A\sigma_o$  is computed. (Go to NOTE 8.).

NOTE 8. The upper accumulator is checked for negative. If  $P_a/A\sigma_o < P_b/A\sigma_o$ , the difference between  $P_c/A\sigma_o$  and  $P_b/A\sigma_o$  is computed. (Go to NOTE 10.).

NOTE 9. The upper accumulator is checked for zero. If zero, index register B is increased by one to give new value of K and Equations 21 and 22 are solved for four new values of N. If non-zero,  $1/q$  is decreased by 0.04,  $P_c/A\sigma_o$  is set equal to  $P_a/A\sigma_o$ , index register A is set to -2 so as to solve Equations 21 and 22 for three new values of N.

NOTE 10. The upper accumulator is checked for negative. If positive,  $1/q$  is increased by 0.12, index register A is set to -2 so as to solve Equations 21 and 22 for three new values of N. If negative, interpolate to obtain correct value of  $1/q$ , increase index register C by 1, set index register A to -2 so as to solve Equations 21 and 22 for three new values of N.

NOTE 11. The dimensionless load,  $P_a/A\sigma_o$ , is stored in a print location. The dimensionless curvature,  $h\psi/\epsilon_o$ , is computed and stored in a print location. The two values of N (see Equations 21 and 22) may be negative. Each of these is checked for sign and  $C_{|-N|}$  is made negative. The dimensionless moment,  $M/\sigma_o Ah$ , is computed and stored in a print location.

NOTE 12. The computer is directed to print the results for one point on one interaction curve. Then index register B is increased by one.

NOTE 13. Index register B is checked for zero. If not zero,  $1/q$  is increased by 0.12 and the computations are repeated. If zero, the difference between  $P_b/A\sigma_o$  and 2.0 is computed.

NOTE 14. The upper accumulator is checked for negative. If negative,  $P_b/A\sigma_o$  is increased by 0.1 and the computations are repeated. If not negative, the computer is ordered to stop. If the stop is ignored, a new No. 4 card is read and computations are repeated for a new cross-section. Computations will continue until all of the No. 4 cards are used up.



Table I  
Comparison of Theoretical and Experimental Collapse Loads  
for Beam-Columns at 972°F

Column Number	Column Depth in.	$\frac{\ell}{r}$	e/h %	Time min.	$\frac{M_Q}{\sigma_{Qh}} \%$	Actual	Experimental Adjusted to 30 min psi	P exp. /P theo.
Rectangular-Section Beam-Columns								
1	0.500	50.0	0	51	50	33,150	35,640	1.06
2	0.500	50.0	0	39	50	34,070	35,130	1.05
3	0.500	50.0	0	26	50	34,950	34,460	1.03
4	0.500	50.0	15	38	50	22,120	22,770	0.97
5	0.500	50.0	15	23	50	23,450	22,850	0.97
6	0.500	50.0	15	16	50	23,450	21,650	0.92
7	0.420	75.0	0	34	50	19,880	20,120	1.01
8	0.420	75.0	0	34	50	19,880	20,120	1.01
9	0.420	75.0	0	14	50	20,950	19,000	0.95
10	0.420	75.0	15	30	50	14,400	14,400	0.98
11	0.420	75.0	15	50	50	14,400	15,420	1.05
12	0.420	75.0	15	13	50	15,240	13,680	0.93
13	0.420	100.0	0	16	50	12,380	11,420	0.93
14	0.420	100.0	0	9	50	13,020	10,830	0.88
15	0.420	100.0	0	8	50	13,750	11,240	0.92
16	0.420	100.0	15	38	50	9,890	10,170	1.05
17	0.419	100.0	15	21	50	10,170	9,800	1.02
18	0.420	100.0	15	13	50	10,450	9,250	0.96
T- Section Beam-Columns								
19	0.600	60.2	0	14	50	31,000	27,900	0.88
20	0.600	60.2	0	15	50	32,300	29,400	0.93
21	0.600	60.2	15	32	50	20,000	20,100	0.96



Table 2  
Digital Computer Program

1	LOAD VS CURVATURE
1	ARC HYPERBOLIC SINE
1	GENERAL I SECTION
	BLR 0000 0040
	BLR 1900 1999
	REG L0041 0049
START	LDD KEY1
	STD 0022 A1
KEY1	00 0088 8888
A1	RD1 9000
	RD1 9008
	RD1 9010 A2
A2	RD1 9020
	RSB 0011
	LDD 8006
	STD 9033
	RAU 9014 A9
A9	STU 9019
	STU 9029 A3
A3	RAU 9011 A8
A8	STU 9018
	RSC 0001 A10
A10	RSA 0003
	RAU 9011 B
	LDD C1 B1
B1	STD END
	STU B2
	FMP 8003
	STU B3
	FAD 9000
	STU B4
	FAD B3
	STU B5
	RAU B4
	LDD B6 FLSQR
B6	STU B7
	FAD B2
	LDD B8 FLLNX
B8	STU B9
	FMP B2
	FSB B7
	STU 9055 A
	RAU B7
	FMP B2
	STU B10
	RAU B9
	FMP B5
	FSB B10
	STU 9059 -A
	AXA 0001 END
C1	RAU 9000
	FSB 9018

NOTE 1  
NOTE 2  
NOTE 3  
NOTE 4  
NOTE 5



Table 2 (Continued)

	BMI	C2	
	RSU	8003	C2
C2	FMP	9011	B
	LDD	C3	B1
C3	RAU	9020	
	NZU		C9
	FMP	9018	
	FAD	9000	
	BMI		C5
	RSU	8003	C5
C5	FMP	9011	B
	LDD	C6	B1
C9	AXA	0001	C6
C6	RAU	9021	
	NZU		D1
	FMP	9018	
	FAD	9000	
	BMI		C8
	RSU	8003	C8
C8	FMP	9011	B
	LDD	D1	B1
D1	RAU	9011	B
	FMP	9018	
	STU	9016	
	RAU	9023	
	NZU	E1	
	RAU	9052	
	FSB	9053	E6
E6	FDV	9016	
	NZC		D6
	STU	9028	
	FSB	9019	
	BMI		D3
	RAU	9018	
	FSB	9011	
	NZU	D4	
	AXB	0001	
	LDD	8006	
	STD	9033	A10
D3	STU	9030	
	RAU	9029	
	FSB	9019	
	BMI	D5	
	RAU	9018	
	FAD	9012	
	STU	9018	
	RSA	0002	C1
D4	RAU	9018	
	FSB	9013	
	STU	9018	
	LDD	9028	
	STD	9029	
	RSA	0002	C1



Table 2 (Continued)

D5	RAU	9028	
	FSB	9029	
	STU	9031	
	RAU	9030	
	FDV	9031	
	FMP	9013	
	FAD	9018	
	STU	9018	
	AXC	0001	
	RSA	0002	C1
D6	STU	0013	NOTE 11
	LDD	9016	
	STD	0015	
	RAU	9000	
	FDV	9018	
	STU	0014	
	FSB	9027	
	FMP	0013	
	STU	9017	
	RAU	9023	
	NZU	F1	
	RAU	9000	
	FSB	9018	
	BMI		D7
	RSU	9057	
	STU	9057	D7
D7	RAU	9056	
	FSB	9057	F6
F6	FDV	9005	
	FDV	9016	
	FDV	9016	
	FSB	9017	
	STU	0016	
	WR2	0013	NOTE 12
	AXB	0001	
	NZB		NOTE 13
	LDD	9019	
	STD	9029	
	RAU	9018	
	FAD	9012	A8
D9	RAU	9019	
	FSB	9002	
	NZU		NOTE 14
	RAB	9033	
	RAU	9019	
	FAD	9015	
D8	HLT	0000	A2
E1	RAU	9055	NOTE 6
	FMP	9024	
	STU	9055	
	RAU	9053	
	FMP	9025	
	STU	9053	



Table 2 (Continued)

	RAU	9054	
	FMP	9023	
	STU	9054	
	RAU	9052	
	FMP	9022	
	FSB	9054	
	FAD	9055	
	FSB	9053	
	FDV	9026	E6
F1	RAU	9021	
	FMP	9018	
	FAD	9000	
	BMI	F2	
	RAU	9059	
	FMP	9024	
	STU	9059	F3
F2	RSU	9059	
	FMP	9024	
	STU	9059	F3
F3	RAU	9000	
	FSB	9018	
	BMI	F4	
	RAU	9057	
	FMP	9025	
	STU	9057	F5
F4	RSU	9057	
	FMP	9025	
	STU	9057	F5
F5	RAU	9058	
	FMP	9023	
	STU	9058	
	RAU	9056	
	FMP	9022	
	FSB	9058	
	FAD	9059	
	FSB	9057	
	FDV	9026	F6

NOTE 11



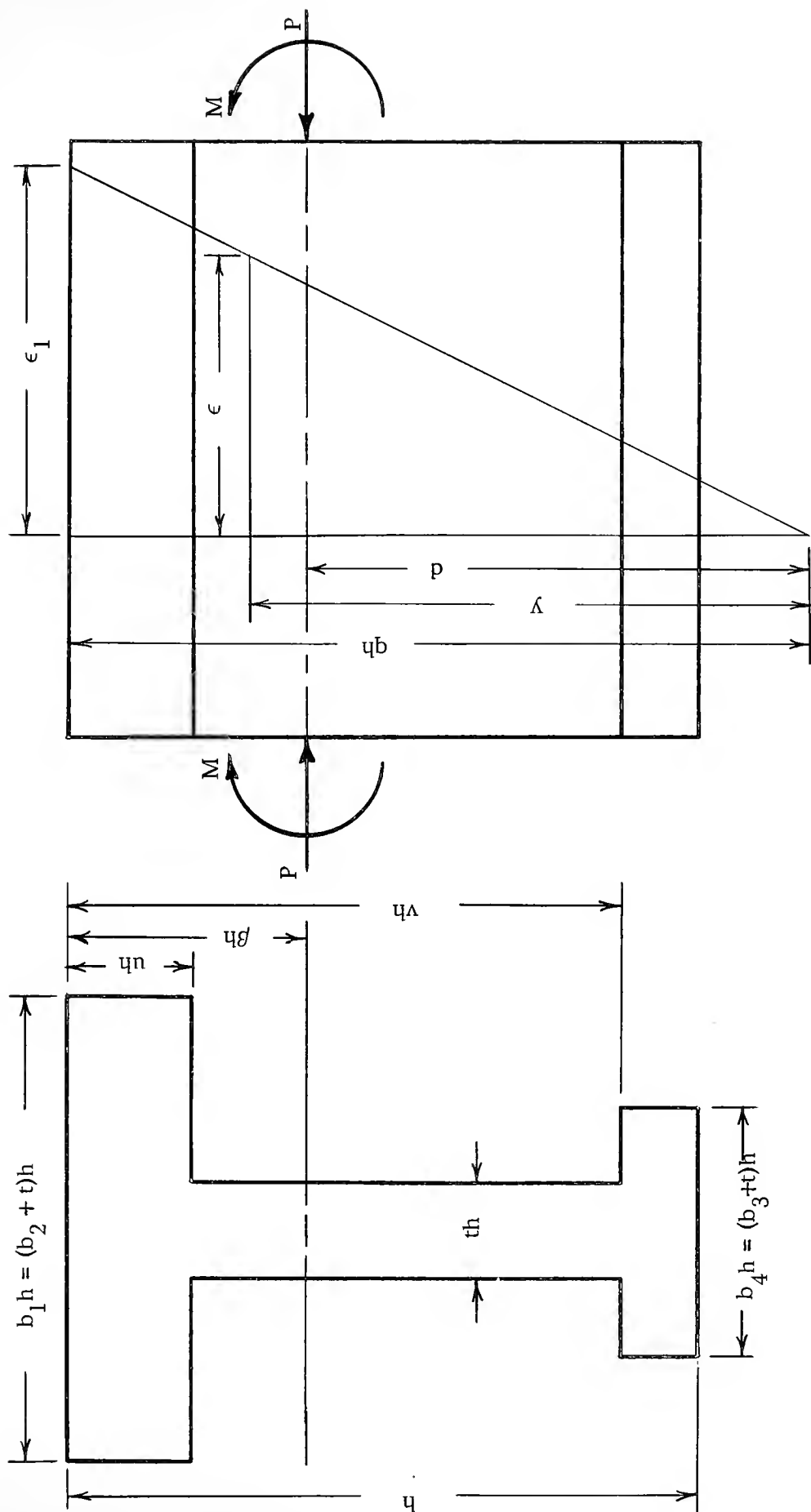


Figure 1 I - Section Member Showing Dimensions of Cross - Section Loading Arrangement and Strain Distribution



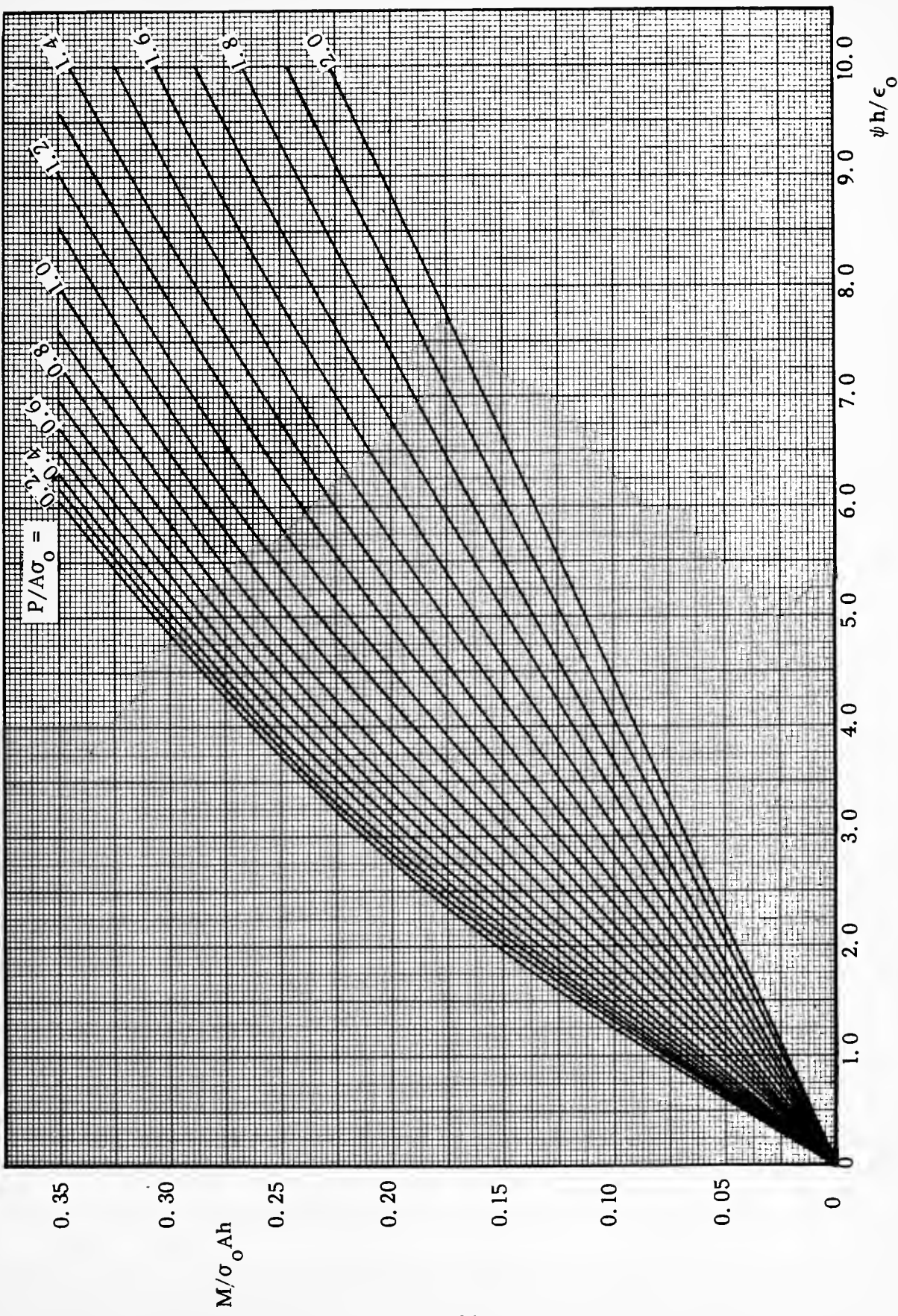


Figure 2. Dimensionless Moment-Curvature Interaction Curves for Rectangular-Section



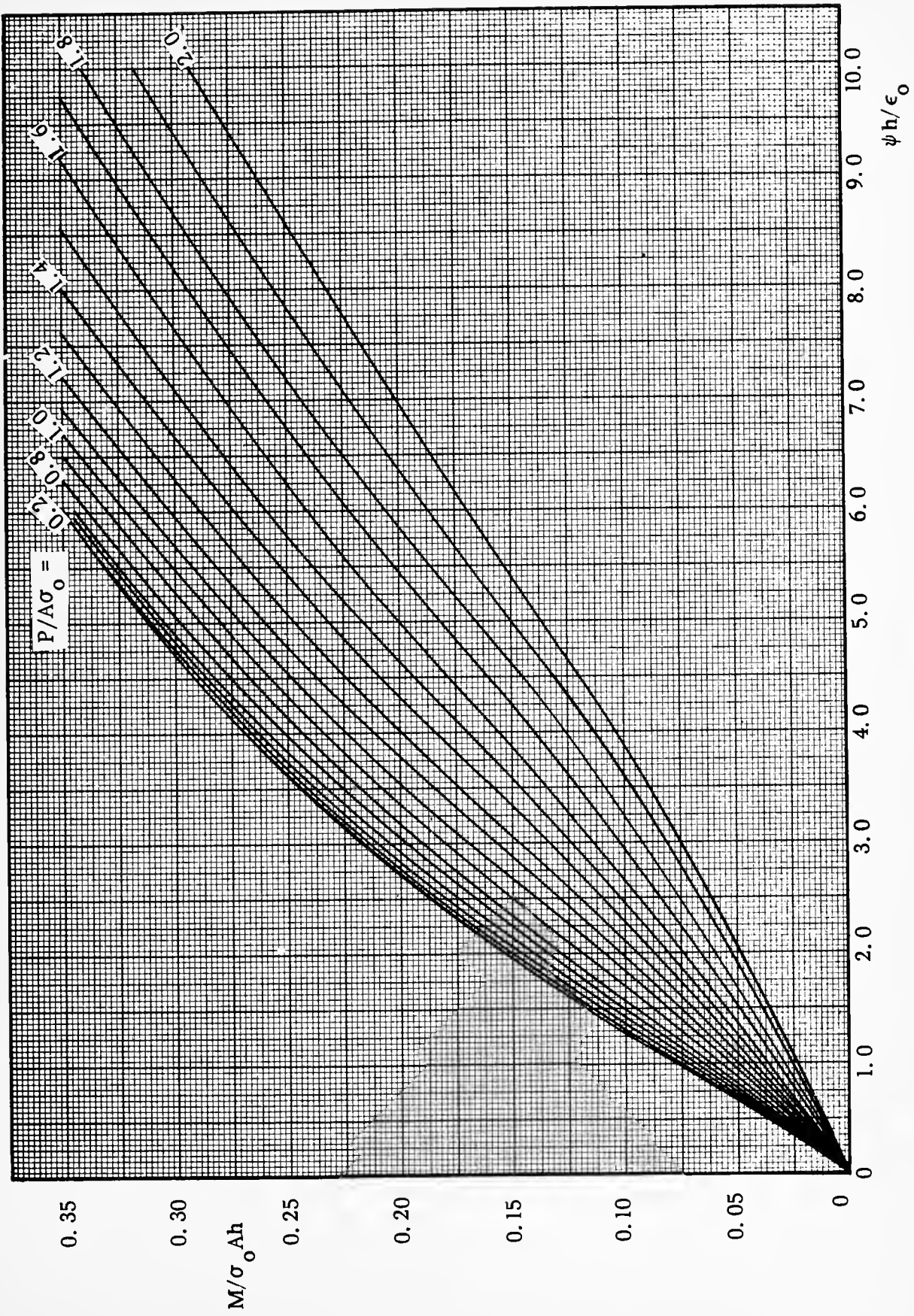


Figure 3. Dimensionless Moment-Curvature Interaction Curves for T-Section



	f	d	c	b	a	Common Factors
$M_Q/\sigma_o Ah$	0	.0159	.0319	.0479	.0638	
Assumed $\delta$	0	.050	.219	.113	.125	
$\Delta = \delta + e$	.150	.200	.219	.263	.275	
$M_P/\sigma_o Ah$	.1050	.1400	.1673	.1841	.1925	
$M/\sigma_o Ah = (M_P + M_Q)/\sigma_o Ah$	.1050	.1559	.1992	.2320	.2563	
$h\psi/\epsilon_o$	1.49	2.22	2.93	3.52	3.96	
Equiv. Concentrated $\psi$		26.4	35.0	42.1	22.9	$\epsilon_o \lambda / 12$
Average Slopes	126.4	100.0	65.0	22.9		$\epsilon_o \lambda / 12$
Calculated $\delta$	0	126.4	226.4	291.4	314.3	$\epsilon_o \lambda^2 / 12$
Calculated $\delta$	0	.057	.103	.132	.142	
Assumed $\delta$	0	.064	.115	.148	.159	
$A = \delta + e$	.150	.214	.265	.298	.309	
$M_P/\sigma_o Ah$	.1050	.1497	.1855	.2085	.2165	
$M/\sigma_o Ah$	.1050	.1656	.2174	.2564	.2800	
$h\psi/\epsilon_o$	1.49	2.35	3.25	3.96	4.98	
Equiv. Concentrated $\psi$		28.2	38.8	47.3	25.9	$\epsilon_o \lambda / 12$
Average Slopes	140.2	112.0	73.2	25.9		$\epsilon_o \lambda / 12$
Calculated $\delta$	0	140.2	252.2	325.4	351.3	$\epsilon_o \lambda^2 / 12$
Calculated $\delta$	0	.064	.114	.142	.159	

Figure 4. Sample Deflection Calculation for T-Section Beam-Column



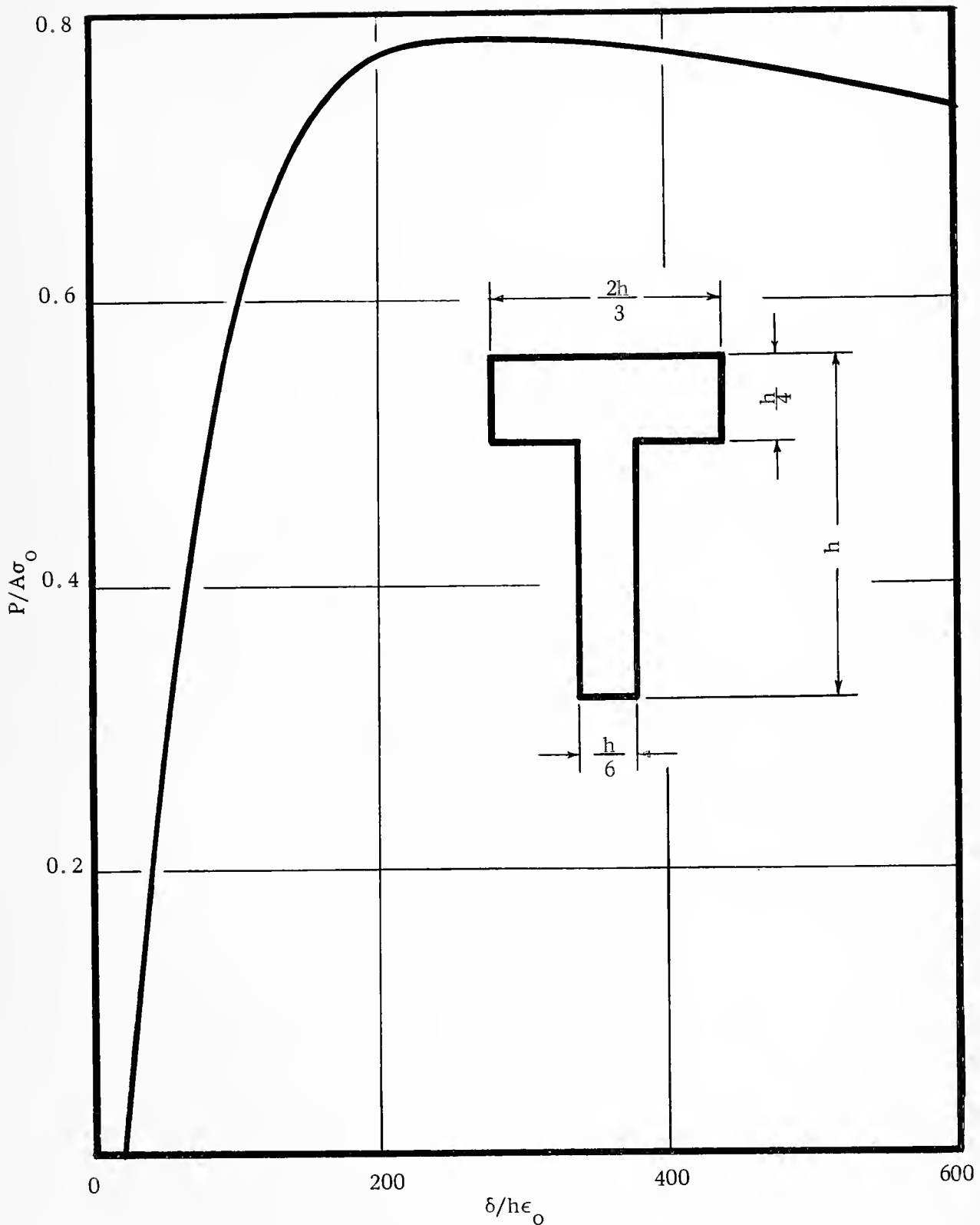
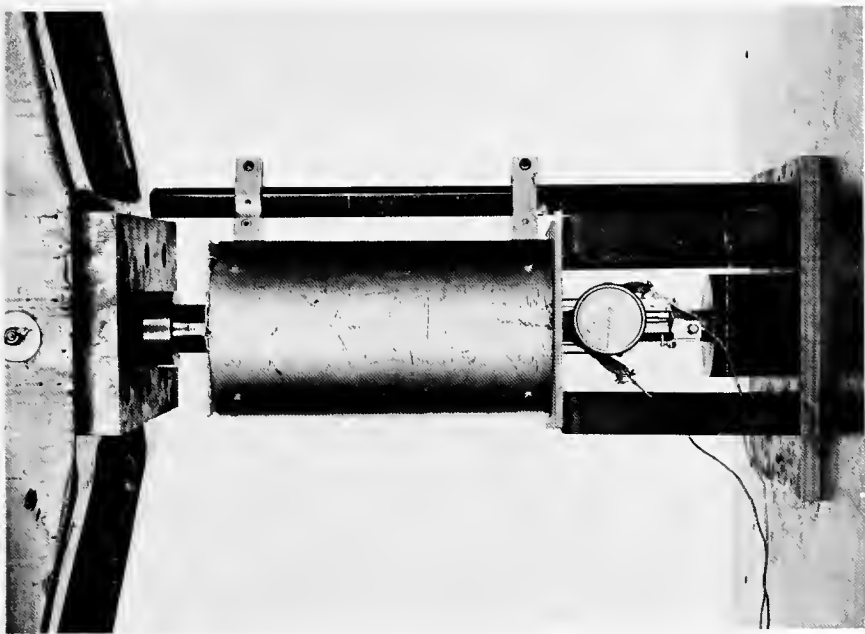


Figure 5 Dimensionless Load-Deflection Curve for T-Section Beam-Column  
 $(l/r = 60.2, Q = 2\sigma_0 I/c l, e/h = 0.15)$



(b) Furnace in Place



(a) Compression Specimen With Extensometer Attached

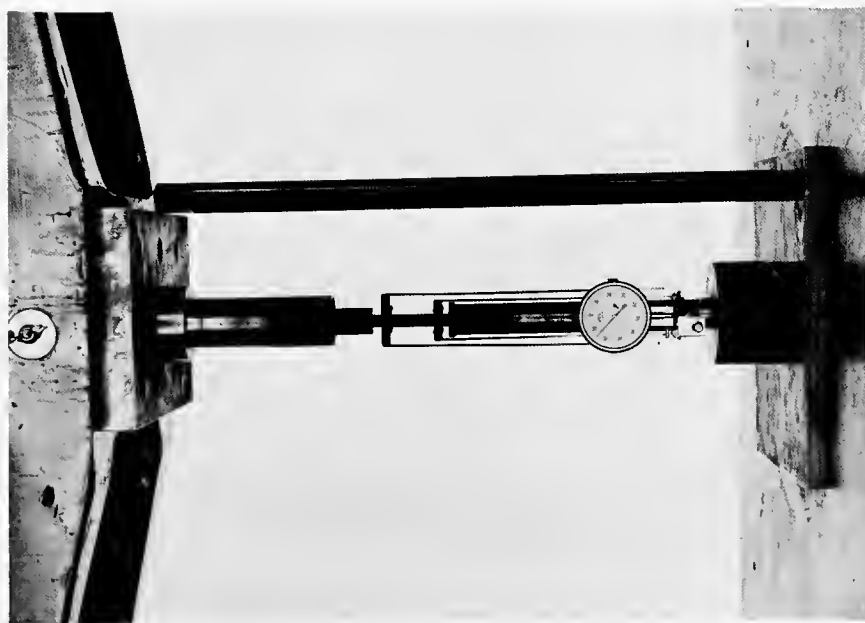


Fig. 6. Fixture for Testing Compression Creep Specimens at Elevated Temperature



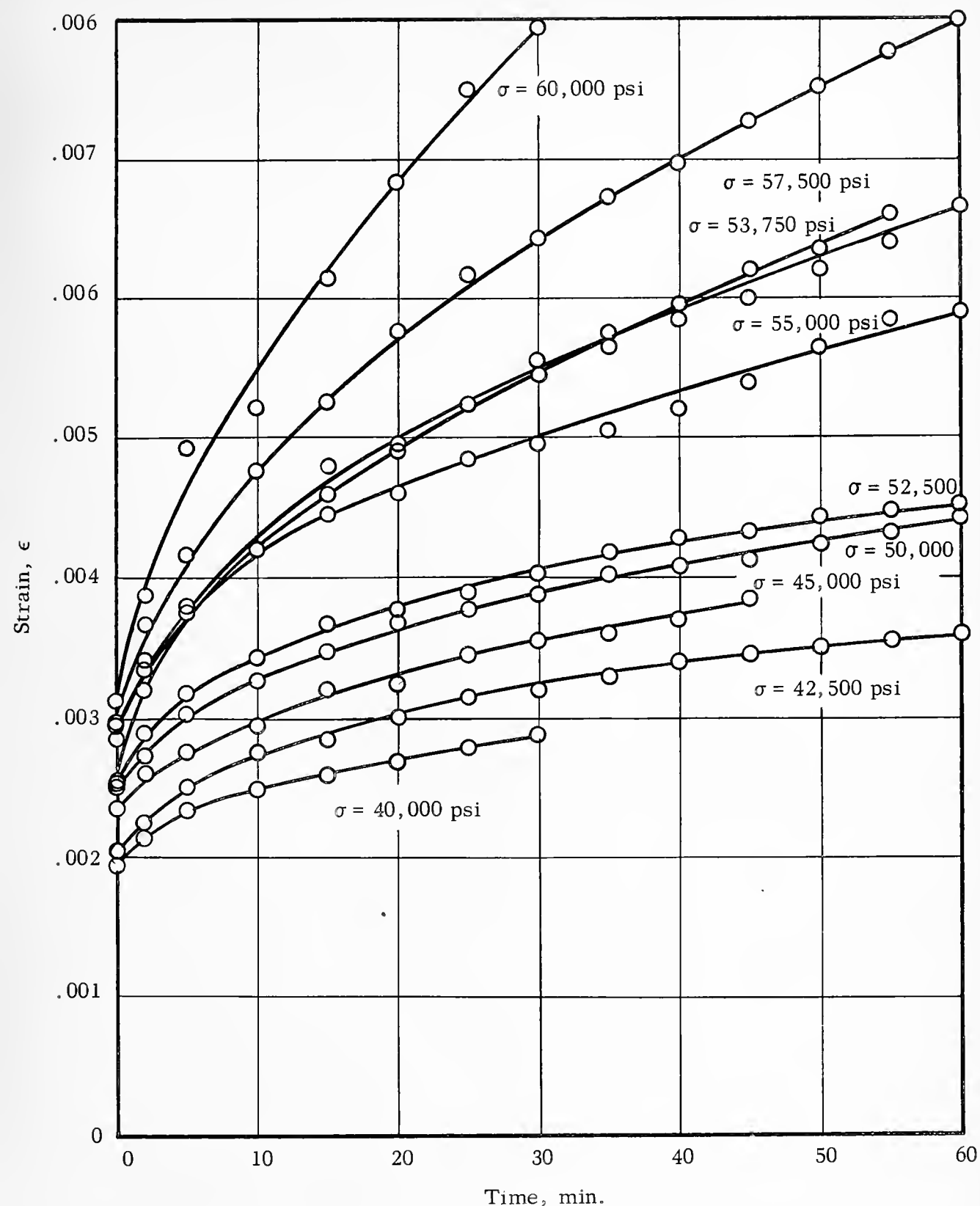


Figure 7. Compression Creep Curves for 17-7PH Stainless Steel at 972°F.



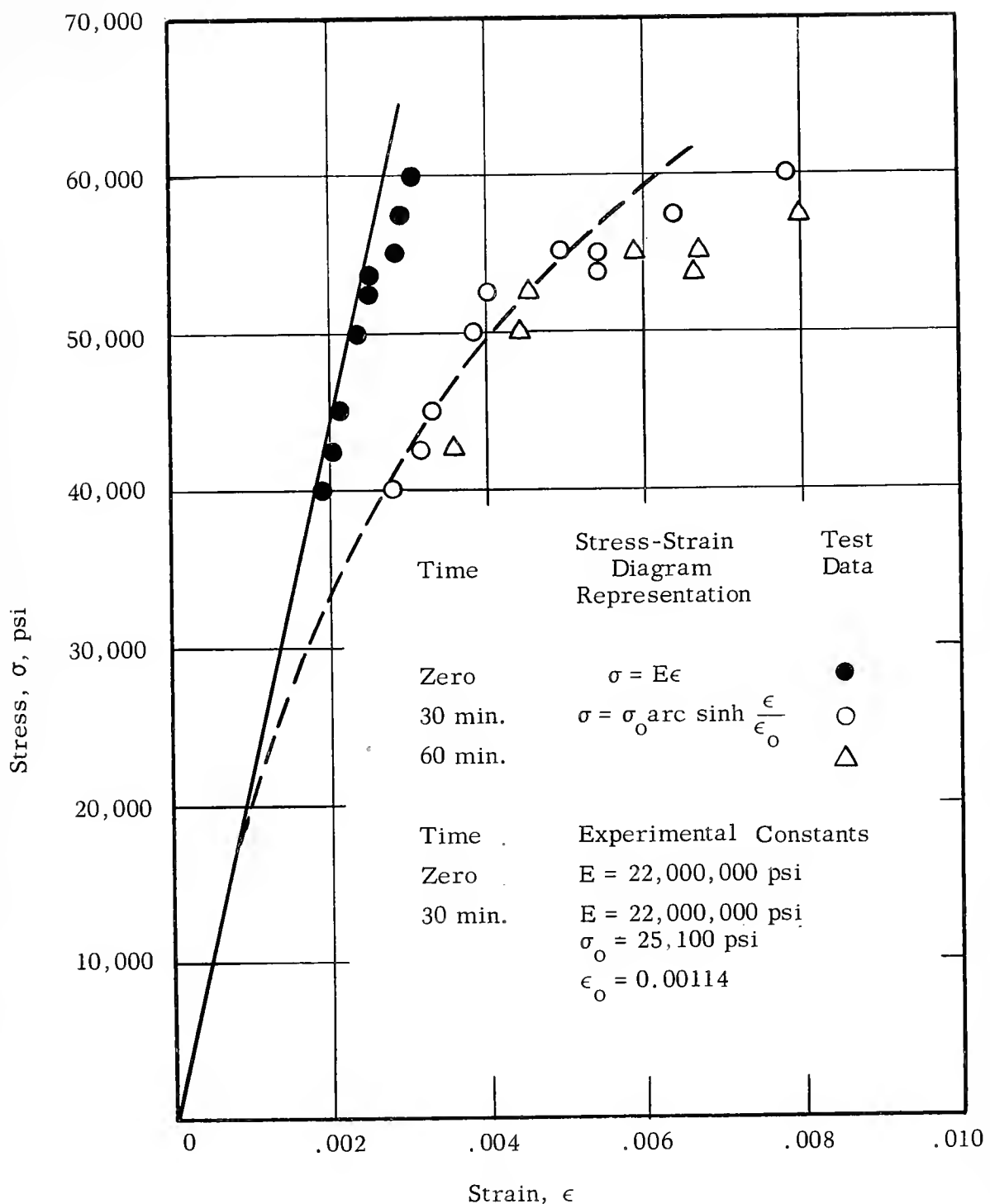


Figure 8. Compression Isochronous Stress-Strain Diagrams for 17-PH Stainless Steel at 972°F.



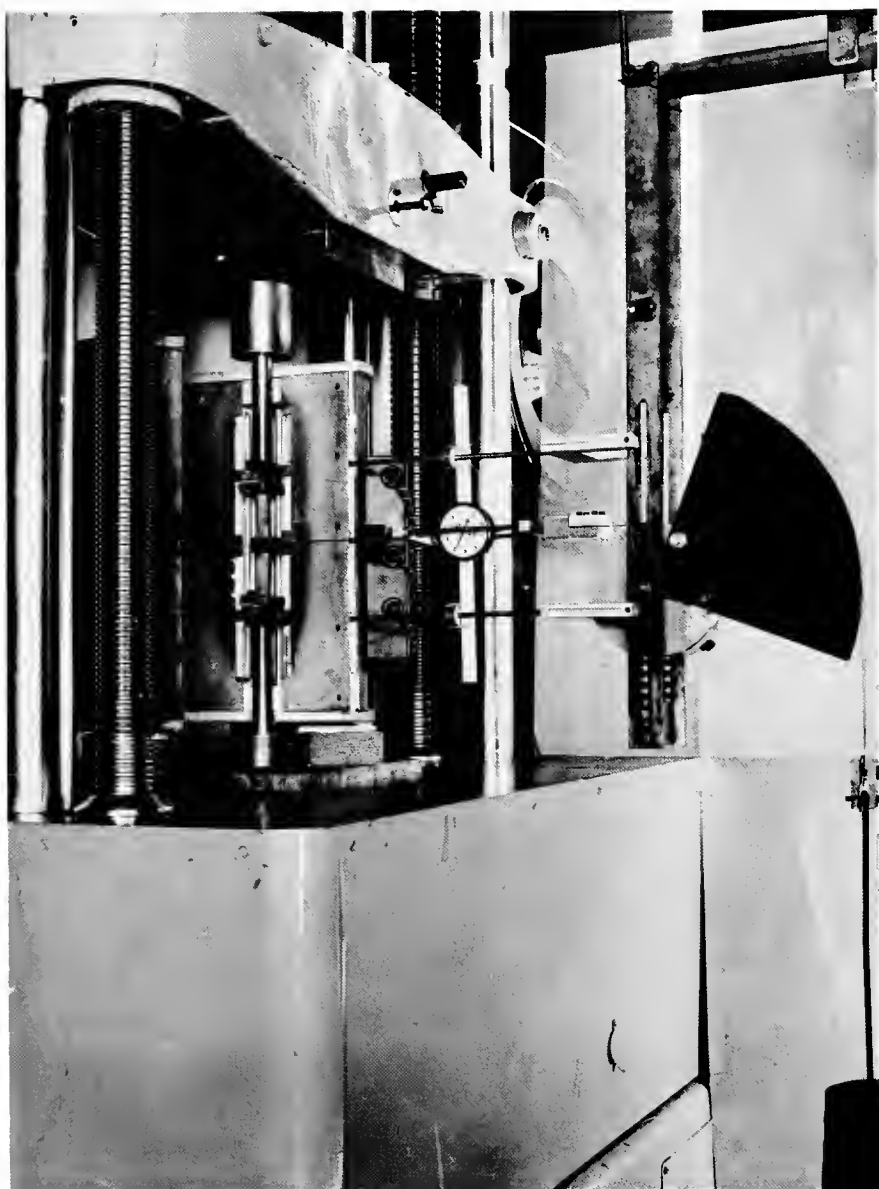
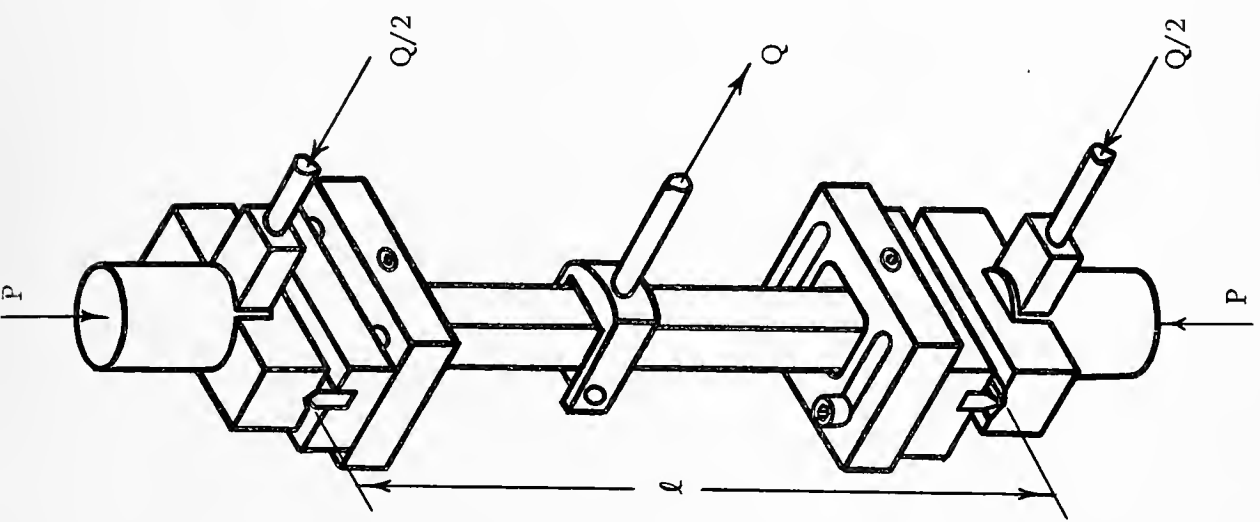
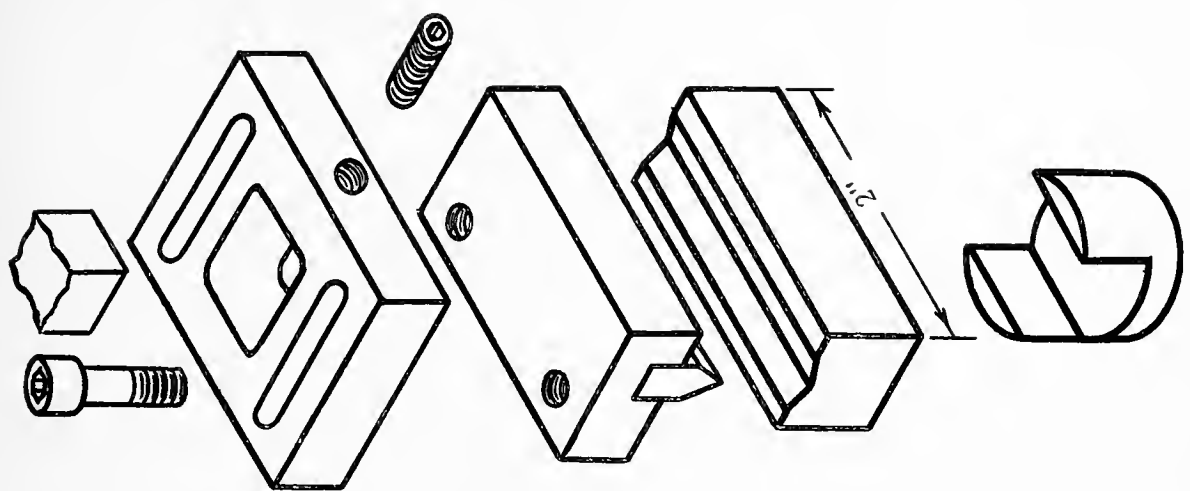


Figure 9. Test Apparatus with Beam-Column in Furnace.



Figure 10. Schematic Diagram of Fixtures for Loading Beam-Column, with Exploded View of Knife Edge.





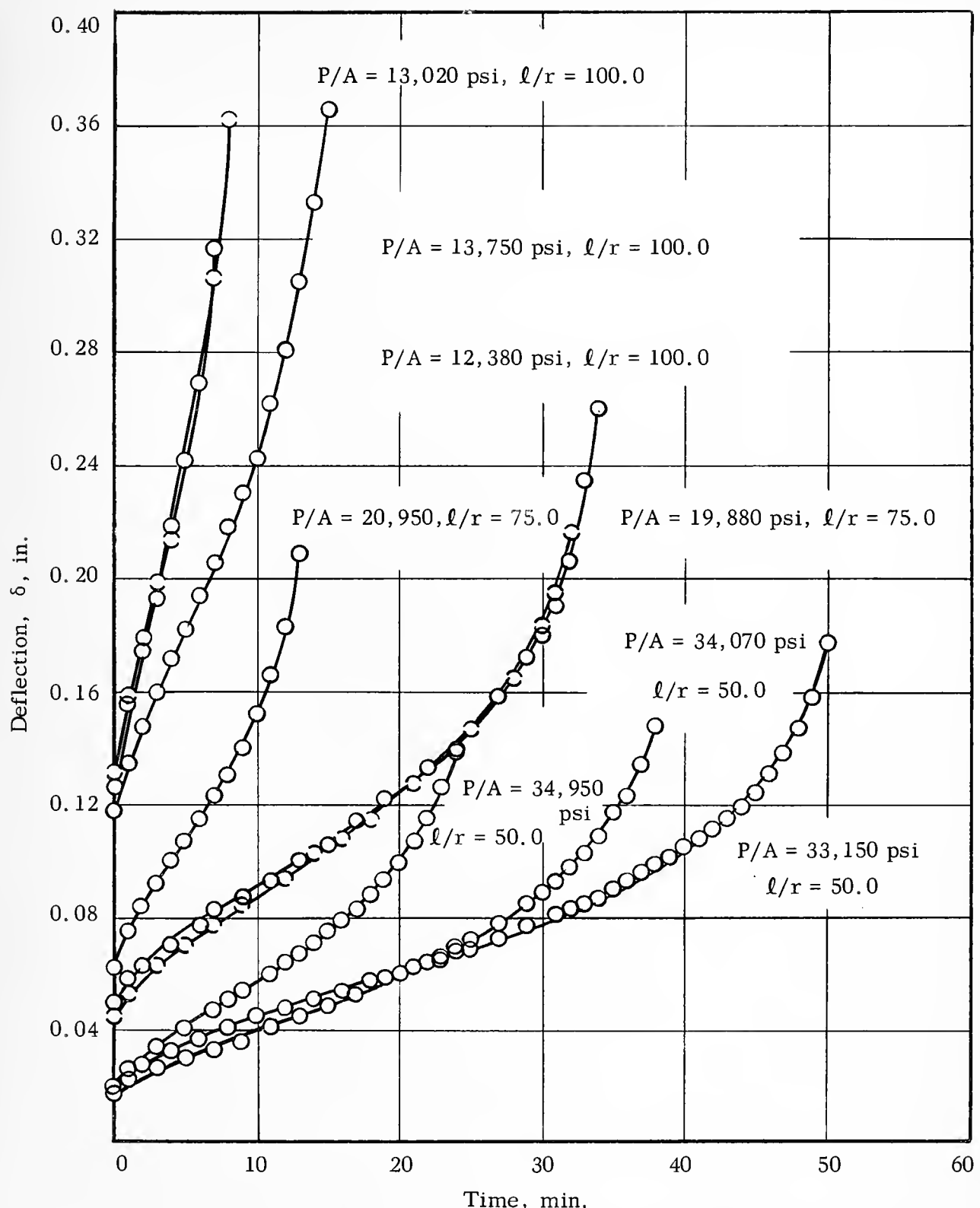


Figure 11. Deflection-Time Curves for Rectangular-Section Beam-Columns Having Zero Initial Eccentricity, Made of 17-7PH Stainless Steel and Tested at 972°F.



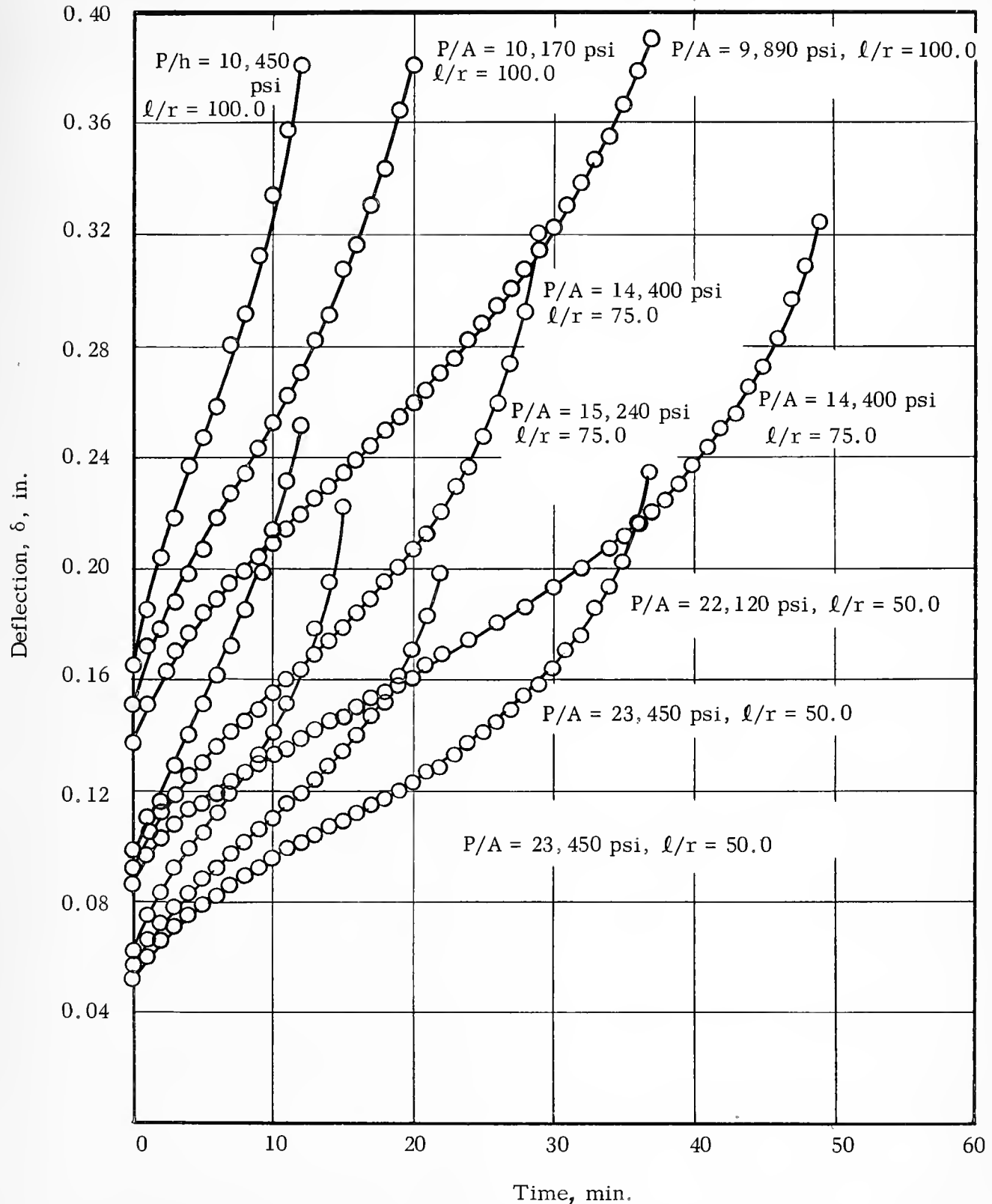


Figure 12. Deflection-Time Curves for Rectangular-Section Beam-Columns Having 15 Per Cent Initial Eccentricity Made of 17-7PH Stainless Steel and Tested at 972°F.



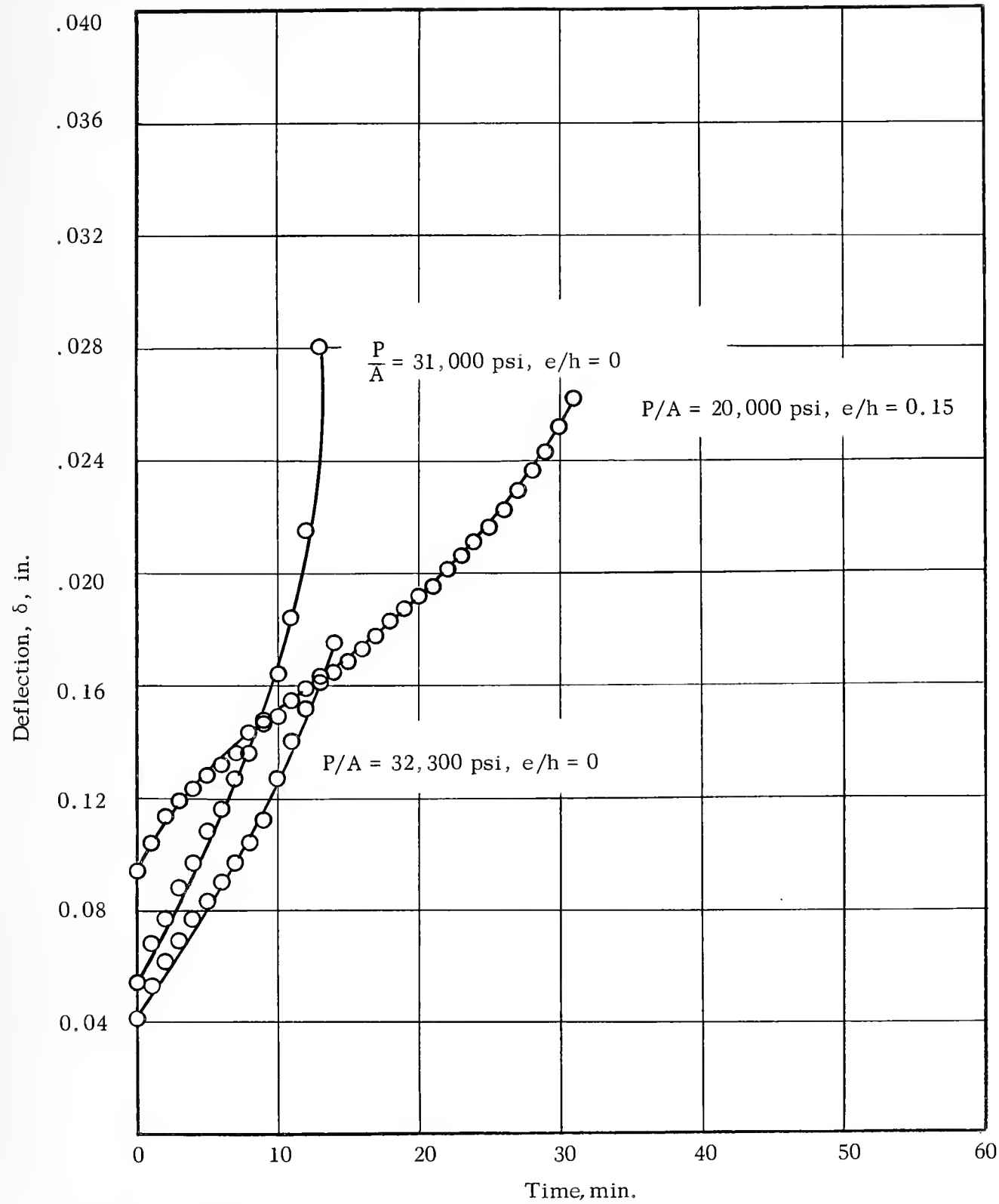


Figure 13. Deflection-Time Curves for T-Section Beam-Columns Made of 17-7PH Stainless Steel and Tested at  $972^{\circ}\text{F}$  ( $\ell/r = 60.2$ ).



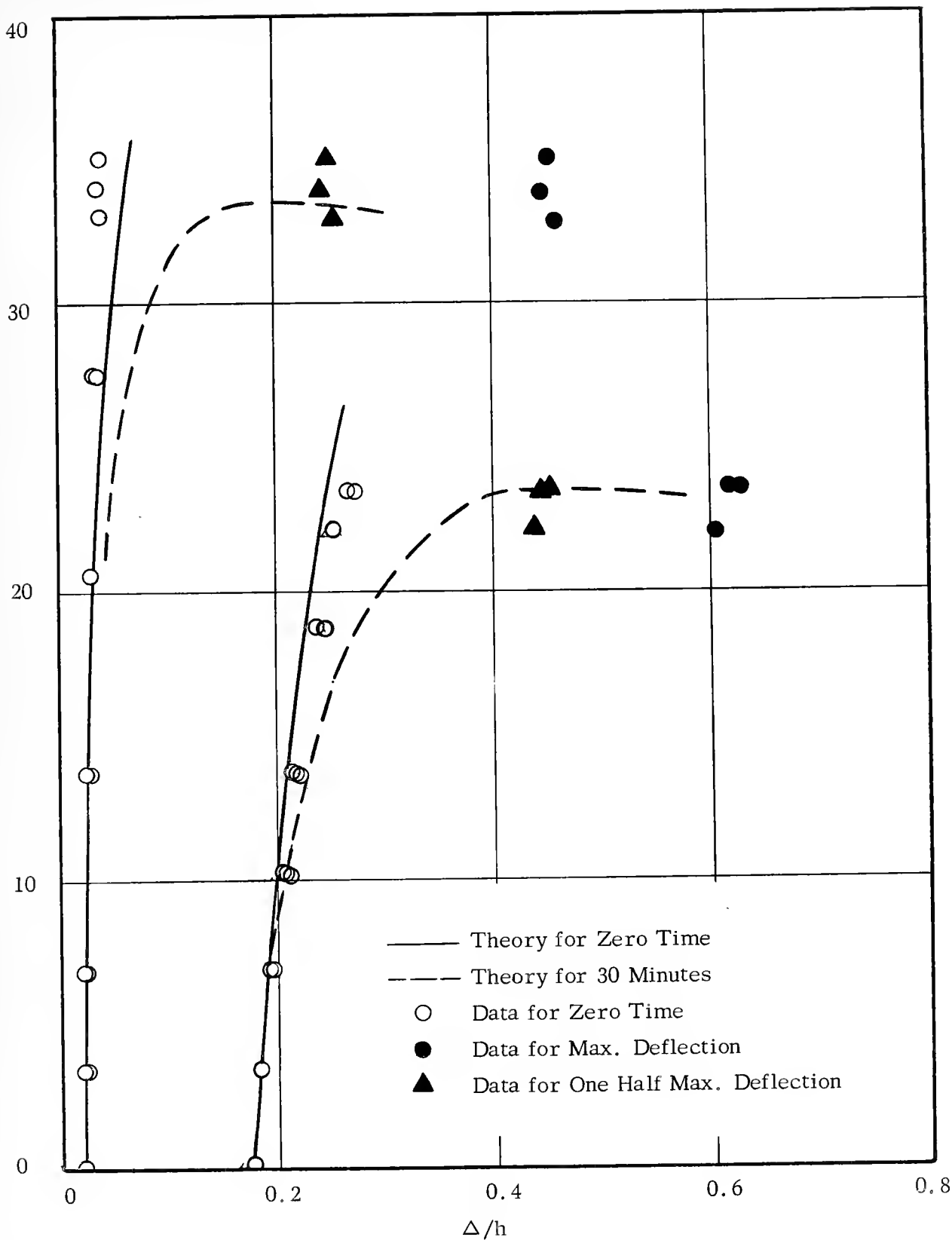


Figure 14. Load-Deflection Curves for Rectangular-Section Beam-Columns Made of 17-7PH Stainless Steel and Tested at 972°F. ( $\ell/r = 50.0$ ).



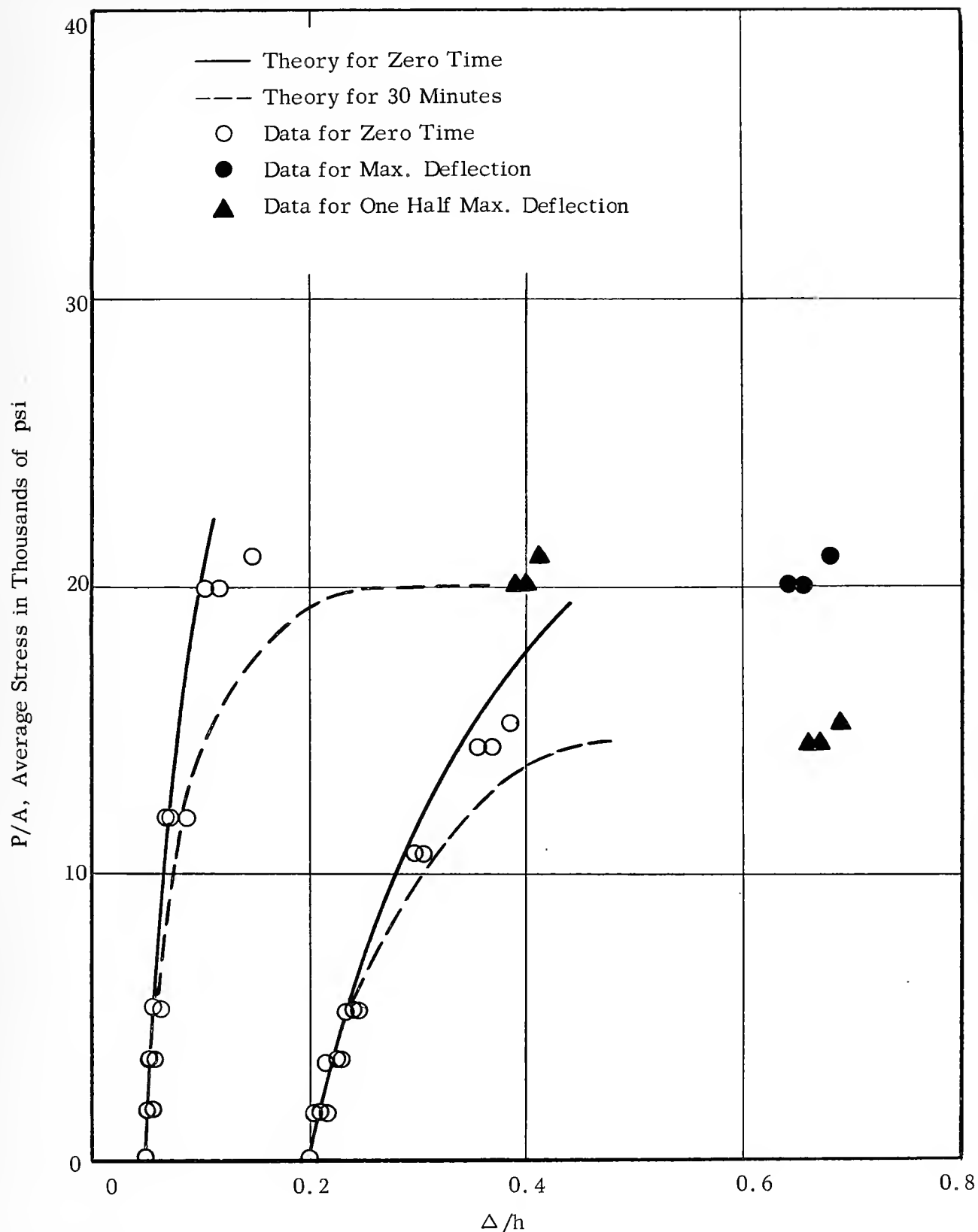


Figure 15. Load-Deflection Curves for Rectangular-Section Beam-Columns Made of 17-7PH Stainless Steel and Tested at 972°F ( $l/r = 75.0$ ).



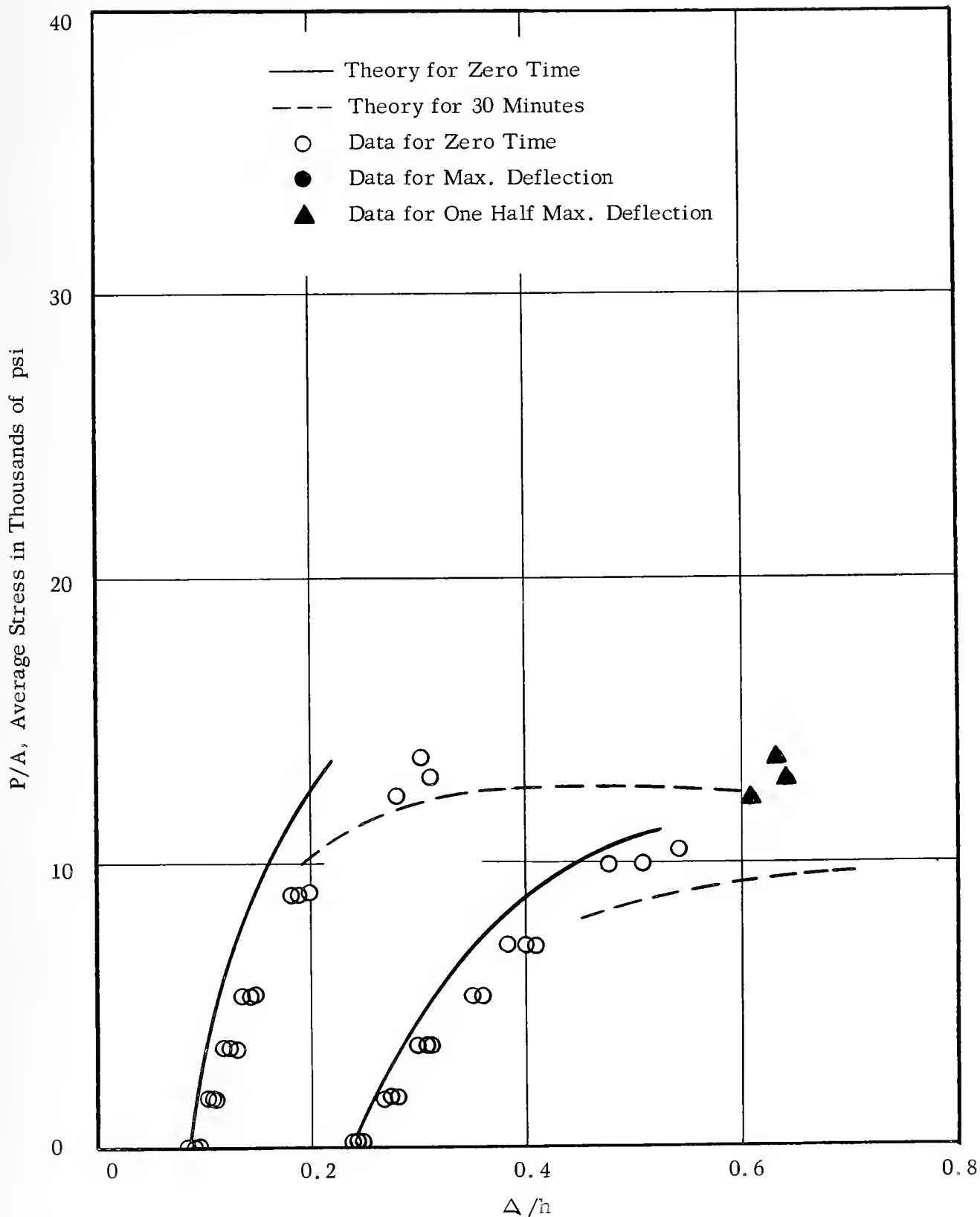


Figure 16. Load-Deflection Curves for Rectangular-Section Beam-Columns Made of 17-7PH Stainless Steel and Tested at 972°F ( $\ell/r = 100.0$ ).



P/A, Average Stress in Thousands of psi

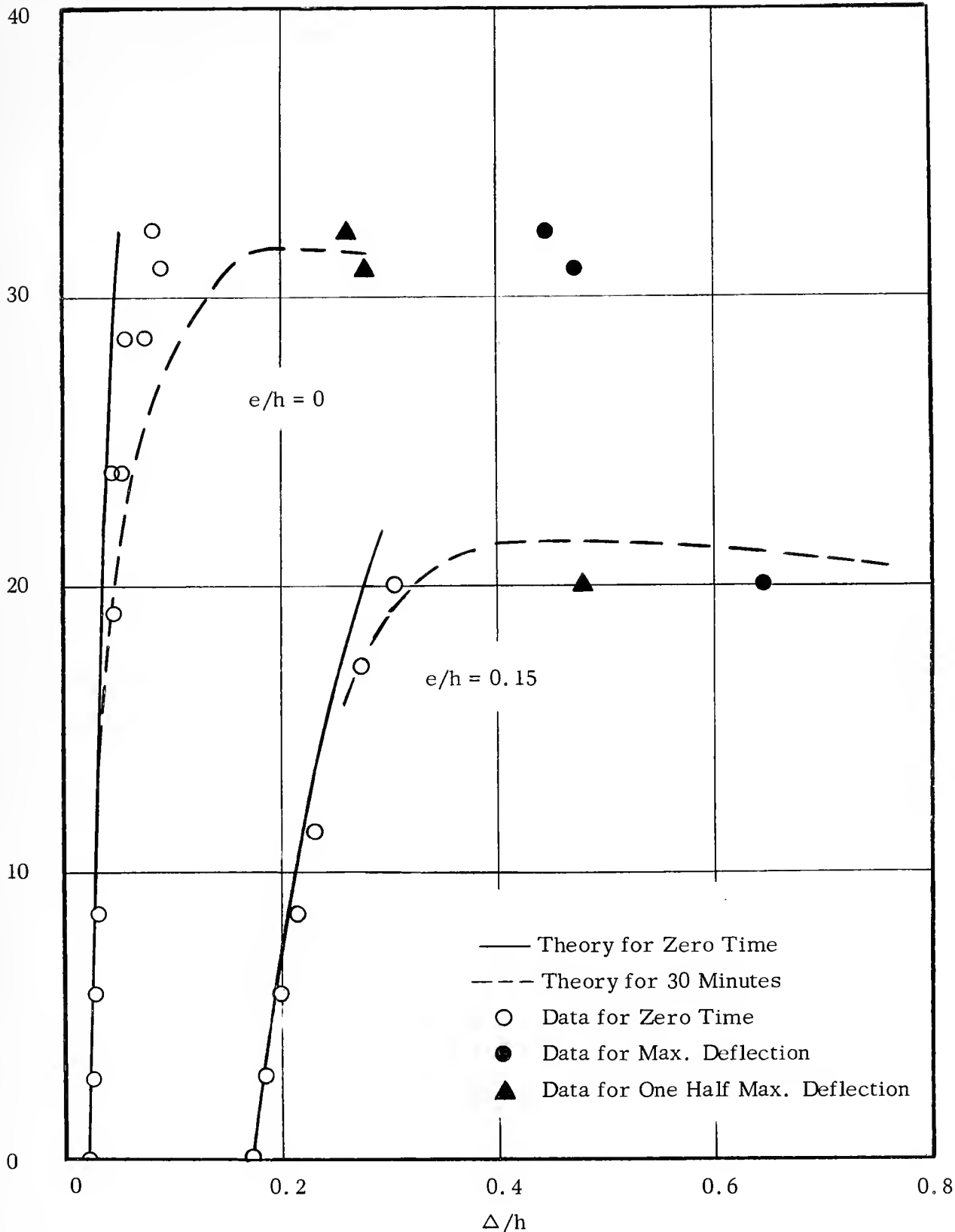


Figure 17. Load-Deflection Curves for T-Section Beam-Columns Made of 17-7PH Stainless Steel and Tested at 972°F ( $l/r = 60.2$ ).



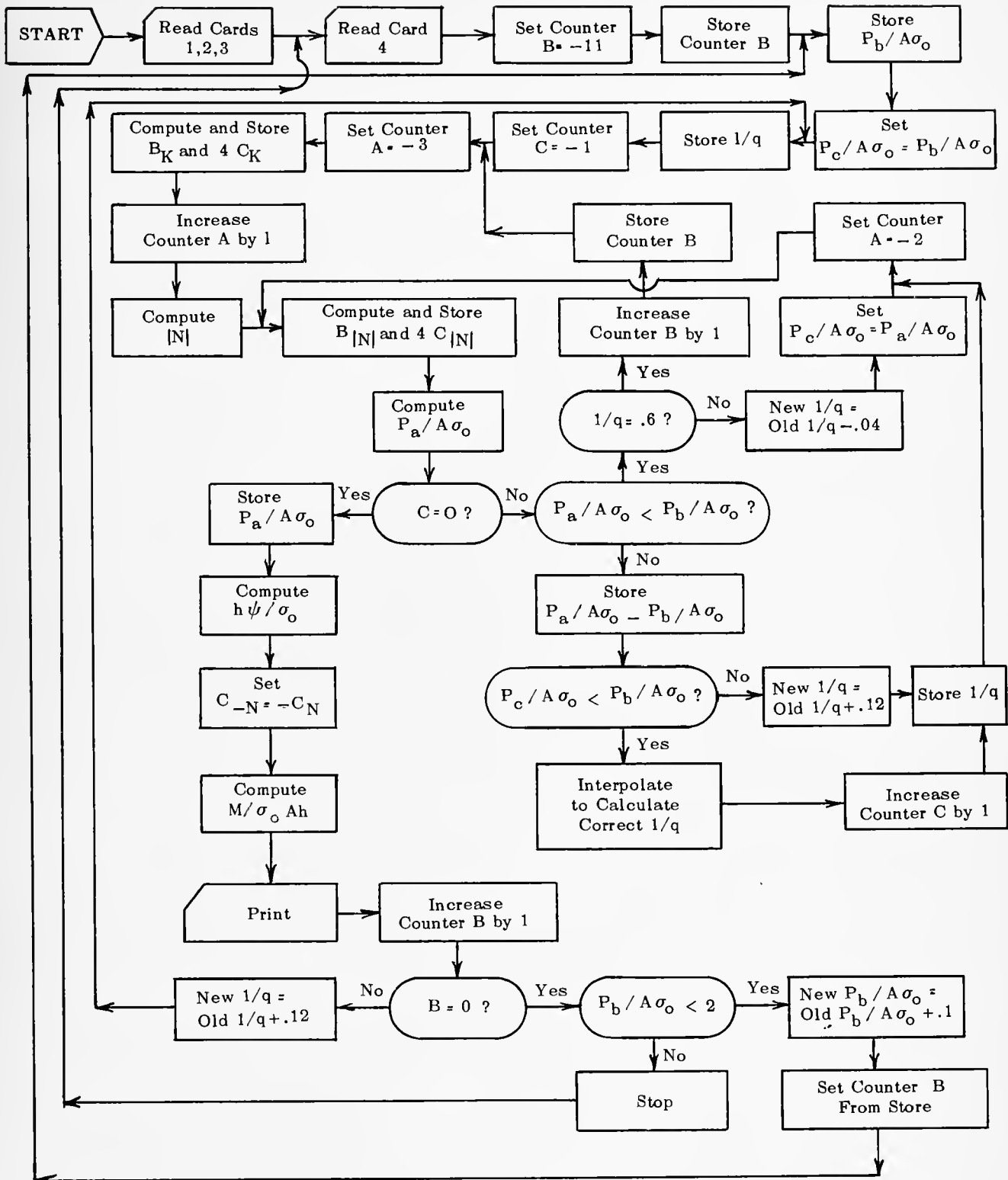


Figure 18. Flow Diagram for Digital Computer Program



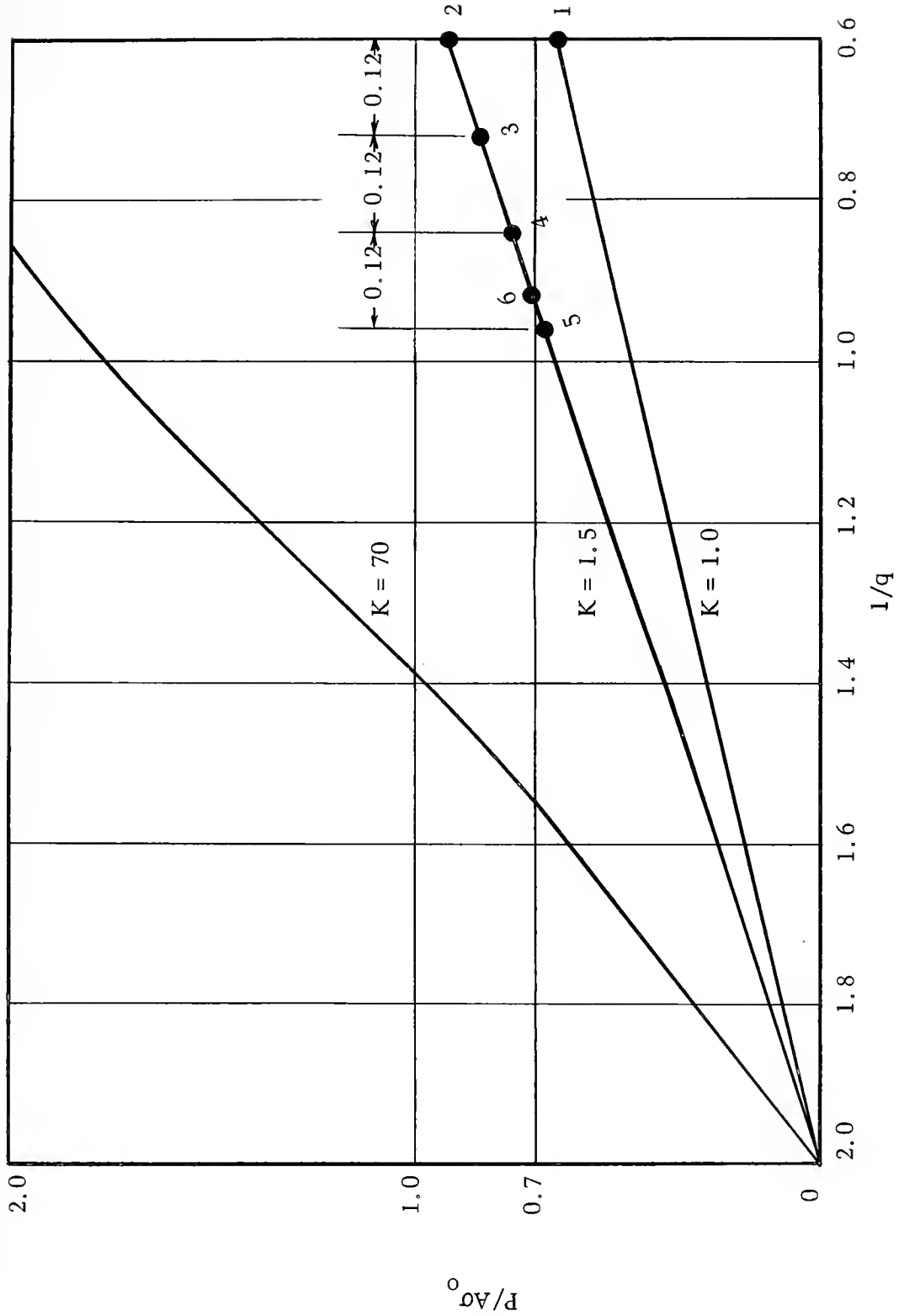


Figure 19.  $P/A\sigma_0$  Versus  $1/q$  Curves Showing Procedure Followed by Computer to Make First Calculation at  $P/A\sigma_0 = 0.70$ .













UNIVERSITY OF ILLINOIS-URBANA



3 0112 083268745